Extracellular Electrical Stimulation of Retinal Ganglion Cells

by

Andrew Eli Grumet

Submitted to the Department of Electrical Engineering and Computer Science
in partial fulfillment of the requirements for the degree of

Master of Science

at the

MASSACHUSETTS INSTITUTE OF TECHNOLOGY

September 1994

© Massachusetts Institute of Technology 1994. All rights reserved.

Author .....
Department of Electrical Engineering and Computer Science
July 5, 1994

Certified by .....
John L. Wyatt, Jr.
Professor, Department of Electcal Engineering and Computer Science
Thesis Supervisor

Accepted by .....
Frederic R. Morgenthaler
Chairman, Departmental Committee on Graduate Students

ARCHIVES

MASS. INST. TECH.
NOV 16 1994
LIBRARIES

Extracellular Electrical Stimulation of Retinal Ganglion Cells

by
Andrew Eli Grumet

Submitted to the Department of Electrical Engineering and Computer Science
on June 1, 1994, in partial fulfillment of the
requirements for the degree of
Master of Science

Abstract

The research conducted for this thesis was part of an overall effort to develop a retinal prosthesis to aid blind patients suffering from disease of the photoreceptors. We hope to restore vision to such patients by implanting a device which electrically stimulates the healthy cells of the inner retina. Preliminary experiments indicate that the threshold amounts of current required to stimulate retinal ganglion cell bodies and axons typically fall within the same range. We believe that stimulation of ganglion cell axons will hinder our ability to elicit phosphenes of discernible resolution in implanted patients. For this reason, current research efforts are directed in part at finding a way to stimulate retinal ganglion cell bodies without exciting the axons which overlie them at the innermost layer of the retina.

The goal of this thesis is to design a stimulating electrode which employs a novel geometry to selectively stimulate retinal ganglion cell bodies. Discussions of the retina and of the retinal prosthesis are provided at the outset of the thesis. Simple models of nerve cells are then constructed and analyzed both to guide the design process and also to develop a general understanding of electrical stimulation. Analysis leads to the specification of a new experimental electrode and a description of how it was constructed. A description of preliminary experiments which were conducted to test the electrode follows. Due to a number of unresolved experimental issues, experimental results were inconclusive. Suggestions for further study are made in the concluding chapter of the thesis.

Thesis Supervisor: John L. Wyatt, Jr.
Title: Professor, Department of Electcal Engineering and Computer Science

Contents

1 Introduction **5**
1.1 Thesis problem 5
1.2 Thesis outline 5

2 The Retina and the Retinal Implant **7**
2.1 Overview of retinal anatomy and physiology 7
2.1.1 Cross-sectional view of the retina 7
2.1.2 Topographical view of the retina 15
2.1.3 Information processing in the retina 18
2.2 The retinal implant 23
2.2.1 Motivation 23
2.2.2 Description and selected design issues 24
2.3 Electrical stimulation of retinal cells 26
2.3.1 Previous work 26
2.3.2 Thesis problem revisited 32

3 Theory of Extracellular Electrical Stimulation **34**
3.1 Statement of Assumptions 38
3.2 Cell Body in a Uniform Electric Field 41
3.2.1 Solution form and boundary conditions 42
3.2.2 Time-independent solution 44
3.2.3 Interpretation of the time-independent solution 45
3.3 Axon in a longitudinal field 51
3.3.1 Cable equation for extracellular stimulation 54
3.3.2 Activating function 55
3.3.3 Time-independent solutions 56
3.3.4 Interpretation of the time-independent solutions 58
3.4 Comparison of thresholds 61
3.5 Limitations of approach 65
3.5.1 Nonlinearity of the cell membrane 65
3.5.2 Time-dependent behavior 65
3.5.3 Role of the cell in determining the extracellular voltage 67
3.5.4 Inhomogeneity of biological tissue 67
3.5.5 Anode-break excitation 67
3.5.6 Non-uniformity of the cell membrane 68

4 Electrode Design **69**
4.1 Geometry 69
4.2 Construction 71
4.3 Predicting the electric field 77

5 On experimental verification **79**
5.1 Three hypotheses 79
5.2 Outline of the experimental procedure 81
5.3 Unresolved experimental issues 83
5.3.1 Stimulus artifact 83
5.3.2 Position of the stimulating electrode relative to the cell 83
5.3.3 Movement of the stimulating electrode 86
5.3.4 Variations with time 87

6 Conclusion **90**
6.1 Summary 90
6.2 Suggestions for further study 90
6.2.1 Modeling and analysis 90
6.2.2 Electrode construction 91
6.2.3 Experimental methods 91

A Additional mathematical derivations **93**
A.1 Time dependent responses of cell body in a uniform field 93
A.2 Axon in a uniform, transverse field 96
A.2.1 Solution form and boundary conditions 96
A.2.2 Time-independent solution 98
A.2.3 Time-dependent solutions 99

B SPICE simulation of axon in longitudinal field **102**
B.1 Circuit description 102
B.2 Results 103
B.3 Abbreviated SPICE input file 104

Chapter 1

Introduction

The research conducted for this thesis was part of an overall effort to develop a retinal prosthesis to aid blind patients suffering from disease of the photoreceptors. Millions of people worldwide are affected by two such diseases, retinitis pigmentosa (RP) and age-related macular degeneration (AMD) [3, 40, 65]. Preliminary evidence suggests that while these diseases result in degeneration of the outer retina, inner retinal elements may remain healthy to some degree [60]. Furthermore, it has long been known that visual sensations are created when the retinal cells of healthy subjects are stimulated electrically [6, 23, 37]. In light of these two facts, we hope to restore vision to patients suffering from RP and AMD by implanting a device which electrically stimulates the healthy cells of the inner retina. Lending support to our approach is a more recent study which demonstrated that phosphenes could be elicited in a patient with RP [25].

1.1 Thesis problem

Preliminary experiments have been conducted to characterize the response of rabbit retinal ganglion cells to electrical stimulation *in vitro*. Results to date indicate that the threshold amounts of current required to stimulate ganglion cell bodies and axons typically fall within the same range [26, 64]. We believe that stimulation of ganglion cell axons will hinder our ability to elicit phosphenes of discernible resolution in implanted patients. For this reason, current research efforts are directed in part at finding a way to stimulate retinal ganglion cell bodies without exciting the axons which overlie them at the innermost layer of the retina.

The goal of this thesis is to design a stimulating electrode which employs a novel geometry to selectively stimulate retinal ganglion cell bodies. All stimulating electrodes used in previous experiments have had radially-symmetric geometries. For this reason, the current investigation focuses on non-radially-symmetric electrodes.

1.2 Thesis outline

The body of the thesis is divided into four chapters. Chapter 2 provides a discussion of the retina and of the retinal prosthesis. This chapter is intended to broaden the reader's understanding the thesis problem described above. We will attempt to solve the thesis problem through a combination of theoretical and experimental approaches. The theory of extracellular electrical stimulation of nerve cells is discussed in Chapter 3. Simple models

of nerve cells are constructed and analyzed in this chapter to guide the design process and also to broaden our general understanding of electrical stimulation. The design and construction of an experimental stimulating electrode are covered in Chapter 4. A model for numerically predicting the electric fields produced by the electrode is presented at the end of the chapter. Chapter 5 describes preliminary experiments which were conducted to test the electrodes. Due to a number of unresolved experimental issues which are described in the final section of the chapter, experimental results were inconclusive. Suggestions for improved experimental methods are made in the concluding chapter of the thesis.

Chapter 2

The Retina and the Retinal Implant

The essence of the thesis can be clarified by a general description of the retina and of the retinal implant. The chapter is divided into three sections. The first section deals in a general way with the anatomy and physiology of the normal retina. Where appropriate, known correlations between retinal structure and function will be given. The second section provides the motivation for and a functional description of the retinal implant. In addition, two design issues relevant to this work will be discussed. The third section of the chapter is devoted to one of the many lines of research towards the development of a successful retinal prosthesis, electrical stimulation of retinal cells. A review of the literature in this area will lead to a more complete formulation of the thesis problem.

2.1 Overview of retinal anatomy and physiology

The retina is a delicate tissue that lines the back of the interior of the eye (Figure 2-1). The retina (*ret*) resides between the choroid (*ch*) and vitreous (*vitr*). From a functional viewpoint, the retina lies at the front end of the visual system. Light enters through the eye and is transduced at the retina to neural signals. These signals propagate through the retina and incite a number of processing operations, some of which will be discussed below. The signals are then conducted from the retina to the visual areas of the brain via the optic nerve (Figure 2-2).

2.1.1 Cross-sectional view of the retina

A cross-sectional view of the retina, suggested by the dashed box in Figure 2-1, reveals a multi-layered cellular organization. A common feature among vertebrates is the interposition of two synaptic layers between three cellular layers [14]. This feature is evident in layers (4) through (8) of Figure 2-3. There are six basic classes of retinal neurons [14]. These are photoreceptors, horizontal cells, bipolar cells, amacrine cells, interplexiform cells[1], and gan-

[1]It has been argued that interplexiform cells should in fact be classified as amacrine cells [62], reducing the number of classes to five. I have arbitrarily chosen to include the interplexiform cell as a distinct class, as in [14].

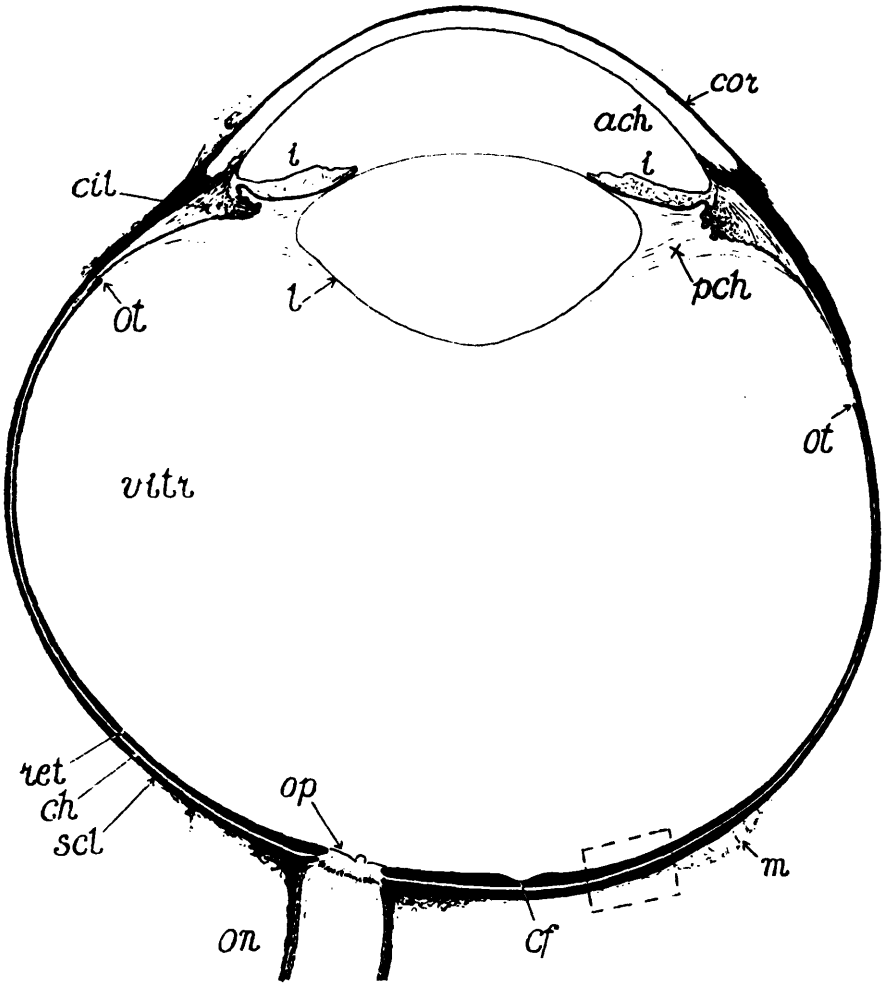

Figure 2-1: View of a horizontal section through the right eye of a Rhesus Macaque (*macaca mulatta*). From Polyak [42]. Abbreviations - *scl:* sclera; *ch:* choroid membrane; *ret:* retina; *on:* optic nerve; *op:* optic papilla, or disc; *cor* cornea; *cil:* ciliary body; *i:* iris; *l:* lens; *ach:* anterior chamber; *pch:* posterior chamber; *vitr:* vitreal chamber; *ot:* ora terminalis; *cf:* central fovea; *m:* extrinsic muscle.

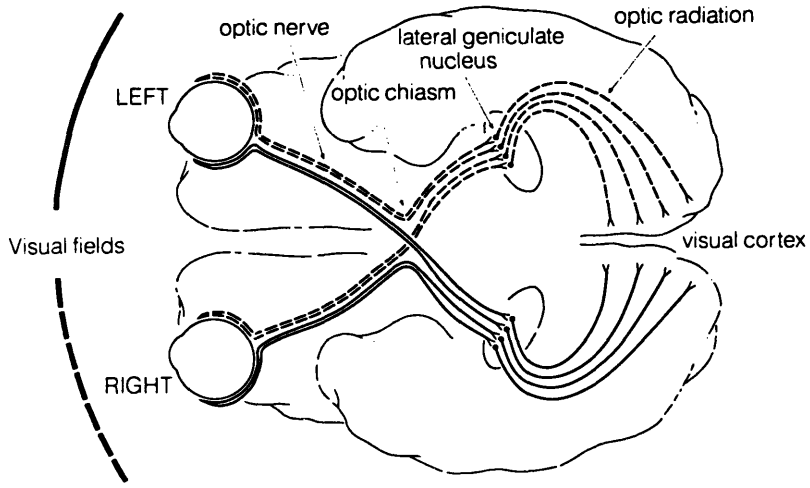

Figure 2-2: Diagram of the visual pathways in primates viewed from the underside of the brain. From Dowling [14].

glion cells. Each type of neuron will be briefly discussed below[2]. In addition to neurons, the retina also contains *glial cells*. These cells do not have axons or conduct action potentials [32], but may be responsible for a variety of physiological functions [63]. One such cell, the Müller cell, is considered first.

Müller cells

The dominant type of glial cell in the retina is the Müller cell. These cells and their processes fill most of the space between neural elements in the retina, leaving extracellular gaps about 20nm wide. The nuclei of Müller cells reside in the inner plexiform layer (see layer 6c) and the cell bodies extend vertically through the retina, spanning the distance between the outer and inner limiting membranes. Also, Müller cells have large *endfoot* regions which extend downwards through the optic nerve fiber layer as triangular or conical structures that form the inner limiting membrane. While Müller cells are integral to the functioning of the retina, they are not in the direct line of signal flow from the outer to the inner retina [49]. On the other hand, the cells appear to be the main contributor to the electroretinogram b-wave. The model for b-wave generation in Müller cells posits two potassium current sinks along the cell's length, one in the outer plexiform layer and one in the inner plexiform layer, and a source of potassium current at the cell's endfoot region.

Photoreceptors

The photoreceptor cells are named after their function; these cells capture light and transduce it to neural signals. Since no other type of retinal cell can perform this feat, only the photoreceptors are stimulated directly by light. When the light-evoked responses of other cell types are discussed below, it should be remembered that these responses are secondary to photoreceptor stimulation. Transduction occurs at the outermost portion of the retina, where incoming light is absorbed by the outer segments of the photoreceptors (layer 2a in Figure 2-3). Since light entering the eye impinges on the retina at the layer of optic nerve fibers, it must travel through the tissue's transparent layers in order to reach the rod and cone outer segments.

There are two types of photoreceptors: rods and cones. The inner segments (see layer 2b) of cones are typically thicker than those of nearby rods. The cell bodies of both types of cells are found in the outer nuclear layer. The photoreceptor terminals extend into the outer plexiform layer, where they make well-characterized synapses onto horizontal and bipolar cell dendrites. Photoreceptors are also known to make contacts with one another, typically via electrical gap junctions.

Rods and cones exhibit distinct types of light sensitivity. The rods are responsible for dim-light or *scotopic* vision, while the cones mediate bright-light or *photopic* vision. In addition, cones are sensitive to the different wavelengths of the visible light spectrum, allowing us ultimately to perceive color. Rods, on the other hand, are not color-sensitive.

Both types of photoreceptors hyperpolarize in response to light. The amount of hyperpolarization produced by a photoreceptor is proportional to the logarithm of light intensity. For this reason, the responses are called *graded potentials*. Photoreceptor responses are also

[2]The better part of the material presented in the remainder of this section and in section 2.1.2 is derived from [14], [42], and [62]. Unless otherwise noted, the information presented applies specifically to primate retinas.

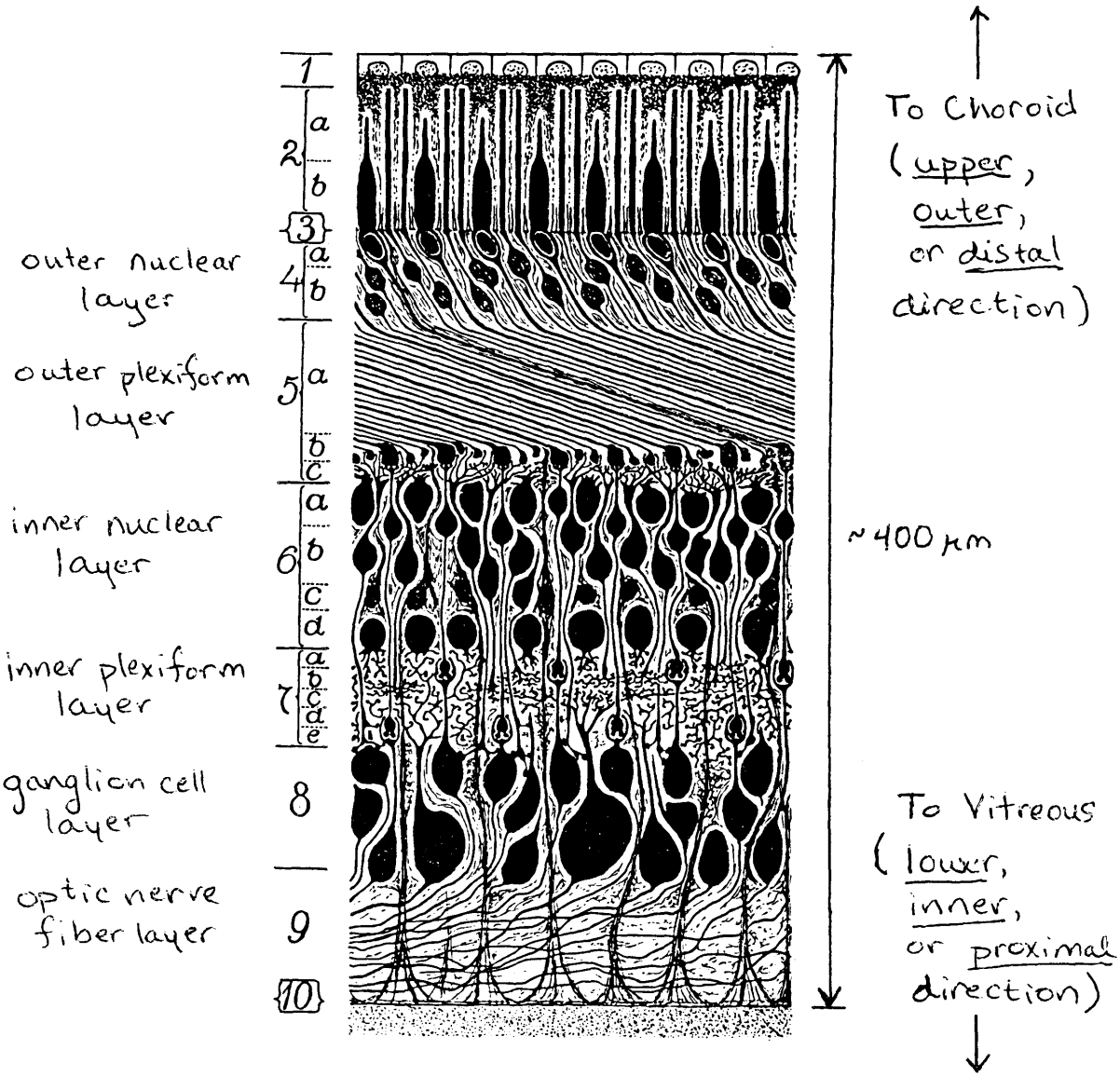

Figure 2-3: Cross-section through the adult human retina in the periphery of the central area. From Polyak [42]. Labeling: (1) pigment epithelium; (2) bacillary layer; (3) outer limiting membrane; (4) outer nuclear layer; (5) outer plexiform layer; (6) inner nuclear layer; (7) inner plexiform layer; (8) ganglion cell layer; (9) optic nerve fiber layer; (10) inner limiting membrane. The pigment epithelial cells (1) are found at the back of the retina, closest to the choroid membrane (*ch* in Figure 2-1), while the inner limiting membrane (10) is closest to the vitreal chamber (*vitr*).

sustained in the sense that, barring adaptation effects, the graded hyperpolarizing potentials are maintained as long as a stimulus is present.

Horizontal cells

Cell bodies of horizontal cells are found at the outer edge of the inner nuclear layer (6a in Figure 2-3). These cells extend their dendritic processes to form a dense network in the outer plexiform layer. There are two basic morphological types of horizontal cells found in vertebrates. The first has a relatively short axon which is several hundred microns long and ends in a prominent terminal expansion. Several subtypes of this cell have been observed and classified in different species. The second type of horizontal cell, which has not been found in primates (as of 1987), is axonless.

Horizontal cells of the same class are known to make contacts with one another via electrical gap junctions. The probable effect of such contacts is to increase the total retinal area over which a given cell is sensitive to light. This area, termed the horizontal cell's *receptive field*, is generally much larger than the area spanned by its dendrites. In addition to making connections amongst themselves, there is substantial physiological evidence indicating that horizontal cells make inhibitory synapses onto photoreceptors.

Horizontal cells generally respond to illumination of the retina with graded, sustained hyperpolarization.

Bipolar cells

The cell bodies of bipolar cells are found in the inner nuclear layer, usually in layer 6b (Figure 2-3). Bipolar cells spread their dendrites in the outer plexiform layer, and extend their axons into the inner plexiform layer. This fact suggests a simple functional polarity, whereby information is conducted away from the outer plexiform layer by the bipolar cell and delivered as input to the inner plexiform layer.

Based on both anatomical and physiological evidence, three types of bipolar cells have been identified. The first type, the *rod* bipolar cell, receives input exclusively from rods at characteristic, invaginating synapses and has a relatively large dendritic field. The other two types of cells receive input exclusively from cones. *On-center* bipolar cells connect to cones at characteristic, invaginating synapses and extend their axons to the inner portion of the inner plexiform layer. *Off-center* bipolar cells connect to cones at characteristically flat synapses and extend their axons to the outer portion of the inner plexiform layer.

Bipolar cells of all three types make synapses onto two postsynaptic processes at a structure called a dyad. The postsynaptic processes are most often either a ganglion cell dendrite and an amacrine cell process, or two amacrine cell processes.

The two types of cone bipolar cells are named after their responses to light stimuli. On-center bipolar cells respond to illumination of their receptive field centers with graded, sustained depolarizing potentials. Off-center bipolar cells respond with graded, sustained hyperpolarizing potentials. For both types of cells, the center response is reduced, and in some cases reversed, by illumination of a region surrounding the center of the receptive field. The On/Off dichotomy of cone bipolar cell responses has a known pharmacological basis (see section 2.1.3). The antagonistic center/surround receptive field organization is thought to stem from opposing influences produced by inputs from the two types of retinal neurons described above. In this scheme, direct interactions between photoreceptors and bipolar cells produce a center response, while the surround response is mediated by horizontal cells.

Rod bipolar cells have been found in some mammalian retinas to depolarize in response to illumination.

Amacrine cells

Amacrine cell bodies are found in both the inner nuclear layer (6d in Figure 2-3) and in the ganglion cell layer (8). The latter group are referred to as *displaced* cells. As a literal translation of their name would imply, amacrine cells do not have axons.

While as many as 30 distinct morphological types of amacrine cells have been found in some species, a simple binary classification scheme can often be applied. *Diffuse* amacrine cells extend processes throughout the inner plexiform layer, while the processes of *stratified* amacrine cells are usually confined to a single plane. This scheme has been further subdivided in some cases to include narrow- and wide-field diffuse amacrine cells and mono-, bi-, and multi-stratified cells. Another way to classify amacrine cells is through the neurotransmitters they use. Examples of a *glycinergic* and a *cholinergic* cell are given below[3]. As these examples will indicate, correspondences have been found between the two classification schemes discussed here.

In the inner plexiform layer, amacrine cell processes make synaptic contacts with ganglion cell dendrites, bipolar cell terminals, interplexiform cell processes, and other amacrine cell processes. While these cells do not have axons in the conventional sense, their processes can both transmit and receive information through synapses. In some cases, sites of synaptic input and output occur over very short distances along the length of a process. One example of this is the *reciprocal* synapse, whereby a bipolar cell makes a synapse onto an amacrine cell, which in turn makes a synapse back onto the bipolar at a nearby location. Reciprocal synapses between two adjacent amacrine cells have also been found (i.e. amacrine 1 synapses onto amacrine 2, which in turn synapses back onto amacrine 1). The wiring scheme inherent in the reciprocal synapse suggests a local feedback interaction. Another local interaction is the *serial* synapse, whereby an amacrine cell synapses onto another amacrine cell, which in turn synapses onto a third process at a nearby location. The functional nature of amacrine cell processes which make reciprocal and serial synapses is somewhat ambiguous; the processes exhibit properties of both axons and dendrites.

On the other hand, some types of amacrine cells exhibit a characteristic segregation of synaptic interaction, suggesting a functional polarity. For example, the AII amacrine cells found in the cat are glycinergic, have diffuse dendritic fields, and make well-characterized contacts with three types of retinal neurons. AII amacrine cells receive input from rod bipolar cells in the inner half of the inner plexiform layer, form electrical gap junctions with On-center cone bipolars in the middle portion of the layer, and make synapses onto either ganglion cell dendrites, Off-center cone bipolar terminals, or other amacrine cell processes in the outer portion of the layer. Thus the AII amacrine cell might be thought of as conducting information from the inner to the middle and outer portions of the inner plexiform layer. The starburst amacrine cell also exhibits functional polarity. This cell type has been found in all mammalian species in which it has been looked for, including humans. Starburst cells are cholinergic and have stratified, radially symmetric dendritic fields. Starburst amacrine cells receive inputs throughout their dendritic fields, but only make output synapses along the fields' outer edges. This synaptic arrangement suggests a functional polarity which points radially outward from the cell body.

[3] A cell which either releases or is activated by neurotransmitter X is referred to as X-ergic.

In most cases, amacrine cell responses are either transient or, less frequently, sustained. Transient amacrine cell responses are depolarizing, and usually are produced at both the onset and cessation of illumination. The amount of depolarization is graded with stimulus intensity, though over a much narrower range of intensities than bipolar, horizontal, and photoreceptor cells. Action potentials are often superimposed on the transient potentials. The number of superimposed spikes is usually small - one or two - and is not sensitive to changes in stimulus intensity.

Transiently responding amacrine cells are very responsive to moving stimuli. Unlike bipolar cells, these cells do not usually have antagonistic center/surround receptive field organization. Sustained responses generated by amacrine cells can be both depolarizing and hyperpolarizing, and a number of these have antagonistic center/surround receptive field organization. Finally, some amacrine cells exhibit responses containing both transient and sustained components.

Interplexiform cells

The cell bodies of interplexiform cells are found among those of amacrine cells. The main difference between these cells and their neighbors is that interplexiform cells extend processes into the outer plexiform layer, where they make output synapses. This suggests a functional polarity opposite to that of bipolar cells. Interplexiform cells receive input mainly from, and synapse rarely onto, amacrine cell processes.

Interplexiform cells are not stained well by the Golgi method - a fact that accounts for their relatively recent discovery. These cells have been studied less extensively than the other cells discussed above, though there are indications that they respond to illumination of the retina with both transient and sustained components [14].

Ganglion cells

Cell bodies of ganglion cells are found both in the ganglion cell layer and in the inner plexiform layer. Cells of the latter type are often referred to as *displaced* cells. Ganglion cells spread their dendrites in the inner plexiform layer, and extend their axons to the optic nerve fiber layer. When examined in a cross-section (Figure 2-3), ganglion cell axons typically emerge from the cell body at its lower end, and assume a horizontal or level course leading to the optic disk (see section 2.1.2). On the retinal surface, ganglion cell axons are normally unmyelinated[4].

Like amacrine cells, ganglion cells come in a variety of shapes and sizes. One morphological classification scheme for these cells developed from observations of dendritic branching patterns. The *monosynaptic* or midget ganglion cell has a relatively small cell body and dendritic field, and is believed to make synaptic contacts with a single bipolar cell. In contrast, *polysynaptic* ganglion cells have larger cell bodies and dendritic fields. Cells of this second type may be further subdivided according to the diffuse and stratified criterion discussed above for amacrine cells. Examples of midget and diffuse cells from monkey retina are shown in Figure 2-4.

A second classification scheme stems mainly from work on the cat retina. In this scheme, α cells have larger cell bodies, thicker axons, and more expansive dendritic trees than β

[4]In the rabbit, ganglion cell axons are myelinated near the optic disk.

cells. A general correlation exists between the α and β morphologies and the Y and X functional classes (see section 2.1.3), respectively [59].

Intracellular recordings from mudpuppy retina suggest that ganglion cell responses are closely related to the inputs provided by bipolar and amacrine cells. *On-off* ganglion cells, for example, respond to stimuli in a manner similar to most amacrine cells, with transient depolarizing potentials at light onset and cessation. Other ganglion cells respond in a manner similar to bipolar cells, with sustained potentials and antagonistic center/surround receptive field organization. *On-center* cells depolarize to illumination of their receptive field center, and *Off-center* cells hyperpolarize.

Unlike their bipolar counterparts, ganglion cells produce action potentials. When no stimuli are present, ganglion cell firing is referred to as *spontaneous activity.* Hyperpolarization of ganglion cells is associated with a suppression of spontaneous activity, and depolarization is associated with an increase of cell activity above the spontaneous level. The rate at which ganglion cells fire (measured in spikes per second) is typically dependent on the intensity of the light stimulus generating the response.

Response rate vs. intensity curves for On-center and On-Off ganglion cells are comparable in domain and shape to those exhibited by bipolar and amacrine cells, respectively. The correlation between cell response types indicates that some ganglion cells may receive input primarily from a single type of inner nuclear layer neuron. Additional evidence which supports this view comes from studies of the cat retina, where it has been shown that the dendrites of On-center and Off-center ganglion cells branch at levels of the INL comparable to those at which On-center and Off-center bipolar cells terminate, respectively.

2.1.2 Topographical view of the retina

In addition to its recognizable cross-sectional structure, the retina possesses distinct topographical features. A prominent landmark is the *optic disk*, where ganglion cell axons originating at all portions of the retina converge to form the optic nerve (Figure 2-5). Nasal to the disk (left side of Figure 2-1, right side of Figure 2-5), axons form straight line paths. Temporal to the disk (the opposite side), axons not originating in the fovea form arched paths around it. The *fovea* is a round region located on the left side of the optic disk as drawn in Figure 2-5. In cross-section, the fovea is a pit-shaped depression on the inner surface of the retina. The foveal depression is characterized by decrease in thickness of the inner layers (5-9) and an increase thickness of the photoreceptor layers (2-4). Cone densities are highest within the fovea, with a minimum center to center spacing of two to three microns. Presumably, the inner layers in this region are thinned in order facilitate light transmission to the foveal cones. The retina is thickest at the outer margin of the fovea, where ganglion cells are stacked as many as seven or eight layers deep. The high cell density and specialized connections (see section 2.1.3) of the fovea account for the fact that the portion of the visual field which projects onto this region can be seen with greatest spatial resolution. The fovea is part of a larger region of the retina known as the *macula.* Neurons in the macula are smaller and more uniform in size than elsewhere, and are present at higher densities. Ganglion cells within this area, for example, are stacked at least two layers deep. The remaining regions outside of the macula are called the *peripheral retina.*

Cell densities decrease and cell sizes increase at increasing distances from the central area[5]. While there is a loss in visual acuity corresponding to the lower cell density in more

[5]An exception to this rule are the rods, which are absent in the central fovea and whose density increases

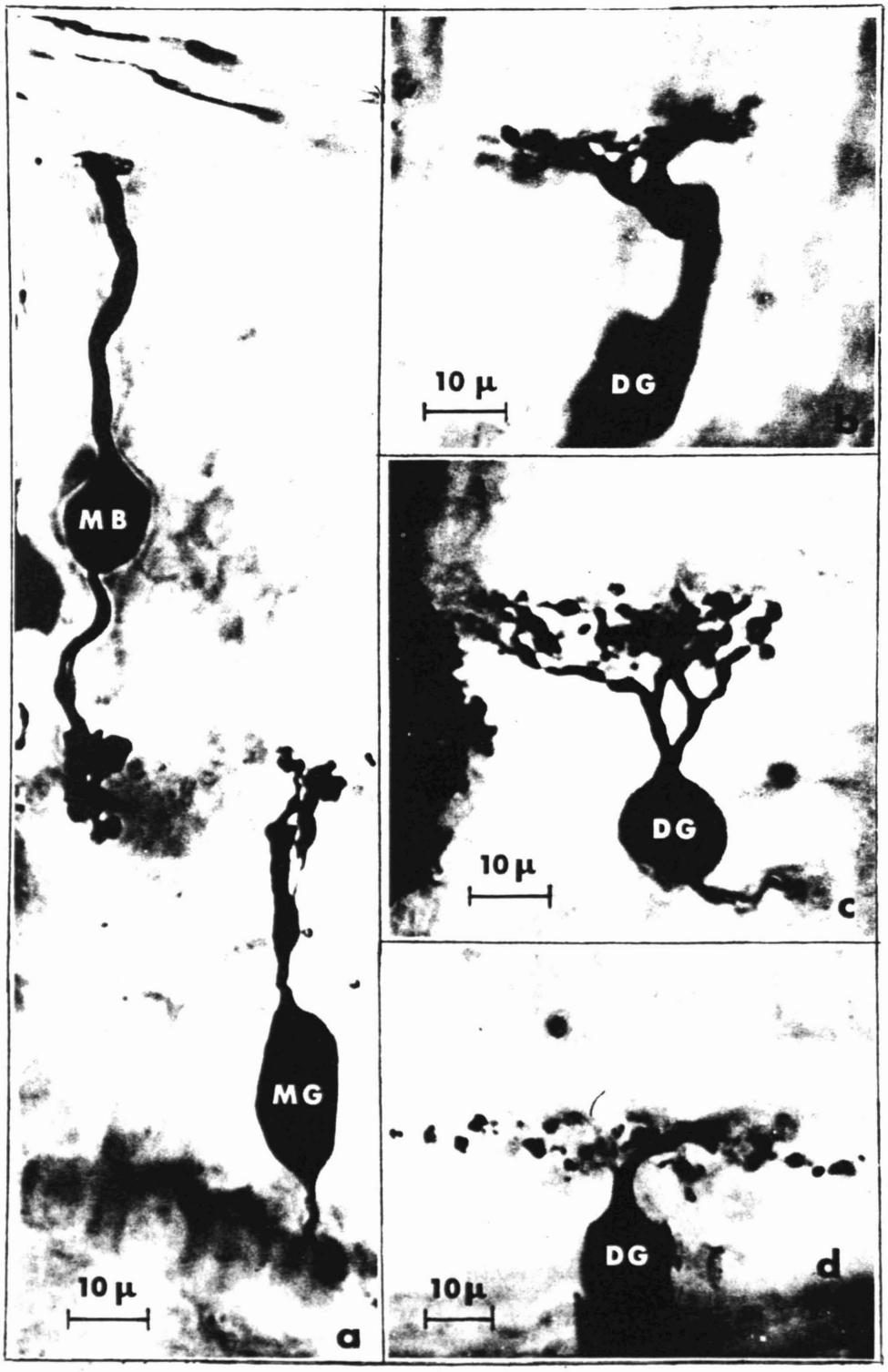

Figure 2-4: Typical diffuse and midget ganglion cells from the parafoveal region of the monkey retina. From Dowling and Boycott [15]. Abbreviations: (MB) midget bipolar; (MG) midget ganglion; (DG) diffuse ganglion.

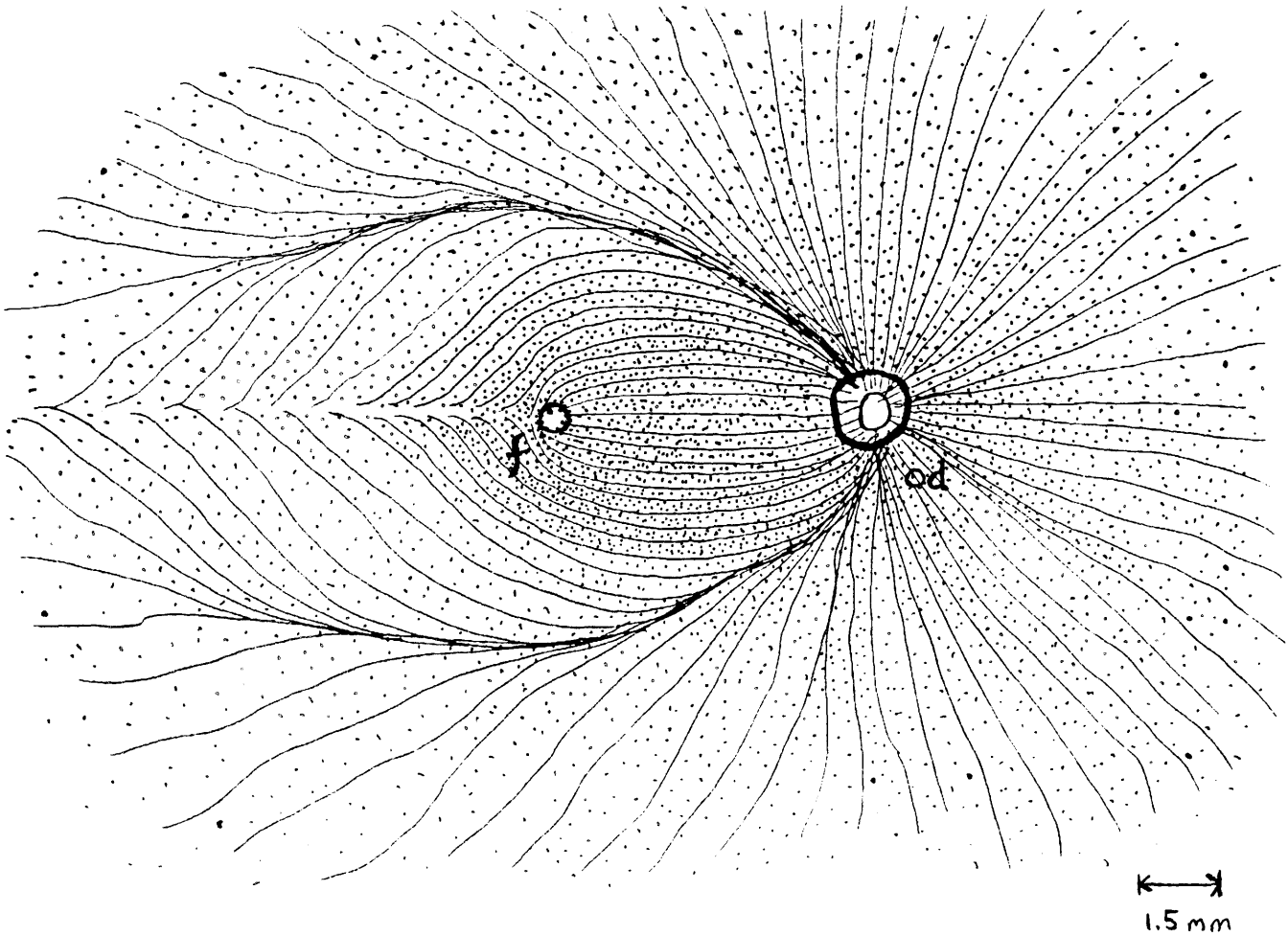

Figure 2-5: Distribution of retinal ganglion cell bodies (small dots) and axons (thin lines) in the human retina. Drawing by Dr. Joe Rizzo. Abbreviations: *f* - fovea; *od* - optic disk.

peripheral regions, physiological recordings from central and peripheral cells suggest that the same basic functional classes of cells exist throughout the retina. In the central retina, a small number of cells will converge upon a ganglion cell of a given type through its small dendritic field. In the peripheral retina, by contrast, a larger number of cells converge upon a ganglion cell of the same type through its large dendritic field.

2.1.3 Information processing in the retina

In the preceding description of retinal neurons, certain types of cells were subdivided according to their responses to small spots of light. This criterion distinguished, for example, the On-center ganglion cells from the Off-center cells. The fact that a given cell will respond preferentially to certain stimuli leads us to regard it as an information processing element, and by extension to think of the retina as an information processing system.

The input to this system is a spatial and temporal pattern of light entering the eye from the visual field. The output is a collection of ganglion cell responses, each a temporal pattern of action potentials conducted away from the retina by a single axon. Between input and output, as we have seen, is an alternating series of cellular and synaptic layers. Signal flow through these layers might be described in terms of *vertical* and *lateral* components. A signal propagating in the pure vertical direction traverses the cellular layers, from photoreceptors to bipolar cells to ganglion cells. A signal traveling in the pure lateral direction, on the other hand, propagates within a single cellular layer, either through networks of horizontal or amacrine cells. This section will focus both on observed characteristics of such input/output relationships and also on their related signal pathways within the retina.

Receptive fields and spatial sampling

While efforts are currently being made to record activity from several cells simultaneously [34], most studies of retinal input/output behavior have concentrated on individual cells. The basic experiments performed in these studies consisted of presenting various light stimuli to the retina while monitoring the behavior of a single cell with a recording electrode. These experiments revealed that light must fall on the retina within a restricted area, referred to as the *receptive field*, in order to influence a cell's behavior. Ganglion cell receptive fields in the cat retina were found to vary between 0.8mm and 2mm in diameter for centrally located cells[31]. In general, receptive fields become progressively larger with increasing eccentricity [49].

Because its receptive field is restricted, each ganglion cell is concerned with light emanating from the restricted area within the visual scene. Thus a spatial decomposition takes place in the retina whereby the visual field is parceled according to ganglion cell receptive fields. Receptive fields of adjacent ganglion cells may overlap, however, so that light impinging on any one region of the retina will produce output from many different ganglion cells.

Spatial sampling in ganglion cells originates at the photoreceptors. To a first approximation, the size of a photoreceptor's receptive field will be determined by the diameter of its outer segment[6]. Though photoreceptors and ganglion cells are alike in that both possess

with retinal eccentricity.

[6]Lateral interactions between photoreceptors will also contribute a given cell's receptive field, though the role of such interactions in retinal signal flow is not well understood [14].

receptive fields, it would be an oversimplification to assume a one-to-one correspondence between those of the photoreceptors those of the ganglion cells. In general, signals from many photoreceptors will converge on a single ganglion cell through a combination of vertical and lateral pathways.

The On and Off channels

On-center and Off-center ganglion cells were described briefly in section 2.1.1. Two important characteristics of On-center and Off-center responses are illustrated in Figure 2-6. First, the cells respond to both *temporal* and *spatial* variations in illumination. Temporal response properties are revealed by the middle trace of the Figure ("Center and surround illumination"), where illumination of the receptive field is spatially uniform: On-center cells are excited by temporal increases in illumination and inhibited by decreases, whereas Off-center cells are excited by temporal decreases in illumination and inhibited by increases. The top and bottom traces of the Figure ("Center stimulation" and "Surround stimulation", respectively) reveal spatial response properties: when more light falls on the receptive field center than on the surround, On-center cells respond vigorously and Off-center cells are inhibited; when less light falls on the center than on the surround, the responses are reversed. It should also be noted that certain types of cell responses are generated by both the spatial and temporal pattern of a stimulus. For example, On-center Y cells (see below) are maximally excited at the onset of center stimulation (not shown in the Figure). The second important characteristic is the antagonistic, center/surround receptive field organization exhibited by On-center and Off-center cells. As revealed in Figure 2-6, both excitatory and inhibitory effects are most pronounced when illumination is restricted to either the receptive field center (top trace) or the surround (bottom trace).

Both the On/Off dichotomy and the antagonistic center/surround receptive field organization arise at the level of bipolar cells. The receptive field organization, as discussed in section 2.1.1, is thought to stem from opposing influences produced in the bipolar cell by photoreceptors and horizontal cells. Direct interactions between photoreceptors and bipolar cells produce a center response, while the surround response is mediated by horizontal cells. As for the On/Off dichotomy, recall that On-center and Off-center cone bipolar cells are distinguished by the polarity of potential they produce in response to illumination of the retina. On-center cells depolarize to illumination of their receptive field centers, while Off-center cells hyperpolarize. By contrast, photoreceptors and horizontal cells only hyperpolarize.

It is initially mysterious in light of these facts that cone bipolar and ganglion cells produce both hyperpolarizing and depolarizing potentials. The single polarity to double polarity conversion which takes place in the retina is due in part to two mechanisms. First, it has a pharmacological basis: though photoreceptors are believed to use a single type of neurotransmitter [54], the On-center and Off-center bipolars differ in the type of neurotransmitter receptor found in their dendritic membranes [62]. Second, anatomical evidence suggests that the conversion may be carried out within the rod pathway as well. While rod bipolar cells are thought to only produce depolarizations, these cells terminate mostly on the AII type amacrine cell. AII amacrine cells make inhibitory or hyperpolarizing synapses onto Off-center cone bipolar and ganglion cells, but make excitatory or depolarizing gap junctions with On-center cone bipolars [62].

It has been argued that the On-center and Off-center ganglion cells operate within two distinct and independent information processing channels[54]. Three lines of evidence support this claim. First, the dendrites of the On-center and Off-center ganglion cells

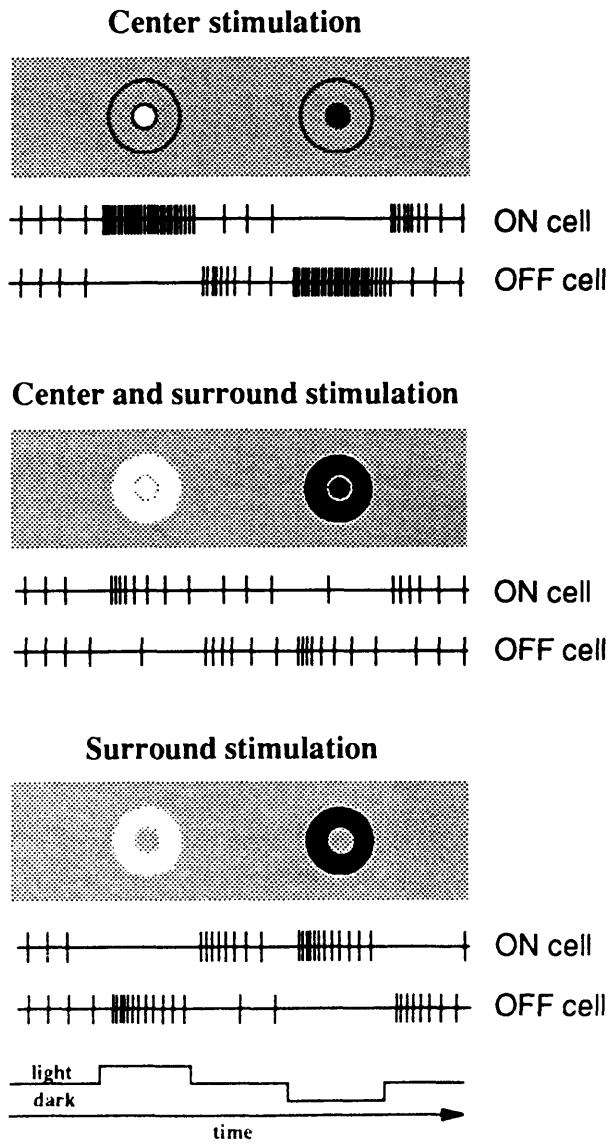

Figure 2-6: Idealized responses of On-center and Off-center ganglion cells. From Schiller [54].

stratify in different sublayers of the inner plexiform layer. Within these sublayers, it has been shown that the On-center and Off-center dendrites are each regularly arrayed so as to provide complete coverage of the retina [62]. In theory, either type of cell should be able to respond to light falling anywhere on the retina. Second, studies with the neurotransmitter analogue 2-amino-4-phosphonobutyrate (APB) have shown that blockage of On-center cone bipolar cells does not interfere with normal Off-center responses [54]. This fact indicates that center/surround antagonism is produced independently in the two channels, rather than through their interaction with one another. The third line of evidence comes from behavioral studies with APB. Under photopic conditions (where the cones are most active) intra-ocular APB injections in experimental animals led to difficulty in detecting bright-spot illumination, but did not effect performance in detection of dark spots [54]. Since only the ON channel is blocked by APB, these results are in agreement with the notion that the ON channel is sensitive to incremental light stimuli, while the OFF channel is sensitive to decremental stimuli.

The color-opponent and broad-band channels

Another classification scheme for ganglion cells has emerged from studies of chromatic responses. Color-opponent cells have small, color-specific receptive fields, while broad-band cells have large, color-insensitive fields. These two types of cells differ in several additional respects as well. The color-opponent ganglion cells have β morphology (see section 2.1.1), project their medium conduction velocity axons to the four parvocellular layers of the lateral geniculate nucleus of the thalamus (LGN), and respond to illumination of retina in a sustained fashion. The broad-band cells have α morphology, project their fast conduction velocity axons to the two magnocellular layers of the LGN, and respond transiently to visual stimuli [55].

Like the On-center and Off-center cells, both types of cells have antagonistic center/surround receptive field organization. A color-opponent cell might respond preferentially to illumination of its receptive field center with red light, for example, while a broad-band cell would respond identically to center illumination of various visible frequencies. The surround of color-opponent cells is not color-specific, so that in both cases, center responses would be reduced by any illumination of the surround.

The origins of the antagonistic center/surround receptive field organization were considered above in the discussion of the On and Off information processing channels. The underlying anatomy responsible for color-opponent responses is now considered. Recall from the discussion of photoreceptors (section 2.1.1) that the cones are sensitive to the different wavelengths of the visual light spectrum. Humans and many other species have three types of cones, which absorb maximally in the red, green and blue regions of the spectrum [14]. In the fovea, it is believed that midget ganglion cells connect via midget bipolar cells to a single cone [62]. This singular connection is probably responsible for color-specific receptive field centers of the color-opponent cells. The color-insensitive surrounds of the color-opponent cells are likely to receive input from all three cone types [55].

The characteristics of the color-opponent and broad-band ganglion cells lead us to think of them as parts of two distinct and independent information processing channels, much as in the case of the On-center and Off-center cells. The color-opponent channel plays a central role in color vision and perception of fine spatial detail, while the broad-band channel is concerned with mainly with perception of motion, low-contrast stimuli, and night vision when only the rods are active [55]. It must be noted that the color-opponent and broad-band

channels, while distinct from one another, are not distinct from the On and Off channels. In the midget system of the primate central retina, for example, there are On and Off systems for each of the three cone types [54]. Under these functional schemes, an On-center, broad-band cell would respond transiently to illumination of its receptive field center, unlike the "ON cell" of Figure 2-6.

Other ganglion cell groupings

X and Y

From studies of the cat retina comes a retinal ganglion cell classification scheme known as X/Y. The X/Y distinction was originally made on the basis of the cells' responses to changes in luminance across their receptive fields. While cells of both types exhibit On-center and Off-center responses, they differ substantially when a sinewave grating is overlayed such that the transition between bright and dark bars is centered over the receptive field. Since the two sides of the receptive field receive equal and opposite amounts of light, the net luminance across the field is zero. An X cell does not respond to this type of stimulus, and is considered to be "linear" because its lack of response reflects the (zero) sum of the light intensities. By contrast, a Y cell responds in a transient fashion to the same stimulus, and is therefore described as "nonlinear".

Substantial parallels exist between the cat Y and X cells and the broad-band and color-opponent cells, respectively. The receptive field centers of the Y cells generally larger than those of the X cells. Like the broad-band cells, the Y cells have the fastest conduction velocity. Like the midget cells of the primate retina, the cat X cells are relatively frequently encountered in the central area. Y cells have α morphology as do the broad-band cells, and the X cells have β morphology as do the color-opponent cells. Furthermore, Y cells have transient or *phasic* responses, while X cells have sustained or *tonic* responses.

Direction-sensitive cells

Many of the On-Off ganglion cells found in rabbit, turtle and other retinas show direction-sensitive or DS responses. These cells respond most strongly to spots of light moving through their receptive fields in a particular direction, the *preferred* direction, and either don't respond to or are inhibited by a spot moving in the opposite or *null* direction [14]. It has been suggested that DS responses are the result of an asymmetric wiring at the level of amacrine cell dendrites which includes a time delay between excitatory and inhibitory inputs to ganglion cells [62].

Spatial processing, temporal processing, and the plexiform layers

In section 2.1.1, it was suggested that ganglion cell responses strongly reflect two distinct types of input. Ganglion cells responding in a sustained fashion and having antagonistic center/surround receptive field organization are thought to receive their input primarily from bipolar cells. The bipolar cells receive their input from the outer plexiform layer, and are concerned primarily with spatial relationships. Ganglion cells responding in a transient fashion to the onset and cessation of light (On-Off) are thought to receive input primarily from the amacrine cells. Amacrine cells receive their input from the inner plexiform layer, and are concerned primarily with temporal relationships. Thus, there appear to be two basic types of information processing carried out in the retina, a spatial type performed in the outer plexiform layer and a temporal type performed in the inner plexiform layer [14].

Not all ganglion cells fit neatly into one of these categories. An On-center Y cell, for example, has antagonistic center/surround receptive field organization, but responds transiently to illumination of its receptive field center. In the present scheme, these cells might be conceived of as reflecting a combination of outer plexiform and inner plexiform layer processing. Other cells such the DS cells are not so easily explained. DS cells perform a spatial and temporal analysis which is thought to be carried out entirely within the inner plexiform layer by amacrine cells.

2.2 The retinal implant

This section provides the motivation for and a description of an epi-retinal prosthesis which is being developed to aid patients suffering from certain forms of blindness. The background material provided in the previous section will explain both the causes of certain forms of blindness and also how the prosthesis is designed to aid such patients.

2.2.1 Motivation

The retinal implant targets patients who develop blindness secondary to loss of outer retinal function from diseases such as *retinitis pigmentosa* (RP) and *age-related macular degeneration* (AMD). Retinitis pigmentosa is a group of diseases caused by gene abnormalities on one of several chromosomes. About 1 in 4000 develop this hereditary disorder which affects an estimated 1.5 million worldwide. Early symptoms of RP include impaired adaptation to light, night blindness, and difficulty with the mid-peripheral visual field. Eventually, visual loss extends to the central and far-peripheral regions [3, 40]. Well over a million people worldwide are affected each year by a second disease, age-related macular degeneration [49]. At least 10% of the U.S. population in the 65-75 age group have lost some central vision from AMD, and the incidence rises in the older age groups [65]. As the world population ages due to improvements in health care, these numbers are bound to increase. Blindness associated with AMD is attributed to degeneration of the photoreceptors, which might be a secondary result of prior degenerative changes in the retinal pigment epithelium. AMD strikes the macula and therefore impairs the regions of highest visual acuity [65].

A third circumstance which may lead to loss of outer retinal function is infrared laser photocoagulation. Using a diode semiconductor laser delivering energy in the 810nm range, it was found that mild burns could be obtained in rabbit eyes which damaged the outer retina and choroid, but spared the inner retinal cells [5, 57].

Only photoreceptors transduce light (section 2.1.1). A patient who suffers the loss of photoreceptor function will not be able to see because his/her retina can no longer perform this transduction. Would it be possible to perform light transduction artificially, and then introduce the artificially generated visual signals into a healthy region of the visual system?

It is well known that responses can be elicited from living nerve cells through the application of an electric current. Furthermore, semiconductor devices which transduce optical signals to electrical signals are readily available. Based on these two facts, we believe that the answer to the above question - at least from a *functional* point of view - is "yes". The task of artificial light transduction is conceived of as channeling optical signals through an electrical system which stimulates visual system nerve cells. A block diagram representation of such a system is illustrated in Figure 2-7.

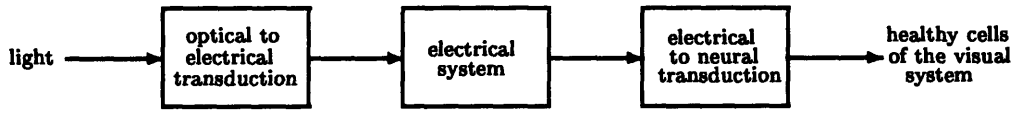

Figure 2-7: Block diagram of an artificial light transduction system.

2.2.2 Description and selected design issues

The retinal implant is currently being developed to accomplish the functions outlined in Figure 2-7. Light from the visual field will be transduced to electrical signals outside of the eye, perhaps by a device which has been mounted on a pair of spectacles (see Figure 2-8). The first stage of the electrical system will transmit information about the visual field to a second stage which has been surgically implanted inside the eye, against the inner margin of the retina. There, the second stage of the electrical system will drive an array of stimulating electrodes, thus providing the electrical to neural transduction.

The choices that have been made to arrive at the current design will not be discussed in this thesis. However, two significant design issues regarding the choice of retinal cells as the stimulation site will be raised. The first regards the health of the retinal cells in the diseases RP and AMD. Nervous system cells may die in the absence of synaptic input through a process known as *transneuronal degeneration*. The horizontal, bipolar, amacrine, interplexiform, and ganglion cells of a retina which has lost photoreceptor function probably receive little or no synaptic input, making them susceptible to this degenerative process. Of particular concern is the health of the ganglion cells. Since the ganglion cells provide the retina's output through their axons, it will be impossible to perform a successful electrical to neural transduction within the retina if these cells degenerate. There is some evidence to support that live ganglion cells may still be found in retinas which have lost photoreceptor function. In a histological study where ganglion cell counts in retinas with RP were compared with those of healthy retinas, it was found that RP patients retain on the order of 50% to 75% of the normal number of cells[60]. This study indicates that ganglion cells are present, albeit in subnormal quantities, in retinas with RP. A second study indicates that the cells are alive and functioning: alert patients with end-stage RP described having sensations of light when current was injected through a bipolar electrode located near the inner retinal surface [25]. As a final note, there appear to be no specific reports describing damage to the ganglion cell layer in the so-called "standard" form of AMD [49].

The second important design issue concerns the psychophysical effects of electrical stimulation of retinal cells. What will a patient perceive when the cells of his/her retina are stimulated? Recall from section 2.1.3 that, due its restricted receptive field, each cell is concerned with a restricted part of the visual scene. We hypothesize that when a retinal cell is stimulated electrically, the brain will perceive that light was present in the part of the visual field with which that cell is concerned. Furthermore, if another cell some small distance away from the first cell is stimulated, there should be a corresponding shift in the location of the perceived light. Based on these hypotheses, we hope to create intelligible

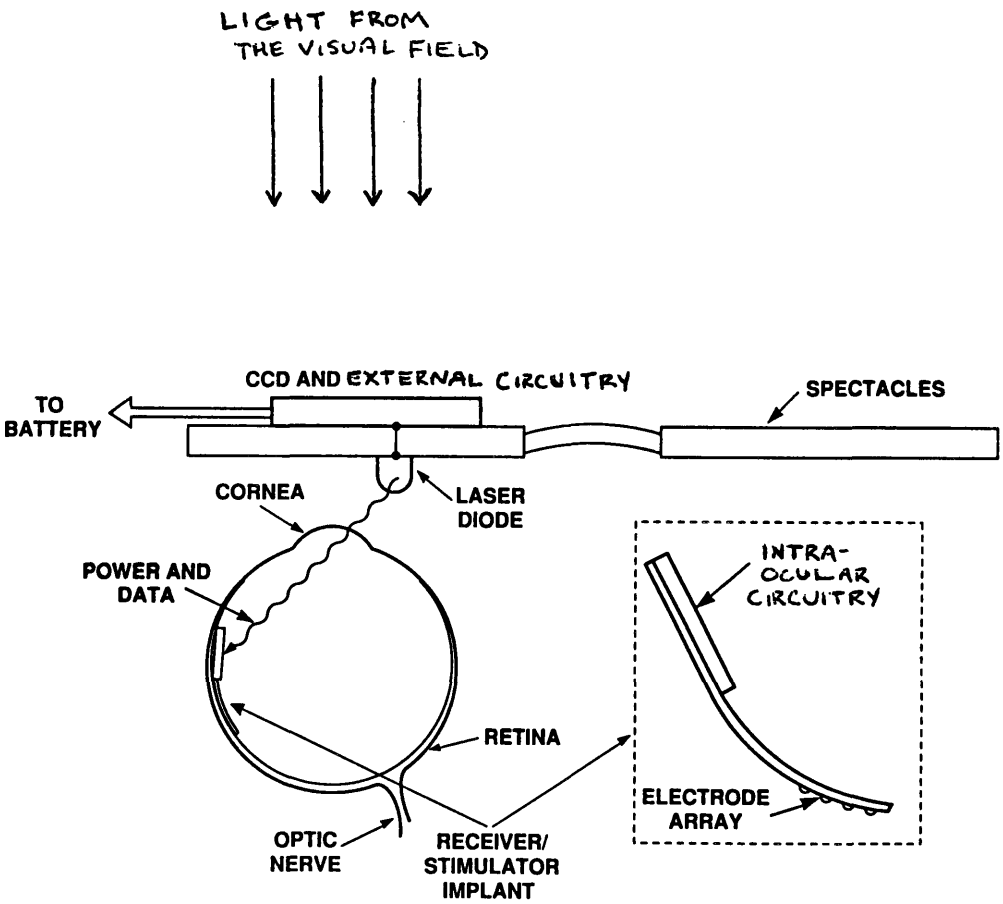

Figure 2-8: Schematic diagram of the retinal implant system. Incoming light is transduced to electricity by a charge-coupled device (CCD) located outside of the eye. Information about the visual field is transmitted into the eye by a laser diode. Inside the eye, the laser diode signals are decoded by a circuit which drives an array of stimulating electrodes.

visual perceptions by using a regularly arrayed group of electrodes to stimulate retinal cells in a pixel-like fashion. For example, if the patient is to perceive a square, we will try to stimulate cells along the borders of an imaginary square which has been projected onto the retinal surface (see Figure 2-9). As we will see below, a substantial challenge to this approach has arisen.

2.3 Electrical stimulation of retinal cells

The development of a successful retinal prosthesis entails several lines of inquiry spanning a broad range of research interests. This thesis is concerned with the electrical to neural transduction depicted in Figure 2-7, which will be accomplished through electrical stimulation of the retinal cells. A review of the work which has been done in this area will help to both motivate and formulate the central problem of the thesis.

2.3.1 Previous work

The literature to date on electrical stimulation of retinal cells reveals a substantial and diverse body of work. An overview of the work is provided below, followed by a summary of the work which is of greatest relevance to this thesis.

Overview

A number of investigators have employed electrical techniques to study aspects of visual system function [10, 11, 13, 18, 19, 20, 35, 36, 37, 39]. These studies were often motivated by the fact that, from a functional point of view, electrical stimulation represents a novel mode of input to the visual system. For example, while visible light necessarily enters the system at the photoreceptor level, electrical currents might act on any of the retinal neurons and possibly on cortical neurons as well. Related studies were devoted explicitly to determining where electrical inputs occur [6, 23, 29, 30, 43, 44]. Since a cell which has been excited by an electrical stimulus will in turn excite other cells through conventional neural pathways, some care must be used when describing the nature of cellular responses. The cells at which such responses originate are said to be stimulated *directly*. A third line of inquiry concerns electrical stimulation of the inner retinal surface elements [2, 24, 25, 26, 38, 64]. These studies have been conducted in efforts to characterize retinal responses to stimulation by an implanted device such as the one depicted in Figure 2-8.

The methods used in the electrical stimulation studies vary considerably. Stimuli were usually delivered using one of three basic configurations. In the first configuration, electrical currents were channeled into the retinas of subjects through electrodes which had been placed outside of the eye (Figure 2-10) [6, 18, 19, 20, 23, 37, 43, 44]. This configuration was the least invasive of the three and was used in many cases on alert human subjects. The second configuration, which has been used to produce current flow perpendicular to the retinal surface, places one electrode inside of the eye and the other outside [10, 11, 29, 30, 35, 36, 39]. For *in vitro* studies, the extraocular electrode was placed off to one side of the eyecup, as depicted in Figure 2-11a. For *in vivo* studies, the extraocular electrode was placed directly behind the eye. In the third configuration, either a monopolar [2, 26, 64] or bipolar [2, 13, 24, 25, 26, 38] electrode was placed at the inner margin of the retina. Stimulating currents delivered using this configuration were thought to be concentrated at the retina's inner surface. An example of this configuration is shown in Figure 2-11b.

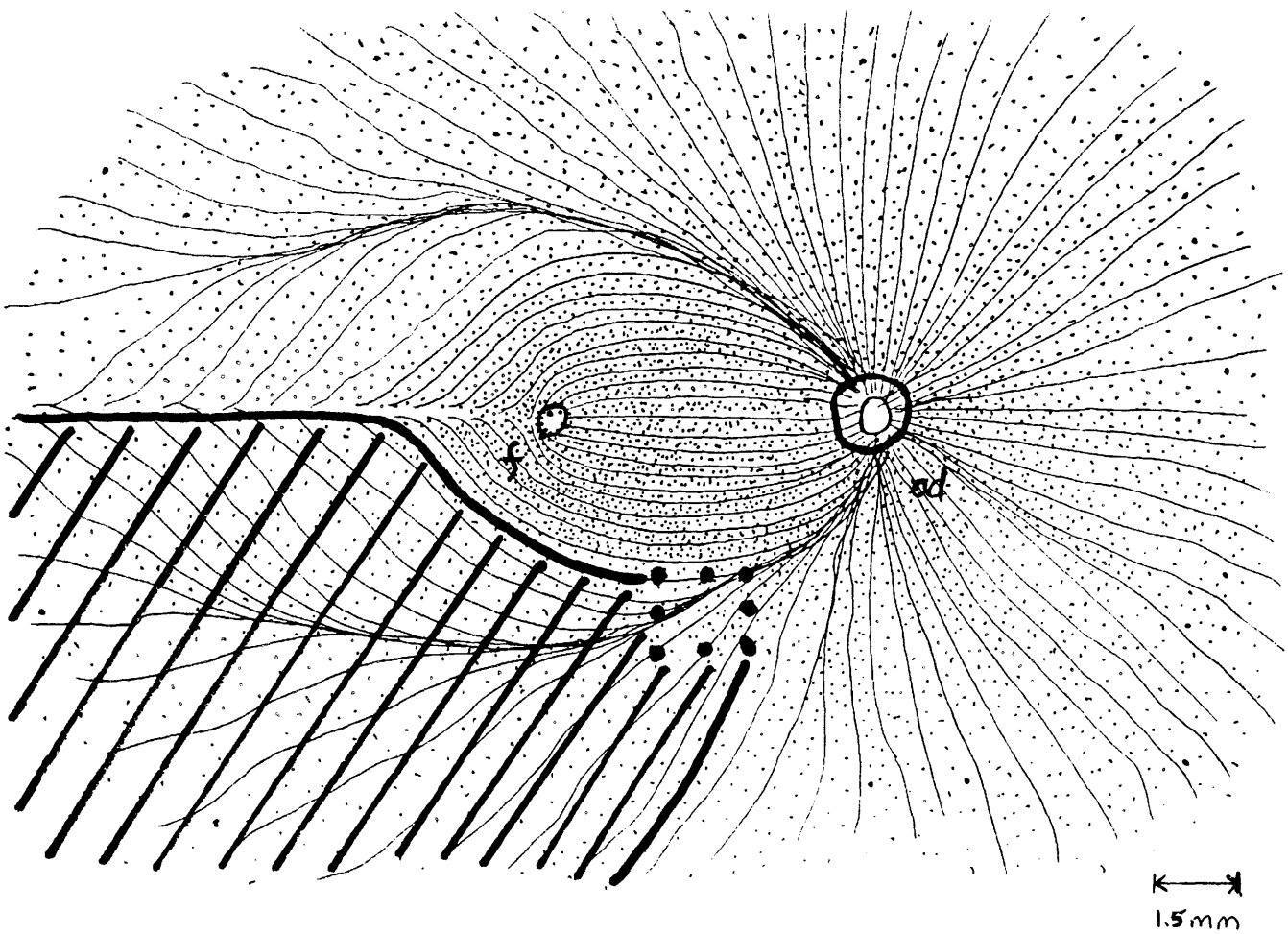

Figure 2-9: To create the impression of a square, we will try to stimulate cells along the borders of the square using a subset of the implant electrodes (large dots). If more peripheral cells are stimulated as well (shaded area), the resulting perception may considerably distorted.

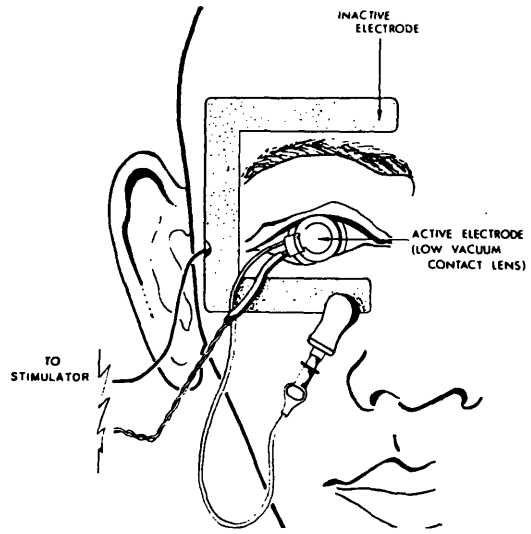

(a)

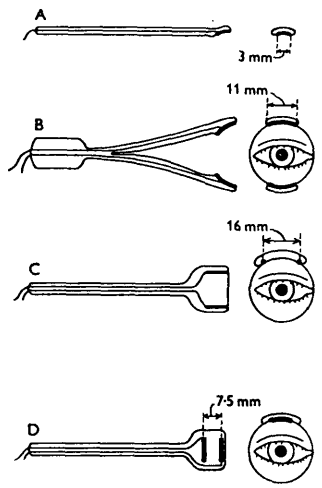

(b)

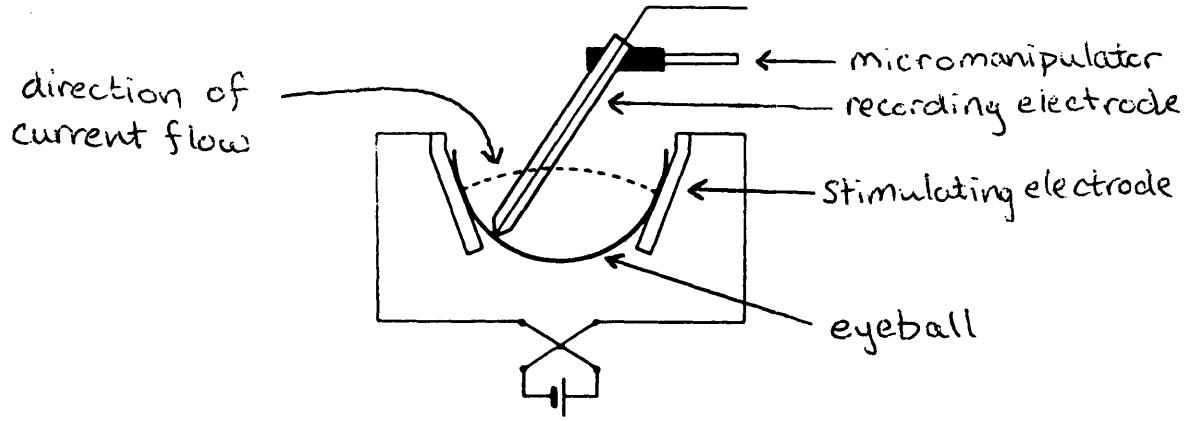

(c)

Figure 2-10: Configurations for electrical stimuli delivered outside of the eye. (a) One pole of the electrode is mounted on a contact lens and placed against the cornea, while the other contacts a large area around the eye. From Potts *et. al.* [44]; (b) Several types of electrodes designed to be placed under the eyelids, against the conjunctiva. From Brindley [6]; (c) Schematic of silver-silver chloride wires placed on opposite sides of the cat eyeball *in vivo.* From Granit [20].

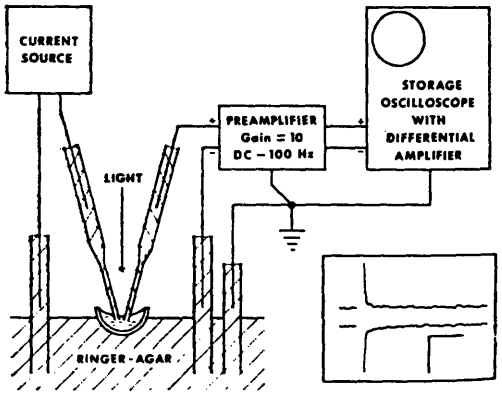

(a)

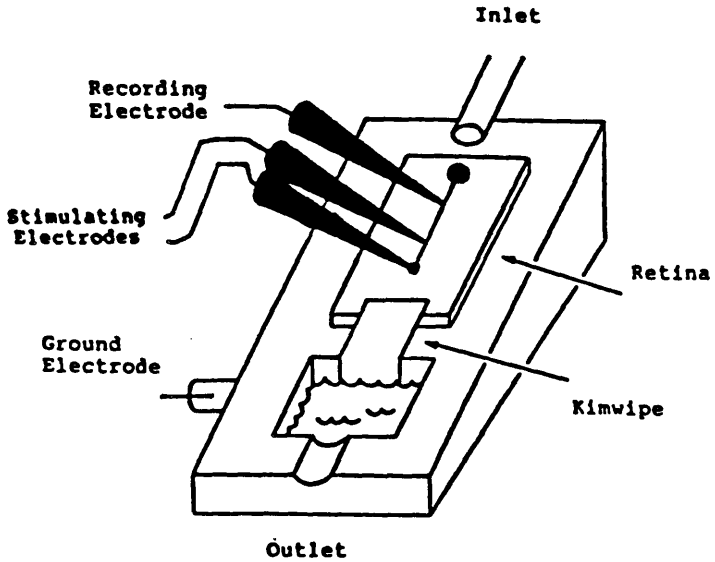

(b)

Figure 2-11: Configurations for electrical stimuli delivered (a) transretinally and (b) to the inner surface of the retina. (a) Current flows between an electrode pole placed in the vitreal cavity of a frog eyecup and an extraocular pole. From Knighton [29]; (b) Current flows between the two poles at the inner surface of the retina. From Jensen [26].

Visual system responses to electrical stimulation were measured in several ways. Some investigators have used visual sensations called *phosphenes*, which may be elicited by delivering electricity to points on the body located inside of or near the eyes, to gauge the effect of stimuli [6, 23, 25, 37]. Central to the phosphene studies is the use of human subjects who can describe the sensation and be easily trained to detect it. A perhaps more flexible and objective method which has been used by other investigators involves recording bioelectrical potentials at the surface of the scalp or cortex in response to electrical stimuli [11, 13, 38, 43, 44]. Brain potentials, however, indicate the gross behavior of a population of neurons and reveal little about interactions at the cellular level. Responses of individual nerve cells have been recorded by a third group of investigators through the use of microelectrodes [10, 18, 19, 20, 26, 35, 36, 64]. Less common forms of visual system response which have been recorded include intraocular potentials in an eyecup preparation [29, 30], potentials at the inner retinal surface [24], intraretinal potentials [39], and potentials at the optic nerve [2].

Summary of relevant work

The site of origin of electrically evoked visual system responses appears to depend strongly on the stimulus configuration used. While transretinal currents seem to stimulate the photoreceptors directly [29], currents applied to the outside of the eye as in Figure 2-10a were thought to stimulate elements proximal to the photoreceptors [43]. Furthermore, while currents applied to the retinal surface stimulate ganglion cell axons directly [2, 26], currents applied using the electrodes of Figure 2-10b do not [6]. In order to avoid ambiguities in the mode of action of applied currents, we will focus on those studies in which electrical stimuli were concentrated at the inner retinal surface [2, 13, 24, 25, 26, 38, 64], as will be those delivered by the retinal implant.

Even within this smaller group of studies, substantial variations in experimental methods are found. In general, three types of stimulating electrodes were used. Bipolar electrodes, illustrated schematically in Figures 2-12a and 2-12b, create more concentrated or *focal* patterns of stimulus current than the monopolar type shown in Figure 2-12c. Also, two distinct types of stimulus waveforms were used. Biphasic waveforms such as those depicted in Figure 2-13b produce less damage to neural tissue and to electrodes than monophasic waveforms such as those of Figure 2-13a [24]. Finally, neural responses were measured either from individual ganglion cells, from a population of cells at the inner retinal surface, from the optic nerve, from the cortex, or in the form of phosphenes. A summary of stimulus and recording parameters used in the studies relevant to this work is provided in Table 2.1.

In spite of the diversity of methods used, two general themes emerge from the studies summarized in Table 2.1. First, all concluded that neural responses to stimulation originated at the inner retina. In such cases, ganglion cells may have been stimulated either directly or as an indirect result of amacrine or bipolar cell stimulation. This result provides support for the basic premise of the retinal implant work, that an array of surface-residing stimulating electrodes such as that depicted in Figure 2-8 may be used to stimulate inner retinal cells. Second, cells close to the stimulating electrode were more likely to be stimulated than cells further away. This supports the notion (presented in section 2.2.2) that intelligible visual perceptions might be created by stimulating the patient's inner retinal cells in a pixel-like fashion. To create the impression of a square, for example, stimulating current might be delivered to a subset of the implant electrodes bordering the square. This situation is depicted schematically in Figure 2-9. If a suitable amount of current is applied, ganglion

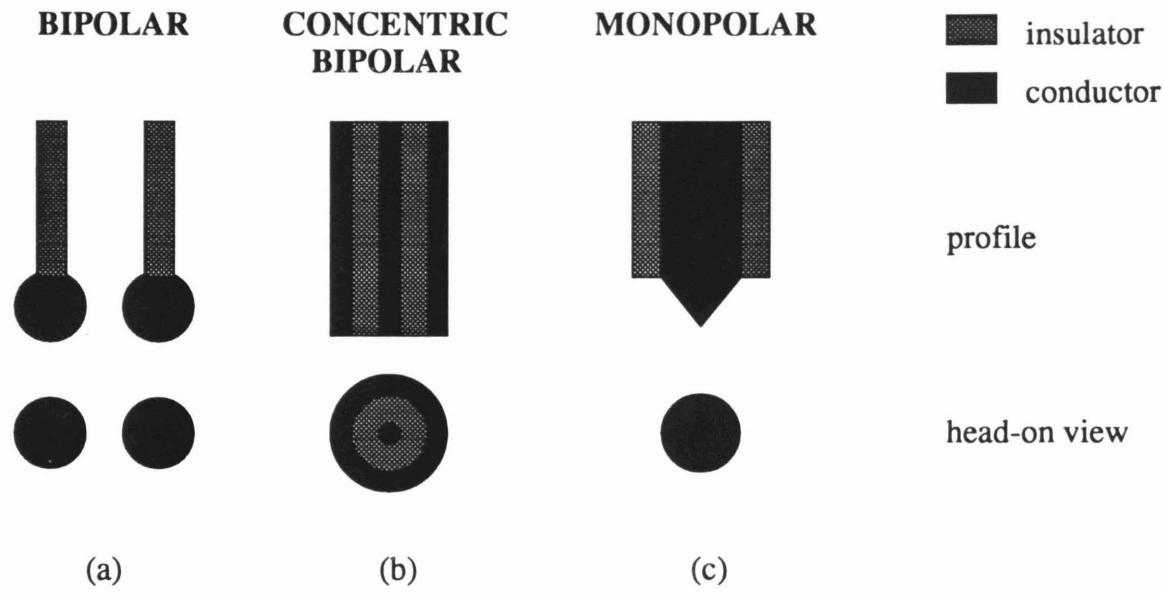

Figure 2-12: Schematic diagram of electrodes used for stimulation of the inner retina. (a) Bipolar electrodes; (b) Concentric bipolar electrodes; (c) monopolar electrode. Electrodes are not drawn to scale.

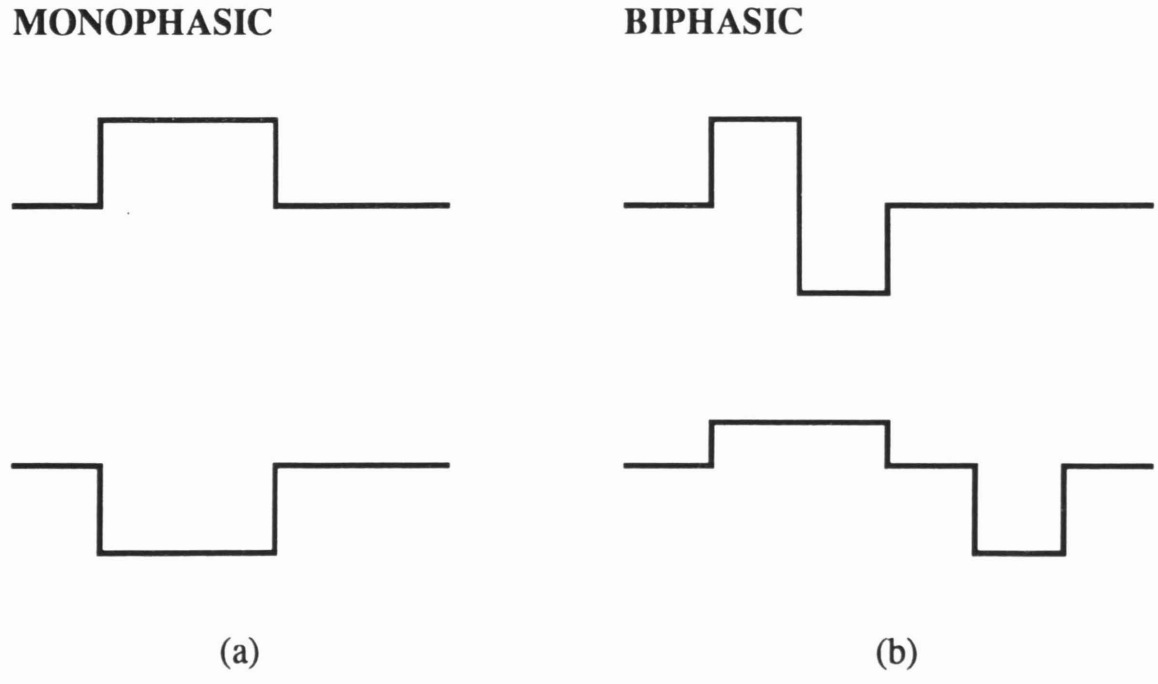

Figure 2-13: Examples of monophasic (a) and biphasic stimulus waveforms. These waveforms represent voltages or currents established across the two poles of a bipolar electrode, or between a monopolar electrode and a return pole which is very far away.

Author(s)	Electrode Type	Stimulus Waveform	Stimulus Duration	Stimulus Amplitude	Recording Site
Benjamin *et. al.* [2]	bipolar	mono- and biphasic	400μs per phase	up to 2mA	optic nerve
Doty & Grimm [13]	bipolar	monophasic	0.1ms or 1ms	1V to 15V	cortex
Humayun *et. al.* [25]	bipolar	monophasic	75μs	up to 100μA	phosphene
Humayun *et. al.* [24]	bipolar	biphasic	75μs per phase	50-300μA (half phase)	retinal surface
Narayanan*et. al.* [38]	bipolar	biphasic	400μs or 700μs total	30-600μA	cortex
Jensen [26]	concentric bipolar	monophasic	200μs	0.4-400μA	single cell
Wyatt *et. al.* [64]	monopolar	monophasic	20-500μs	8-24μA	single cell

Table 2.1: Summary of stimulus and recording parameters which successfully evoked visual system responses when electrodes were placed against the inner retinal surface.

cell bodies in the vicinity of each electrode will be stimulated either directly or indirectly. Because ganglion cells have restricted receptive fields centered approximately over their cell bodies [31, 26], the resulting perception might correspond to the pattern of stimulating electrodes used. That is, the patient might see spots of light bordering a square.

However, the electrodes might also be stimulating ganglion cell axons, which overlie the cell bodies at the innermost portion of the retina (see Figure 2-3). Were this the case, we hypothesize that the the brain would interpret incoming nerve messages from the stimulated axons as if they had originated at their peripherally located cell bodies. As depicted in Figure 2-9, we might expect the resulting sensation to be "referred back" to a more diffuse portion of the visual field than originally expected, corresponding to the receptive fields of the more peripheral cell bodies.

To determine the likelihood of this phenomena, a series of experiments were conducted to compare the threshold amounts of current needed to stimulate ganglion cell bodies and axons. When a stimulating electrode was placed over the center of a ganglion cell's receptive field, measurements were believed to represent thresholds for stimulating ganglion cell bodies, whereas when the electrode was positioned between the receptive field center and the optic disk, measurements were taken to represent axon thresholds. In these experiments, cell body and axon thresholds typically fell within the same range [26, 64]. It would appear from this result that ganglion cell bodies and axons in the vicinity of a stimulating electrode are equally likely to be excited.

2.3.2 Thesis problem revisited

The above discussion suggests that a more careful approach must be taken to extracellular stimulation of retinal cells if the retinal implant is to be used to produce well-defined

phosphenes. In order to achieve this goal, we believe it will be necessary to selectively stimulate retinal ganglion cells at or near the cell body without affecting the overlying axons. It is evident from Table 2.1 that a number of stimulation parameters might be varied in order to achieve selective stimulation. This thesis attempts to address the problem through the design of a novel, non-radially symmetric electrode geometry.

Chapter 3

Theory of Extracellular Electrical Stimulation

In Chapter 2, a functional description of the retinal implant was given. Central to the implant's function is the task of creating action potentials in ganglion cell bodies where the retinal circuitry has failed to do so. The purpose of this chapter is to investigate a general theory of how such a task is accomplished.

Definition of terms

When an action potential is created in a nerve cell, the cell is said to be *stimulated.* Nerve cells in living organisms may be stimulated by electrical, mechanical, or chemical means, depending on the particular cell type. *Electrical stimulation* of many types of cells may be performed by applying an electrical current inside or near the cells. If current is applied directly to the inside of a cell and an action potential is generated as a result, the cell is stimulated *intracellularly* (see Figure 3-1a). If the stimulating current is applied outside of a cell, as in Figure 3-1b, the cell is stimulated *extracellularly.*

The retinal implant will use electrical current to stimulate ganglion cells in the retina. For a variety of reasons, the implant electrodes will not penetrate the retinal cells. Therefore, the retinal implant's mode of operation is *extracellular electrical stimulation.*

Previous work

A number of papers have been written on extracellular electrical stimulation. Broadly speaking, research in the field has been either experimentally or analytically motivated. Research of the first type has generally involved experiments performed on real nerve cells to test or formulate qualitative theories which describe how the cells were stimulated. A useful summary of the data and theories emanating from such research is given by Ranck[46]. Research of the second type is more mathematical and abstract. Models of nerve cells have been constructed based on some particular set of assumptions about cell shape, membrane structure, and environment. Due to the many assumptions that must be made to simplify analysis, few attempts have been made at finding quantitative correspondences between theory and experiment[48, 51, 53]. For the most part, analyses have been matched qualitatively to familiar trends in extracellular electrical stimulation experiments, or have predicted phenomena which remain untested[8, 33, 41, 52, 47, 61].

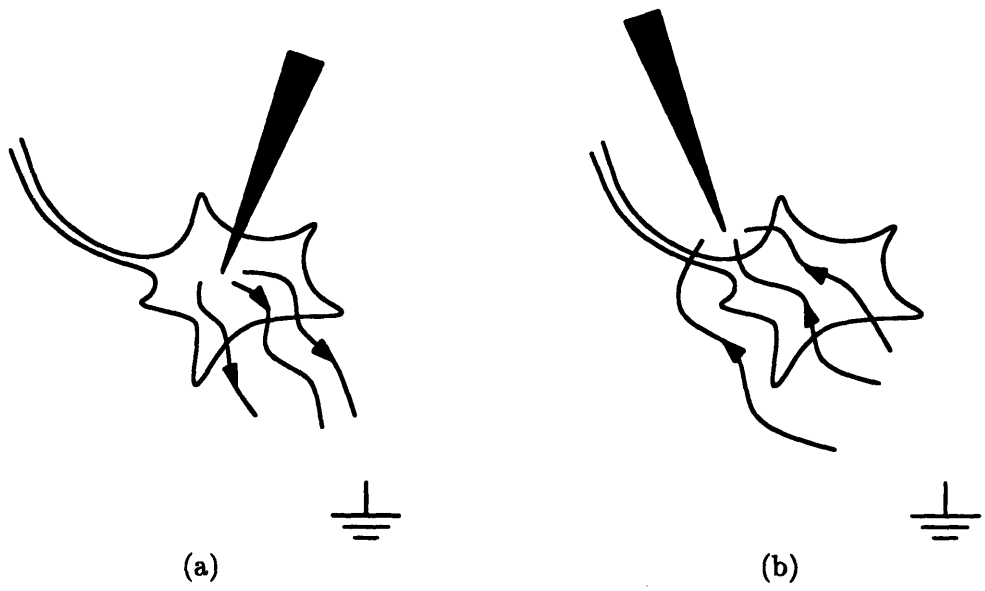

Figure 3-1: (a) Schematic of intracellular stimulation of a cell; (b) Schematic of extracellular stimulation of a cell.

The work of the analytical literature is divided into two parts based on morphological considerations. While the typically bulbous cell body of a nerve cell has been modeled as a perfect sphere, the shaft-like axon has been modeled as a right circular cylinder. To my knowledge, dendrites have not been modeled for extracellular electrical stimulation problems. Spherical cell body models and cylindrical axon models have been analyzed in isolation in order to simplify the math. That is, axon models have been analyzed in the absence of a cell body, and cell body models have been analyzed in the absence of an axon. For reasons that will become clear later in the chapter, analyses of axon models have concentrated on the effects of longitudinal variations in electric potential and largely ignored transverse effects. The analytical methods which have been used to study longitudinal effects in axons and to study cell bodies are now briefly considered.

A general method for analyzing the effects of variations in electric potential along an axon's length is the procedure used by McNeal[33]. The first step of McNeal's method is to calculate the potentials created in the extracellular space by a specified electrode configuration. A familiar configuration is the monopolar spherical geometry. The extracellular medium is commonly assumed to be a uniform, linear, and isotropic conductor of infinite extent. Due to its relatively small size, the axon model is assumed to have negligible effect on the electrode-induced potentials, and is usually ignored during this step. For relatively simple models based on the assumptions described above, closed-form solutions for the extracellular potentials have been found. For more complex models, numerical simulations could be employed to find the extracellular potentials.

Once the electrode-induced potentials are known, an axon model must be chosen. All such models rely on the basic set of assumptions listed in Table 3.1. Implicit in assumptions 2 and 5 is the notion that the electric field creates a radially symmetric equipotential region outside of the axon model at a given position along its length. For most electrode configurations, this will not be strictly true. However, it has been demonstrated by McNeal

1. The cell membrane is a cylindrical boundary that surrounds a conductor of electrical current, the intracellular solution, which is assumed to be homogeneous, isotropic, and obey Ohm's law.
2. All the electric variables have cylindrical symmetry.
3. A circuit theory description of currents and voltages is adequate. That is, the quasi-static terms of Maxwell's equations are sufficient, and electromagnetic radiation effects are negligible.
4. Current flows through the inner conductor in the longitudinal direction only. Current flows through the membrane in the radial direction only.
5. At a given longitudinal position along the axon, the inner conductor and external surface of the axonal membrane are equipotentials, so that the only variation in potential occurs in the radial direction, across the membrane.

Table 3.1: Basic assumptions for analyzing longitudinal effects in axons; adapted from [63].

that the effects of transverse variations in extracellular potential were vastly smaller to those of variations in potential along the axon's length[33]. This fact will also be demonstrated later in the chapter.

In addition to the general assumptions listed in Table 3.1, several specific attributes must be added to the axon model before the second step of McNeal's method can be carried out. For instance, one must decide if the model is to represent a myelinated or an unmyelinated axon. In addition, an axonal length - be it finite or infinite - must be specified. Furthermore, membrane properties such linearity and passivity, as exhibited by the cable model, or nonlinearity, as seen in the Hodgkin/Huxley model of the squid axon[21] must be decided. Finally, the time-dependent behavior of the model must be considered. Will we analyze a steady-state response of a model, a transient effect, or a frequency response? McNeal studied the transient response of two different models of finite-length, myelinated axons to a step of extrinsic current; one model was passive and linear, and the other was the nonlinear Frankenhauser-Huxley model of frog nerve[33].

The second step of McNeal's method is to calculate the transmembrane potentials induced in the axon model by the extracellular potentials determined in the first step. Note from assumption 3 of Table 3.1 that the model generated by each choice of axon model properties will have a circuit theory representation. Once the details of the axon model have been decided, the corresponding circuit is "placed" somewhere in the extracellular medium. The axon model circuit is then solved (either analytically or numerically, depending on the complexity of the circuit) for the case where it is driven by a series of voltage sources connected to the nodes representing the extracellular space along the axon model's length. The voltages at these extracellular nodes are assigned so as to match the voltage profile seen by the axon when placed in the chosen position and orientation relative to the stimulating electrode. The transmembrane potentials can then be easily deduced from the circuit solution.

I have only seen two papers which present models of the cell body for extracellular electrical stimulation problems. In both papers, the cell body is modeled as a perfect sphere with a membrane of zero thickness. Plonsey and Altman attribute a distributed specific resistance (SI units are ohm·m^2) to the membrane and use their model to analyze the effects of steady-state electric fields[41], while Cartee and Plonsey attribute both a specific resistance and a capacitance per unit area to the membrane in order to analyze the transient effects of a step in applied electric field[8]. The analyses in the two papers are similar in most other respects. The intracellular and extracellular fluids are modeled as linear, isotropic, and homogeneous conductors. The applied electric field is uniform far away from the cell body model, corresponding to the parallel plate electrode configuration. The electric potential inside of and outside of the cell body model are found by solving Laplace's equation using standard techniques. The uniformity of the field far from the cell body model and the electrical characteristics of the membrane provide the necessary boundary conditions. The transmembrane potential can be calculated from the resulting solution in a straightforward manner. As in the case of the simpler axon models discussed above, useful analytical results can be found in closed form. Unlike the axon models for longitudinal effects, the cell body model plays a role in determining the extracellular potentials created by the extracellular electrode near the cell.

Chapter overview

The simplest of the models described above, incorporating idealized electric fields and cell shapes, uniformly linear membranes, and steady-state conditions will be analyzed in this chapter. Three representative scenarios, illustrated schematically in Figure 3-2, will be examined. In all cases, two large, perfectly conducting parallel plates are connected to a current source which has been on for a long time relative to any time constants of interest. Neglecting fringing, the electric field in the absence of the cell models will be uniform and horizontally directed between the plates, and zero everywhere else. In section 3.2, the transmembrane potentials induced in the spherical cell body model (Figure 3-2a) will be found from Laplacian solutions for the electric potential. In section 3.3, the transmembrane potentials induced in the infinitely long axon by a longitudinal field (Figure 3-2b) will be calculated using McNeal's method in conjunction with the cable model for unmyelinated axons. The mathematical formula for the transmembrane potentials induced in the cell body model will be related to the general principles described by Ranck[46]. Results from the longitudinal axon model will be related to theoretical work presented by various authors. The analyses of these first two stimulus paradigms will be our our primary means of understanding how nerve cells are stimulated extracellularly. The transmembrane potentials induced in the infinitely long axon by a transverse electric field (Figure 3-2c) can be found from Laplacian solutions for the electric potential, as in the case of the spherical cell body model. While this formulation has not yet been seen in the literature, the derivations bear a strong resemblance to those for the spherical cell (see appendix A.2), and consequently yield little additional insight. The solution for this model is given in section 3.4, where analytical results are used to predict how the minimum-amplitude or *threshold* fields required to generate action potentials using the three stimulus paradigms compare with one another.

The goal of the analyses that follow is to predict as many general phenomena of extracellular electrical stimulation of nerve cells as possible with relatively simple models. This, of course, involves tradeoffs. Due to the large number of assumptions that will be made in modeling cell bodies and axons, the analyses that follow will fail to predict significant aspects of nerve cell behavior. Section 3.1 provides a formal statement of the assumptions made in this chapter. A discussion of the more dramatic consequences of certain assumptions is included in that section. The topic is then reconsidered more thoroughly at the end of the chapter, in section 3.5.

It should also be noted that the models we are proposing may apply to more general situations than those that will be analyzed in this thesis. For example, induced transmembrane potentials in all models may be found for *arbitrary* electrode configurations if numerical simulations are employed. Furthermore, all models take the cell membrane capacitance into account, so that equations derived from the models can be used to evaluate the effects of low frequency time varying fields[1].

3.1 Statement of Assumptions

In addition to the assumptions listed in Table 3.1 for modeling longitudinal effects in axons, the following will be assumed:

[1] Of course, if the time variation of the electric field is rapid enough to produce electromagnetic radiation effects, the models presented in this chapter will be inadequate.

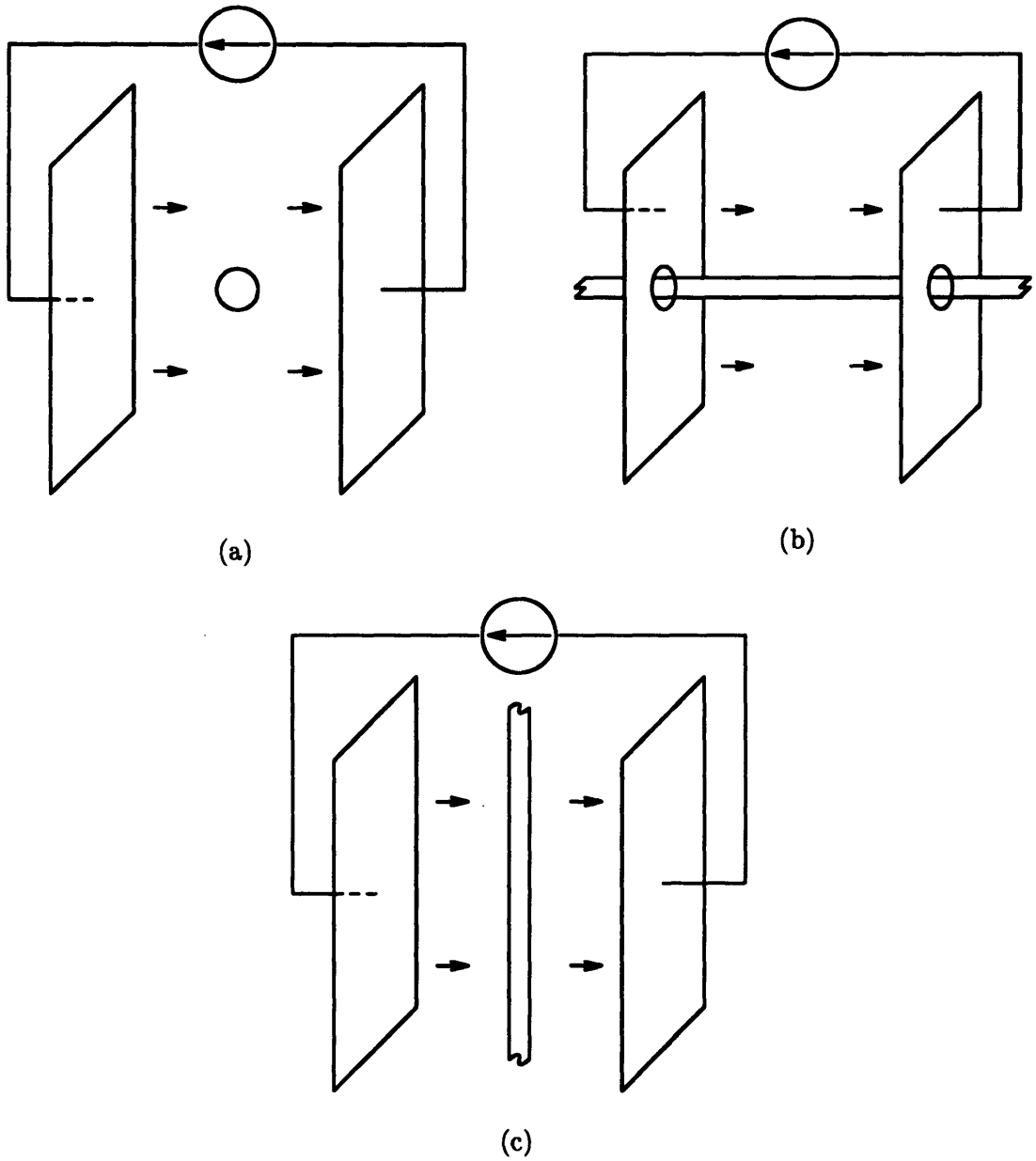

Figure 3-2: Stimulus paradigms. (a) Cell body in a uniform field; (b) Axon in a longitudinal field; (c) Axon in a uniform, transverse field.

1. Extracellular electric fields near a cell body are not affected by the cell's axon, by the cell's dendrites, or by other cells in the vicinity; extracellular fields near an axon are not affected by the cell body, by the cell's dendrites, or by other cells. In other words, cell body and axon models will be analyzed in isolation.

2. Cell bodies are perfect spheres. Axons are right circular cylinders of (doubly) infinite length.

3. Intracellular and extracellular fluids have linear, isotropic, and homogeneous electrical properties.

4. Below a fixed threshold depolarization, cell membranes have passive, linear, and time-invariant electrical properties which are uniform over their entire surface area.

5. There are no fixed charges in the material, so that the electric potential has Laplacian solutions.

6. When electroquasistatic models are used, the applied electric field is uniform far from the cell body and axon models.

7. When circuit models are used, extracellular electrodes are represented with perfect voltage sources whose values are determined by the potentials induced by the electrode in a homogeneous extracellular medium.

Some of the assumptions are stronger than others, and all will have an effect on the validity of the derived results. Probably the strongest of the assumptions is that cell membranes are passive and linear. This assumption has two important consequences. First, nerve cell membranes have active components such as the sodium-potassium pump, which helps maintain a *rest* potential across the membrane. The inside of a resting cell is generally at a lower potential than the outside of the cell, and the membrane is said to be *polarized.* Since the models which will be used here have no active components, they will not predict this polarization. Second, nerve cells can produce highly nonlinear *action potentials.* Since the models which used here are linear, they will not reproduce action potentials or any other properties of excitation.

All is not lost, however. For small enough perturbations of transmembrane potential about its rest value, cell membranes are *incrementally* linear [63]. Through their extensive theoretical and experimental work on crustacean axons, for example, Hodgkin and Rushton demonstrated that the cell membrane will behave linearly for stimulating currents up to half of the threshold for excitation[22]. On the other hand, McNeal's numerical simulations of the Frankenhauser-Huxley equations for myelinated frog nerve show that linear behavior persists up to 80% of the excitation threshold[33].

Our models represent a linearization of the membrane's nonlinear electrical properties about the rest potential. Presumably, the linear approximation will be a very good one well below the excitation threshold, and will become progressively worse as the threshold is approached.

The rest potential itself is not accounted for in our models. Derived transmembrane potentials therefore represent incremental deviations about this value. We will speak of *induced* transmembrane potentials when discussing the incremental effect of the applied field. The sign of the induced transmembrane potential will reveal the effective electrophysiological state of the cell model's membrane. In areas where the induced transmembrane

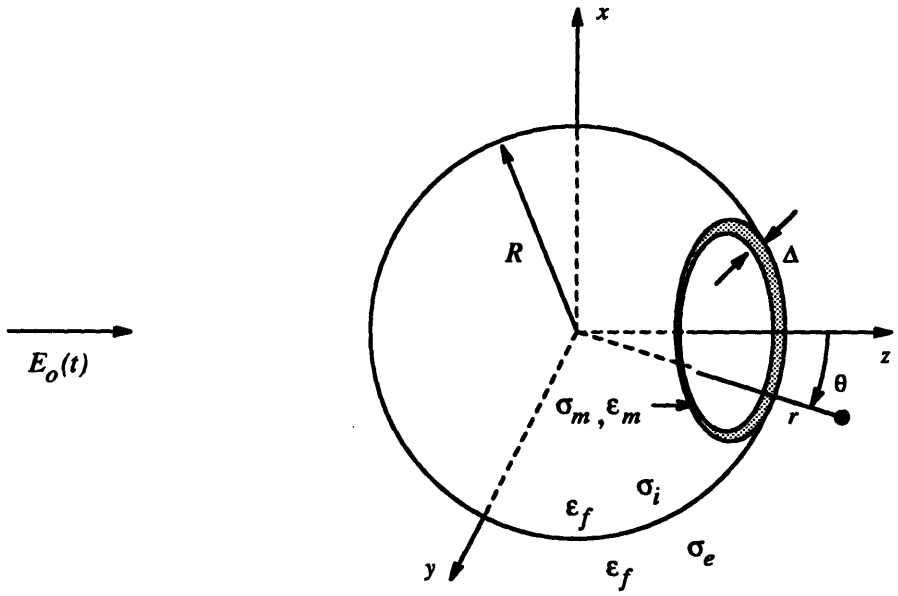

Figure 3-3: Cell body model.

potential is positive, the inside of the cell model is incrementally positive with respect to the outside. Such areas are said to be *depolarized.* In areas where the induced transmembrane potential is negative, the inside of the cell model is incrementally negative with respect to the outside. These areas are said to be *hyperpolarized.*

Excitable cells will produce action potentials if their membranes are sufficiently depolarized. Under assumption 4, linear models may be used to predict excitation thresholds explicitly. It is sufficient to calculate the electric field strength required to induce the threshold depolarization in the models. When the threshold is reached, action potentials are produced and the linear models are no longer valid. For the purposes of this thesis, we are not interested in the properties of the action potentials themselves. Therefore, nonlinear models will not be examined. Furthermore, we are less interested in the exact values of the thresholds for the three stimulus paradigms than in how these thresholds compare with one another. Such relationships will be explored in section 3.4.

3.2 Cell Body in a Uniform Electric Field

A model for the cell body is illustrated in Figure 3-3. The model is a perfect sphere of radius R centered on a coordinate axis with the Cartesian coordinates x, y and z and the spherical coordinates r and θ drawn in for reference. The intracellular and extracellular fluids have uniform permittivity ϵ_f. The intracellular fluid has uniform conductivity σ_i, and the extracellular fluid has uniform conductivity σ_e. The cell membrane is modeled as a linear, isotropic, and homogeneous spherical shell of thickness Δ, permittivity ϵ_m, and conductivity σ_m. The model is similar to that analyzed by Cartee and Plonsey[8], but differs in two respects. First, the membrane thickness Δ is assumed to be zero in their model. In the place of permittivity and conductivity, the zero thickness membrane is described by two distributed circuit parameters, a specific resistance and a capacitance per

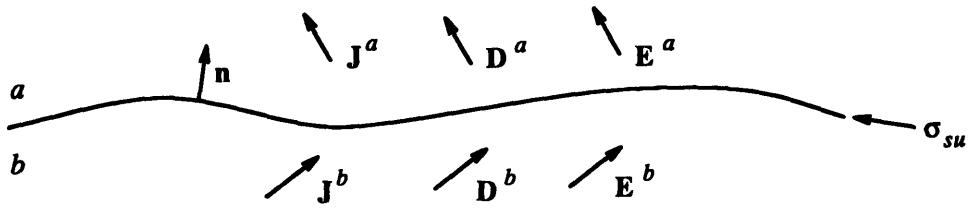

Figure 3-4: Illustration of vectors used for boundary conditions.

unit area. Second, the fluid permittivity ϵ_f is neglected in their model. Laplacian solutions for potentials in and around the model used by Cartee and Plonsey may be found fairly easily using a hybridization of circuit theory and classical electric field theory laws. While requiring slightly more algebra, the model of Figure 3-3 entails fewer assumptions about cell structure and provides a consistent electric field theory representation of the cell body.

3.2.1 Solution form and boundary conditions

The solution for the electric potential is of the form

$$\Phi = \begin{cases} a(t)r\cos\theta & \text{for } r < R, \\ b(t)r\cos\theta + \frac{c(t)}{r^2}\cos\theta & \text{for } R < r < R+\Delta, \\ -E_o(t)r\cos\theta + \frac{d(t)}{r^2}\cos\theta & \text{for } r > R+\Delta. \end{cases} \tag{3.1}$$

Before we determine the boundary conditions that apply to this solution, a few comments are in order. First, notice that for large r, the potential is approximately $-E_o(t)r\cos\theta$ or simply $-E_o(t)z$. This agrees with the previously established condition that the electric field is uniform and horizontally directed far from the cell body model. Second, note that there is no ϕ-variation in the potential. This is due to the uniformity of the applied field and spherical symmetry of the cell body model. More importantly, it points to the relative simplicity of solution (3.1), which for other applied fields and cell body geometries would likely involve a modal expansion in spherical harmonics. Now we will establish the boundary conditions which apply to the solution given above.

The functions $a(t), b(t), c(t)$ and $d(t)$ can be related to one another and to the surface charge densities on the membrane:solution boundaries using three continuity conditions. The conditions follow from, respectively, Faraday's Law, Gauss' Law, and charge conservation:

$$\begin{aligned} \mathbf{n}\times(\mathbf{E}^a - \mathbf{E}^b) &= 0, \\ \mathbf{n}\cdot(\mathbf{D}^a - \mathbf{D}^b) &= \sigma_{su}, \\ \mathbf{n}\cdot(\mathbf{J}_u^a - \mathbf{J}_u^b) &= -\dot{\sigma}_{su}\,. \end{aligned}$$

In above equations, $\mathbf{E}$ is the electric field, $\mathbf{D}$ is the electric flux density, $\mathbf{J}_u$ is the unpaired current density, σ_{su} represents surface charge density, and $\dot{\sigma}_{su}$ is the time derivative of σ_{su}. The vector $\mathbf{n}$ is the unit normal to the boundary. The superscripts ^{a} and ^{b} indicate position with reference to the boundary at which the continuity condition is applied, as shown in Figure 3-4. The cell membrane, intracellular fluid, and extracellular fluid are all assumed to be linear, isotropic, and homogeneous materials. Thus, the constitutive laws

for unpaired current density and displacement flux density may be used on the latter two continuity conditions, yielding

$$\begin{aligned} \mathbf{n}\cdot(\epsilon_a\mathbf{E}^a - \epsilon_b\mathbf{E}^b) &= \sigma_{su}, \\ \mathbf{n}\cdot(\sigma_a\mathbf{E}^a - \sigma_b\mathbf{E}^b) &= -\dot{\sigma}_{su}\,. \end{aligned}$$

Since the cell body is a perfect sphere centered on the origin, the normal vector to the membrane is $\mathbf{n} = \hat{\imath}_r$. Using this fact and the definition of potential,

$$\mathbf{E} = -\nabla\Phi, \tag{3.2}$$

the continuity conditions take the following form:

$$\frac{\partial\Phi^a}{\partial\theta} = \frac{\partial\Phi^b}{\partial\theta},$$

$$-\epsilon_a\frac{\partial\Phi^a}{\partial r} + \epsilon_b\frac{\partial\Phi^b}{\partial r} = \sigma_{su},$$

$$-\sigma_a\frac{\partial\Phi^a}{\partial r} + \sigma_b\frac{\partial\Phi^b}{\partial r} = -\dot{\sigma}_{su}\,.$$

Application of the continuity conditions at $r = R$ and $r = R + \Delta$ yield the following equations.

$$bR + \frac{c}{R^2} = aR, \tag{3.3}$$

$$-E_o(t)(R+\Delta) + \frac{d}{(R+\Delta)^2} = b(R+\Delta) + \frac{c}{(R+\Delta)^2}, \tag{3.4}$$

$$-\epsilon_m\left(b - \frac{2c}{R^3}\right)\cos\theta + \epsilon_f a\cos\theta = \sigma^i_{su}, \tag{3.5}$$

$$-\epsilon_f\left[-E_o(t) - \frac{2d}{(R+\Delta)^3}\right]\cos\theta + \epsilon_m\left[b - \frac{2c}{(R+\Delta)^3}\right]\cos\theta = \sigma^e_{su}, \tag{3.6}$$

$$-\sigma_m\left(b - \frac{2c}{R^3}\right)\cos\theta + \sigma_i a\cos\theta = -\dot{\sigma}^i_{su}, \tag{3.7}$$

$$-\sigma_e\left[-E_o(t) - \frac{2d}{(R+\Delta)^3}\right]\cos\theta + \sigma_m\left[b - \frac{2c}{(R+\Delta)^3}\right]\cos\theta = -\dot{\sigma}^e_{su}\,. \tag{3.8}$$

In the above equations, $a = a(t)$, $b = b(t)$, $c = c(t)$, $d = d(t)$, and σ^i_{su} and σ^e_{su} are the surface charge densities on the intracellular and extracellular membrane:solution boundaries, respectively. These equations completely describe a linear time-invariant system in six variables (a, b, c, d, σ^i_{su}, and σ^e_{su}) which may be solved completely for a given $E_o(t)$.

3.2.2 Time-independent solution

If the applied field is held constant at E_o, and the system described above is in steady state, the time derivatives in equations (3.7) and (3.8) will be zero. In such a case, equations (3.3),(3.4), (3.7), and (3.8) can be solved for a, b, c, and d.

From equations (3.3) and (3.4), it can be shown that

$$b = a - \frac{(R+\Delta)^3}{(R+\Delta)^3 - R^3}\left[a - \frac{d}{(R+\Delta)^3} + E_o\right], \tag{3.9}$$

$$c = \frac{R^3(R+\Delta)^3}{(R+\Delta)^3 - R^3}\left[a - \frac{d}{(R+\Delta)^3} + E_o\right]. \tag{3.10}$$

Substituting into equations (3.7) and (3.8), noting that the time derivatives are zero, and collecting terms yields

$$a\left[\sigma_i + \sigma_m \frac{2(R+\Delta)^3 + R^3}{(R+\Delta)^3 - R^3}\right] + \frac{d}{(R+\Delta)^3}\left[-\sigma_m \frac{3(R+\Delta)^3}{(R+\Delta)^3 - R^3}\right] = E_o\left[-\sigma_m \frac{3(R+\Delta)^3}{(R+\Delta)^3 - R^3}\right],$$

$$a\left[-\sigma_m \frac{3R^3}{(R+\Delta)^3 - R^3}\right] + \frac{d}{(R+\Delta)^3}\left[2\sigma_e + \sigma_m \frac{(R+\Delta)^3 + 2R^3}{(R+\Delta)^3 - R^3}\right] = E_o\left[-\sigma_e + \sigma_m \frac{(R+\Delta)^3 + 2R^3}{(R+\Delta)^3 - R^3}\right].$$

Several of the expressions in the two preceding equations can be written in terms of the membrane conductance per unit area,

$$G_m = \sigma_m/\Delta, \tag{3.11}$$

by noting that

$$\frac{\sigma_m}{(R+\Delta)^3 - R^3} = \frac{G_m}{3R^2 + 3R\Delta + \Delta^2}.$$

After making this substitution, we have

$$a\left[\sigma_i + G_m \frac{2(R+\Delta)^3 + R^3}{3R^2 + 3R\Delta + \Delta^2}\right] + \frac{d}{(R+\Delta)^3}\left[-G_m \frac{3(R+\Delta)^3}{3R^2 + 3R\Delta + \Delta^2}\right] = E_o\left[-G_m \frac{3(R+\Delta)^3}{3R^2 + 3R\Delta + \Delta^2}\right],$$

$$a\left[-G_m \frac{3R^3}{3R^2 + 3R\Delta + \Delta^2}\right] + \frac{d}{(R+\Delta)^3}\left[2\sigma_e + G_m \frac{(R+\Delta)^3 + 2R^3}{3R^2 + 3R\Delta + \Delta^2}\right] = E_o\left[-\sigma_e + G_m \frac{(R+\Delta)^3 + 2R^3}{3R^2 + 3R\Delta + \Delta^2}\right].$$

The equations we have derived thus far can now be greatly simplified by recognizing that membrane thickness Δ is much less than the cell body radius R. Specifically, cell membranes are known to be on the order of 75Å thick[63], whereas the radii of ganglion cell bodies[2] in rabbit retina[3] have been measured at roughly 10μm[1, 26]. Thus the cell body radius is over a factor of 1000 greater than cell membrane thickness. Based on this comparison, we make the approximation $R + \Delta \approx R$ to obtain

$$a(\sigma_i + G_m R) + d\left(-\frac{G_m}{R^2}\right) = E_o(-G_m R),$$

$$a(-G_m R) + d\left(\frac{2\sigma_e}{R^3} + \frac{G_m}{R^2}\right) = E_o(-\sigma_e + G_m R).$$

[2]Of course, retinal ganglion cell bodies are not perfect spheres. Therefore, to speak of cell body "radius" is somewhat misleading. The numbers used here are calculated from measurements of cell body area when viewed under a light microscope, and are used only to demonstrate that cell body size is generally much larger than cell membrane thickness.

[3] At the time this chapter was written, rabbits were the primary animal used for experimental research in the retinal implant group.

Now we can solve for a and d fairly easily, and we find that

$$a = -\frac{3\sigma_e G_m R}{\sigma_i G_m R + 2\sigma_e G_m R + 2\sigma_i \sigma_e} E_o, \tag{3.12}$$

$$d = \frac{\sigma_i G_m R^4 - \sigma_e G_m R^4 - \sigma_i \sigma_e R^3}{\sigma_i G_m R + 2\sigma_e G_m R + 2\sigma_i \sigma_e} E_o. \tag{3.13}$$

Equations (3.1), (3.12) and (3.13) provide a complete solution for the electric potential inside and outside of the cell body model. To determine the potential inside of the cell membrane, it would be necessary to find b and c. This could be done by substituting the solutions for a and d back into equations (3.9) and (3.10). However, the potential inside of the membrane is not of critical importance to this analysis, so we will neglect b and c altogether.

3.2.3 Interpretation of the time-independent solution

For purposes of nerve cell stimulation, the critical effect of an applied field is that it changes the electric potential difference between the inside and the outside of the cell. This effect will be called the *induced transmembrane potential*, and will be defined by

$$V_m = \Phi|_{r=R} - \Phi|_{r=R+\Delta}. \tag{3.14}$$

The potential Φ at a point in space is determined by equations (3.1), (3.12), and (3.13). The particular value V_m takes on depends on where along the cell membrane it is calculated. Due to the symmetry of the cell body model, this position may be described by the angle θ only (see Figure 3-3). As discussed in section 3.1, positive values of V_m will indicate areas of cell membrane which are depolarized, and negative values of V_m will indicate hyperpolarized areas.

Applying the definition of transmembrane potential given by equation (3.14) to the solution found in section 3.2.2 gives

$$\boxed{V_m = \frac{3\sigma_i \sigma_e R}{\sigma_i G_m R + 2\sigma_e G_m R + 2\sigma_i \sigma_e} E_o \cos\theta.} \tag{3.15}$$

This solution agrees with the results of Cartee and Plonsey, who derived the step-response of V_m for a spherical cell body in a uniform field using a similar model[8].

Features of the induced transmembrane potential

While based on highly simplified models, the induced transmembrane potential given by equation (3.15) predicts many of the phenomena described by Ranck for extracellular electrical stimulation of real nerve cells[46]. Mathematical features of the induced transmembrane potential are listed below and accompanied by the related phenomenon reported by Ranck.

- $V_m \propto \cos\theta$

  Regions at the right side of the cell (θ is near zero) are depolarized whereas regions at the left side of the cell (θ is near π) are hyperpolarized. Since the applied electric field points from the left to right, hyperpolarized regions occur where the extracellular potential is relatively high and depolarized regions occur where the extracellular potential is relatively low.

$G_m = 0.001$ S/cm^2
$\sigma_i = 0.005$ S/cm
$\sigma_e = 0.02$ S/cm

Table 3.2: Electrical parameters for a typical cell. From [8].

- $V_m \propto R$ for sufficiently low $G_m R$

  Small cells will suffer smaller induced transmembrane potentials than large cells in the same applied electric field. $G_m R$ will be "sufficiently low" if it is much less than σ_i and σ_e. Using a radius of $R = 10\mu$m and the electrical parameters of a typical cell[8] listed in Table 3.2, we see that $G_m R = 1 \times 10^{-6}$ S/cm. This is at least a factor of 1000 smaller than σ_i or σ_e.

- $V_m \downarrow 0$ as $G_m \uparrow \infty$

  The induced transmembrane potential is greatest for a perfectly insulating ($G_m = 0$) membrane, and decreases as the membrane conductance increases.

- $V_m \propto E_o$

  Larger applied electric fields induce larger transmembrane potential changes. The electric field is defined as the gradient of the electric potential. Therefore, the steeper the extracellular voltage gradient, the greater the induced transmembrane potential.

Potential averaging property

Using the parameters in Table 3.2, a radius of $R = 10\mu$m and an applied electric field $E_o = 1$ V/cm, the plot of Figure 3-5 was produced to illustrate how transmembrane potentials are induced in the cell body model. Potentials in the intracellular and extracellular space are plotted along the z-axis as defined in Figure 3-3. Outside of the cell, $|z| > R$, the potential profiles are approximately straight lines of negative slope, corresponding to the constant electric field that would be established in the absence of the cell body model. Inside the cell, $|z| < R$, the potential is constant and has assumed the average value of the potentials in the neighboring extracellular space. The discontinuities in potential across the dotted lines in Figure 3-5 represent induced transmembrane potentials. At $z = -R$ the interior of the cell model is at a lower potential than the exterior, representing a membrane hyperpolarization. At $z = R$, the interior of the cell model is at a higher potential than the exterior, representing a membrane depolarization.

The potential averaging that takes place inside the cell has a simple circuit theory analogy. A one-dimensional circuit model of the cell body is illustrated in Figure 3-6. Circuit nodes are labeled with circled integers for reference. R_l and R_r represent lumped cell membrane resistances of the left and right halves of the cell body. Voltage drops across these membrane resistances are analogous to induced transmembrane potentials. R_i represents the intracellular resistance. Note that the membrane capacitance has been left out of this model. In steady-state, the capacitances connected in parallel with resistors will

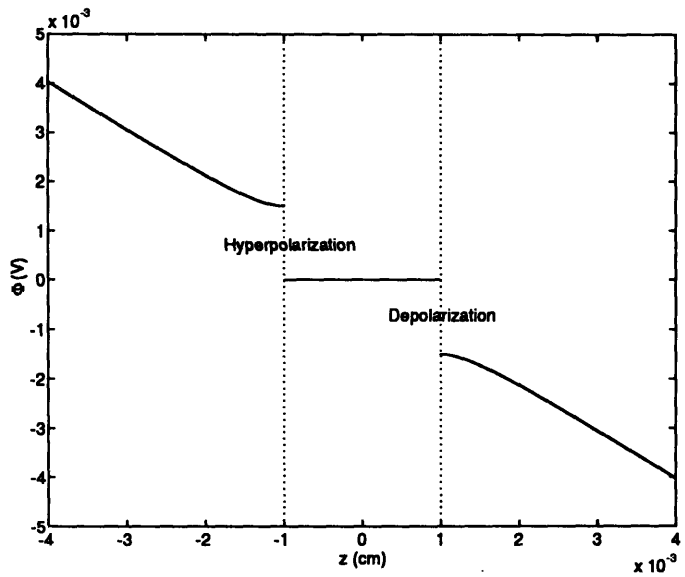

Figure 3-5: Extracellular and intracellular voltages along the z-axis. Dotted lines indicate boundary between the inside and the outside of the cell body model, i.e. the cell membrane.

resemble open circuits, and will therefore not affect the final distribution of voltages in the circuit.

The sources v_l and v_r represent extracellularly applied voltages on the left and right sides of the cell body, respectively. Strictly speaking, extracellular electrodes such as those depicted in Figure 3-2a *will not* behave like perfect voltage sources in the immediate vicinity of a cell, since the cell will play a role in determining the extracellular potentials nearby. To see this relation, recall that the coefficient d in equation (3.1) for the electric potential outside of the cell is shown in equation (3.13) to depend on the cell radius R, the intracellular conductivity σ_i, the extracellular conductivity σ_e, and the membrane conductance per unit area G_m. Assuming the extracellular voltages are known, however, perfect sources may be substituted at the appropriate nodes of the circuit to model the effect of extracellular electrodes.

The intracellular voltages at nodes ② and ③ may be found by solving the circuit equations. These voltages are given by

$$v_2 = v_r + \frac{R_i + R_r}{R_l + R_i + R_r}(v_l - v_r),$$

$$v_3 = v_r + \frac{R_r}{R_l + R_i + R_r}(v_l - v_r).$$

If the intracellular resistance is small and the membrane resistances are equal,

$$v_2 \approx v_3 \approx \frac{v_r + v_l}{2}.$$

Thus, the potentials at the intracellular nodes ② and ③ are the average value of the potentials at the extracellular nodes ① and ④.

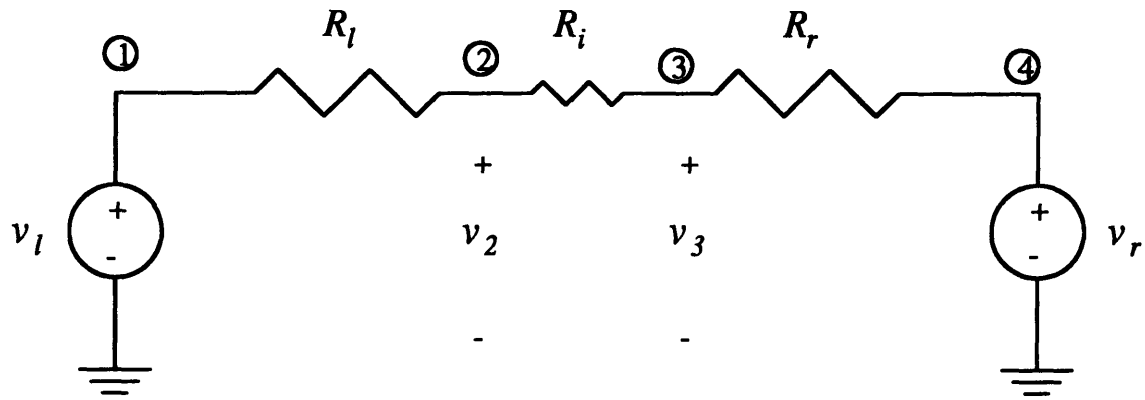

Figure 3-6: One-dimensional circuit model of spherical cell in steady-state.

The induced transmembrane potentials for the circuit model demonstrate the same properties described above for the spherical cell body model. Define

$$v_{ml} = v_2 - v_l = \frac{R_l}{R_l + R_i + R_r}(v_r - v_l),$$

$$v_{mr} = v_3 - v_r = \frac{R_r}{R_l + R_i + R_r}(v_l - v_r),$$

where v_{ml} is the potential induced across the left membrane resistance, and v_{mr} is the potential induced across the right membrane resistance. First, observe that hyperpolarizations occur at the side of the greater extracellular voltage, and depolarizations occur at the side of the smaller extracellular voltage. If $v_l > v_r$, for instance, the induced potential will be negative across the left membrane resistance, corresponding to a hyperpolarization, and positive across the right membrane resistance, corresponding to a depolarization. This property, which is analogous to the cosine proportionality of V_m above, is illustrated with voltage profile plot similar to that of Figure 3-5. A discretized version of the plot may be produced if the distance variable z is replaced with node numbers. The plot in Figure 3-7 was produced in this manner with $R_l = R_r = 10^{11}\Omega$, $R_i = 4\times10^7\Omega$, and $v_r = -v_l = 1.5mV$. These values were chosen so that induced voltages would be comparable to those of the three dimensional model along its z-axis: R_i is the resistance of a cylindrical "core" of conductivity σ_i (see Table 3.2), cross-sectional area $1\mu m^2$ and length $20\mu m$; R_l and R_r are the resistances of a $1\mu m^2$ area patch of membrane; and v_r and v_l are the extracellular voltages at $z = \pm R$, respectively, in Figure 3-5. As before, the dashed vertical lines represent the cell membrane.

Second, the transmembrane potentials induced in the 1-d circuit model decrease with decreasing membrane resistance. The analogous property for cell body model is that $V_m \downarrow 0$ as $G_m \uparrow \infty$. As R_l and R_r become comparable to R_i, the voltage drops over the three resistances become comparable. If the voltage drop $v_l - v_r$ were unchanged, the jumps in potential across the cell membrane resistances would decrease. We have stated above, however, that a change in cell model properties can result in a change in the extracellular voltages created by an extracellular electrode. Consider figure 3-8a, which was created by increasing G_m by a factor of 10,000. The extracellular voltage at $z = R$ has dropped

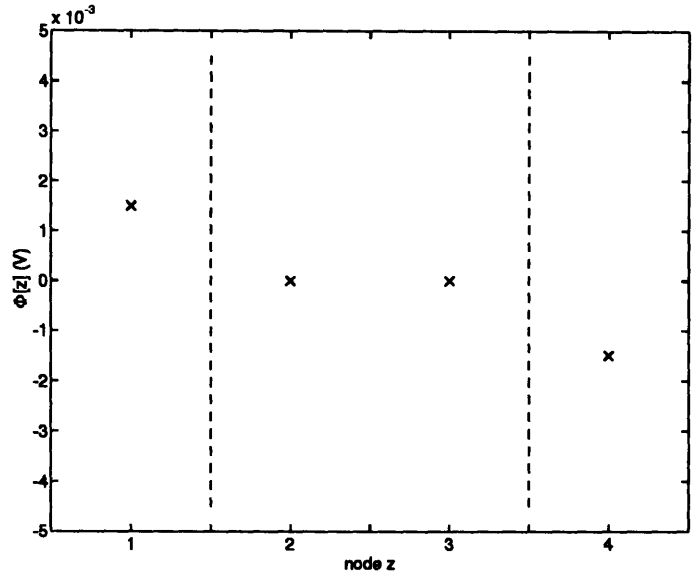

Figure 3-7: Voltage profile for circuit model of cell body.

slightly to 1.38mV. Thus, increasing the membrane conductance actually shrinks the induced transmembrane potentials in two ways: (1) by reducing the total voltage dropped across the cell model diameter; and (2) by causing an increased fraction of this voltage to be dropped across the intracellular resistance. A plot of node voltages for $R_l = R_r = 10^7\Omega$, $R_i = 4 \times 10^7\Omega$ and $v_r = -v_l = 1.38$mV is shown in Figure 3-8b to illustrate the effect of low membrane resistance in the circuit model.

Third, the transmembrane potentials induced in the circuit are proportional to the total voltage applied across it, $v_l - v_r$. This explains the remaining two properties. The total voltage established across the sphere is proportional to both the applied electric field E_o and the radius R. Thus, V_m is proportional to both of these quantities. Note that if the voltages v_l and v_r are equal, no depolarizations or hyperpolarizations will be created. The corresponding voltage profile will be entirely flat, since $v_2 = v_3 = v_l = v_r$ in such a case.

Generalization

The potential averaging property of the simple circuit model of Figure 3-6 may be generalized to an arbitrary number of conductances and voltage sources. This suggests a model such as that of Figure 3-9, where each conductance represents a differentially small patch of membrane and each voltage source represents the extracellular voltage at that patch. The intracellular resistances are assumed to have negligible effect on intracellular potential averaging, and are left out of the model. Comparison of Figures 3-5 and 3-8a suggest that this assumption is reasonable for the cell body model. The model may be used for an arbitrarily shaped cell provided that such intracellular resistances are small.

If G_j is the conductance of patch j and V_j is the extracellular potential, as labeled, we have

$$V_{mj} = \frac{\sum_{i=1}^{n} G_i(V_i - V_j)}{\sum_{i=1}^{n} G_i}$$

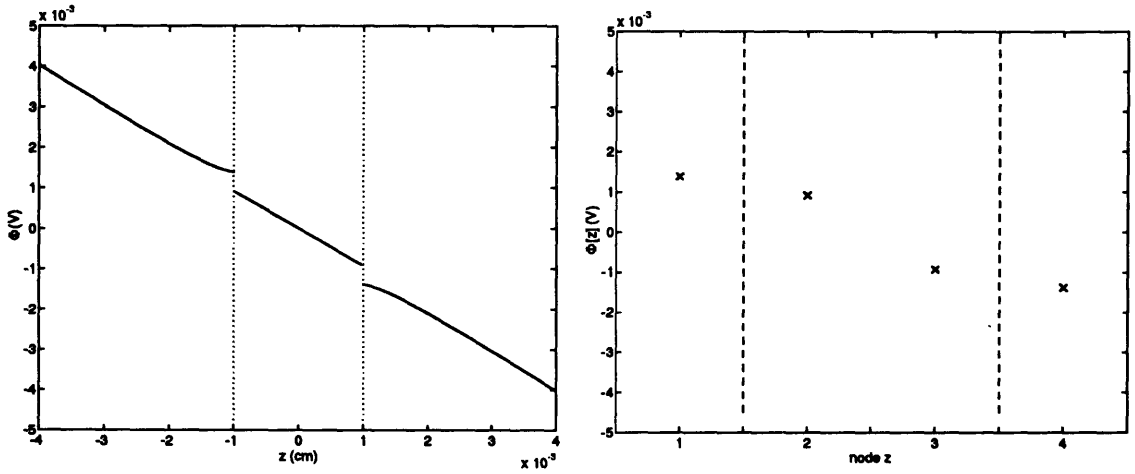

(a) (b)

Figure 3-8: Voltage profiles for (a) spherical cell body model with membrane conductance increased 10000-fold; (b) circuit model with R_l and R_r comparable to R_i.

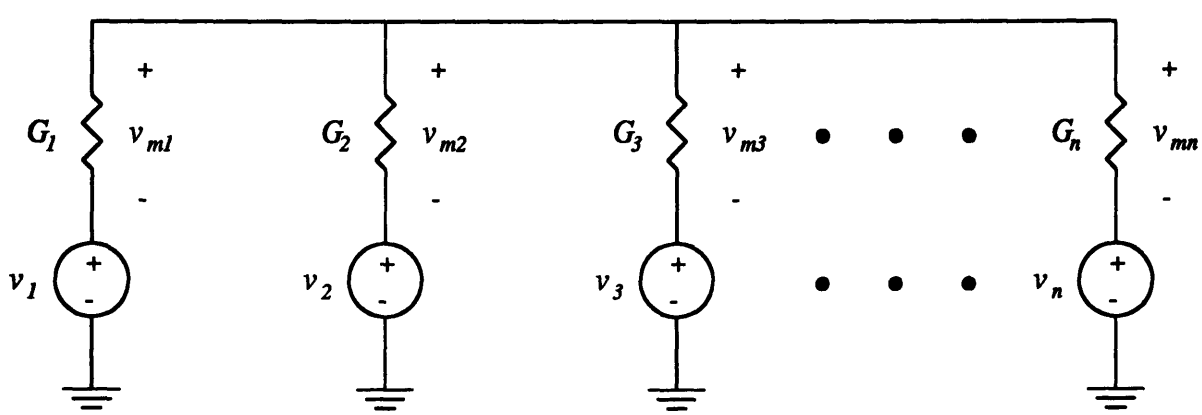

Figure 3-9: Circuit model for cell with small intracellular resistance in steady-state.

for the induced transmembrane potential. Note that V_{mj} will be small in areas where G_m is relatively large. This is because at patch j, G_j appears in the denominator of V_{mj}, which it dominates (by assumption), but is multiplied by zero in the numerator. This result has two important implications. First, for cells with spatially nonuniform membrane conductances, smaller transmembrane potentials will be induced in areas of higher conductance. Second, if the extracellular potentials are near some voltage V_j over a significant fraction of the cell's area, the induced transmembrane potentials will tend to be small in those areas. In this case, the total conductance path associated with V_j will appear large, since it represents a parallel combination of several patch conductances.

This second phenomenon may occur when a cell body stimulated with a point electrode, as in Figure 3-10. The electrode has a needle-like tip which is connected to the negative terminal of a current source. The return path for the current is assumed to be very far away. A potential profile characterized by a sharp, localized drop under the electrode tip is created in the extracellular space, as drawn in the trace labeled V_e in the lower portion of the Figure. Assume this potential drop occurs within a distance comparable to or smaller than the diameter of a cell body. Qualitatively speaking, the extracellular potentials in the vicinity of the electrode will vary more rapidly in the horizontal direction (as drawn) than in the vertical direction. In such a case, the vertical walls of the cell (emphasized with dotted lines in the Figure) will be at roughly the same extracellular potential. Remembering that the cell is a three-dimensional structure, it is clear that the side walls of the cell constitute a dominant fraction of its surface area. Thus the extracellular potential at these regions sees a large membrane conductance. For this reason, the induced intracellular potential profile (dotted line trace in Figure 3-10) will average out to a value which is close to the extracellular potential near the side walls of the cell. On the other hand, the membrane area directly beneath the electrode constitutes a small fraction of the cell's surface area, and thus represents a small conductance. The induced intracellular potential in this region will average out to a value which is relatively far from the local extracellular potential. Since the induced intracellular potential is much greater than the extracellular potential, this area of membrane is strongly depolarized by the point electrode. The actual intracellular voltage is found by adding the induced intracellular potentials to the rest potential V_r, yielding the V_i trace.

Small changes in intracellular potential occur due to intracellular resistances. Since in cell bodies these resistances act over short distances and more or less in parallel, they do not significantly affect the potential profiles. By contrast, intracellular resistances in axons occur over long distances and in series. As we will see in the next section, this dramatically alters the way extracellular voltages induce transmembrane potentials.

3.3 Axon in a longitudinal field

For applied electric fields with components longitudinal to an axon, it is useful to examine the cable model shown in Figure 3-11. The axon model is assumed to be of (doubly) infinite length. The axonal membrane is represented as a distributed series of resistances and capacitances in parallel, separated at the interior of the cell by an axial resistance. There are many variables associated with this model, which are listed in Table 3.3 for reference. The variable meanings are also illustrated in the circuit diagram of Figure 3-12. All currents and potentials are assumed to be radially symmetric, and all currents flowing through the membrane are assumed to flow in a radial direction only. Note that several

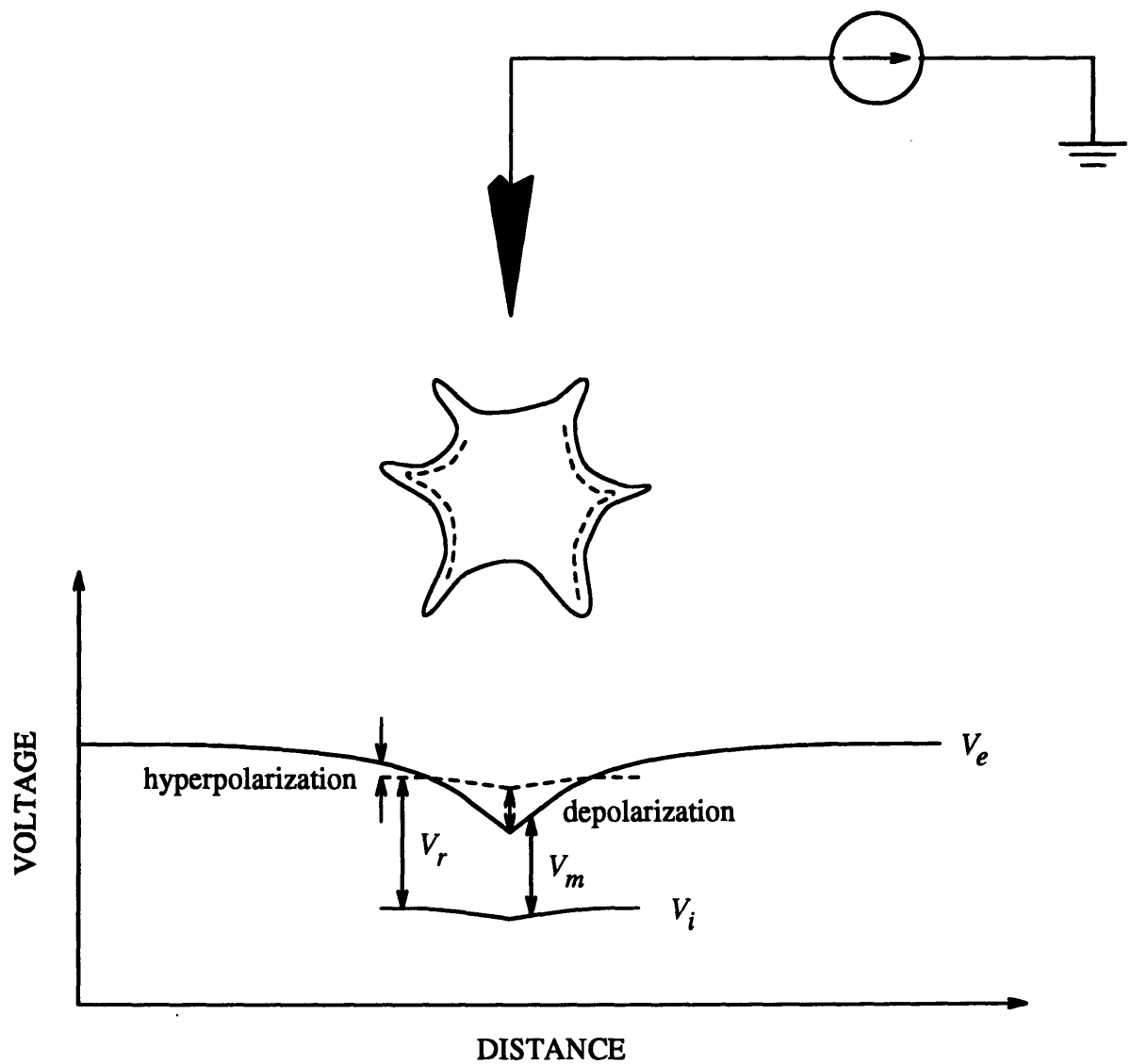

Figure 3-10: Schematic of point electrode stimulation.

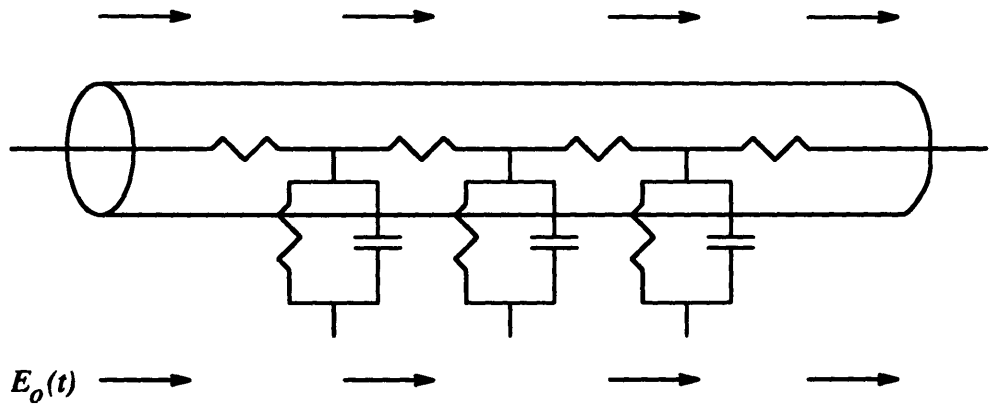

Figure 3-11: Schematic of axon in a longitudinal field.

Variable	Name	SI Unit
$V_m(z,t)$	Transmembrane potential	Volts
$V_i(z,t)$	Intracellular potential	Volts
$V_e(z,t)$	Extracellular potential	Volts
$I_i(z,t)$	Intracellular axial current	Amperes
$k_m(z,t)$	Membrane current per unit length	Amperes/meter
r_i	Intracellular resistance per unit length	Ohms/meter
g_m	Membrane conductance per unit length	Siemens/meter
c_m	Membrane capacitance per unit length	Farads/meter
λ_c	Space constant	meters
τ_m	Time constant	seconds
z	Length variable	meters

Table 3.3: Cable model variables defined.

of the variable expressions are multiplied by Δz. Since these variables are given in "per unit length" units, multiplication by some length is necessary to give the circuit element or current the correct units. Note also that no assumptions about the extracellular medium were made to arrive at the circuit model; the voltages at the extracellular nodes are strictly set by $V_e(z,t)$. To determine the actual values of $V_e(z,t)$, on the other hand, one must know the stimulating electrode configuration, the stimulus waveform and amplitude, the electrical properties of the extracellular medium, and the electrical properties of the axon. Even with such knowledge, however, an analytical solution for $V_e(z,t)$ is not guaranteed. Therefore, following a few initial derivations and remarks, a simple time-independent extracellular voltage will be assumed (see Figure 3-14a).

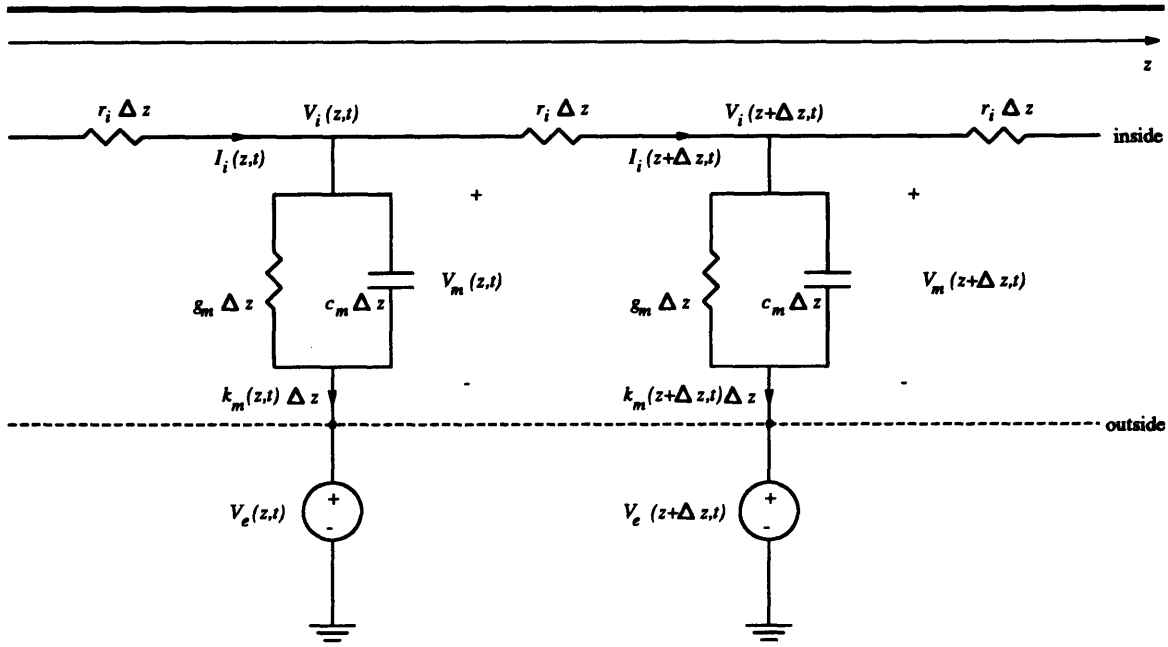

Figure 3-12: Cable model variables illustrated.

3.3.1 Cable equation for extracellular stimulation

Using Kirchoff's Current and Voltage Laws, three equations can be written for the circuit of Figure 3-12 which, in the limit where Δz approaches zero, become

$$\frac{\partial V_i(z,t)}{\partial z} = -I_i(z,t)r_i, \tag{3.16}$$

$$\frac{\partial I_i(z,t)}{\partial z} = -k_m(z,t), \tag{3.17}$$

$$k_m(z,t) = c_m\frac{\partial V_m(z,t)}{\partial t} + g_m V_m(z,t). \tag{3.18}$$

Equations (3.16)-(3.18) can be combined to form a single equation,

$$-\lambda_c^2\frac{\partial^2 V_i(z,t)}{\partial z^2} + \tau_m\frac{\partial V_m(z,t)}{\partial t} + V_m(z,t) = 0, \tag{3.19}$$

where

$$\lambda_c = \sqrt{\frac{1}{g_m r_i}} \tag{3.20}$$

is the length constant of the axon, and

$$\tau_m = \frac{c_m}{g_m} \tag{3.21}$$

is the time constant. Now, noting that

$$V_m(z,t) = V_i(z,t) - V_e(z,t) \tag{3.22}$$

and that the second partial derivative operator is linear, add $\lambda_c^2 \frac{\partial^2 V_e(z,t)}{\partial z^2}$ to both sides of equation (3.19) to obtain

$$-\lambda_c^2 \frac{\partial^2 V_m(z,t)}{\partial z^2} + \tau_m \frac{\partial V_m(z,t)}{\partial t} + V_m(z,t) = \lambda_c^2 \frac{\partial^2 V_e(z,t)}{\partial z^2}. \tag{3.23}$$

This partial differential equation in V_m provides a useful tool for the analysis of extracellularly applied electric fields. Rubinstein and Spelman used a similar equation to calculate the response of V_m to a two-dimensional impulse $V_e(z,t)$ using transform methods[52]. This impulse response may be convolved both in space and time to determine the circuit model response to an arbitrary extracellular potential distribution.

3.3.2 Activating function

Equation (3.23) suggests that V_e itself is not the fundamentally important quantity for inducing transmembrane potentials in the axon model. Rather, the second spatial derivative of the extracellular potential can be thought of as the "drive term". For this reason, the function was dubbed the *activating function* by Rattay[48]. Define the activating function

$$f_a(z,t) = \frac{\partial^2 V_e(z,t)}{\partial z^2} \tag{3.24}$$

and substitute into the previous result to obtain

$$-\lambda_c^2 \frac{\partial^2 V_m(z,t)}{\partial z^2} + \tau_m \frac{\partial V_m(z,t)}{\partial t} + V_m(z,t) = \lambda_c^2 f_a(z,t). \tag{3.25}$$

The activating function has important implications for extracellular electrical stimulation. If the applied extracellular potential depends on z and t only, then by the definition of the electric potential we have

$$E_o(z,t) = -\partial V_e(z,t)/\partial z$$

for the applied electric field. Taking a partial derivative in z on both sides of the above relation and using the definition of activating function, we have

$$f_a = -\partial E_o(z,t)/\partial z.$$

This means that the extracellular electric field must have a nonzero first derivative in the axon's longitudinal direction in order to induce transmembrane potentials. In contrast, recall from section 3.2 that only a spatially constant electric field was required to induce transmembrane potentials in the cell body model.

This fundamental difference in mode of activation can be explained on the basis of geometrical considerations. First, consider the cell body model. Since the spherically shaped intracellular fluid resembles a collection of short-length resistors in parallel with one another, its lumped intracellular resistance is small. Furthermore, the inside of the cell model is at a roughly constant potential due to the low intracellular resistance. Because the intracellular potential is constrained to be constant, transmembrane potentials will be induced at some points on the model if its external surface is not equipotential. Finally, a uniform electric field is sufficient to create a non-uniform extracellular potential distribution. Now consider the axon model geometry. The intracellular fluid resembles a long, *series* connection of

resistors. For this reason, intracellular resistances in the axon model are substantial. If just the right amount of current is flowing inside of the axon, the intracellular potentials can track the linearly varying extracellular potentials created by a constant electric field. Thus, a spatially constant extracellular electric field is not sufficient to induce transmembrane potentials in the axon model. Of course, current must flow into and out of the axon model at some locations; transmembrane potentials are necessarily induced at these locations. If the axon model is of infinite length - the case that is examined in this thesis - transmembrane current flow will only occur in or near regions where the extracellular electric field has a nonzero first spatial derivative (see, for example, Figure 3-16). If the axon model is of finite length, transmembrane currents might flow through the ends of the model.

The response of V_m may be found for the two-dimensional (in z and t) impulse activating function and convolved to find V_m for an arbitrary f_a. Since we are concerned with the steady-state case in this thesis, however, only the time-independent impulse response will be derived.

3.3.3 Time-independent solutions

In cases where the applied electric field is not changing with time and all transients have died out, equation (3.25) reduces to

$$-\lambda_c^2 \frac{d^2 V_m(z)}{dz^2} + V_m(z) = \lambda_c^2 f_a(z). \tag{3.26}$$

Solutions of this time-independent cable equation may be found for an arbitrary extracellular electrode configuration if we obtain its impulse response. Let the activation function be a spatial impulse in z,

$$f_a(z) = E_o \delta(z). \tag{3.27}$$

First solve the homogeneous equation

$$-\lambda_c^2 \frac{d^2 \hat{V}_m}{dz^2} + \hat{V}_m = 0,$$

where the "hat" notation has been introduced to denote the impulse response of the induced transmembrane potential. This equation can be solved using standard techniques for ordinary differential equations with constant coefficients. Let

$$\hat{V}_m = Ae^{pz}.$$

Substituting this expression into the homogeneous equation and solving for p, we find that

$$p = \pm \frac{1}{\lambda_c}.$$

Solutions of this form apply in regions where the drive is zero, i.e. on either side of the V_m axis, so

$$\hat{V}_m = \begin{cases} A_1 e^{-z/\lambda_c} + A_3 e^{z/\lambda_c} & \text{for } z > 0, \\ A_2 e^{z/\lambda_c} + A_4 e^{-z/\lambda_c} & \text{for } z < 0. \end{cases}$$

Since the axon model is infinitely long, on physical grounds we expect the transmembrane potential to decay to zero far away from the stimulus. A_3 and A_4 must then be zero, leaving

$$\hat{V}_m = \begin{cases} A_1 e^{-z/\lambda_c} & \text{for } z > 0, \\ A_2 e^{z/\lambda_c} & \text{for } z < 0. \end{cases}$$

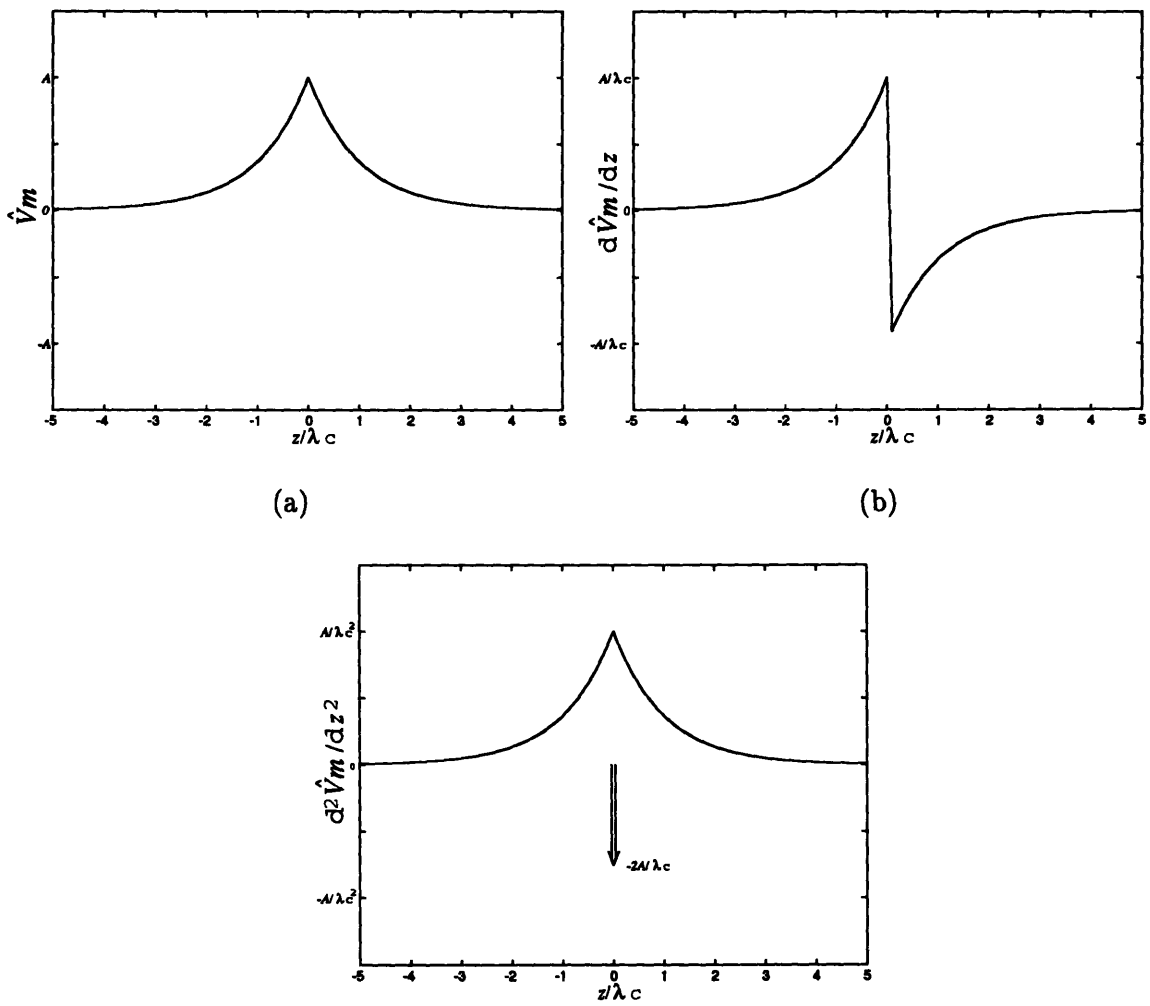

Figure 3-13: Impulse matching to solve the time-independent cable equation for extracellular stimuli. The area of the impulse in plot (c) must be equal to $-E_o$.

It will now be shown that $\hat{V}_m$ must be continuous at the origin. Suppose the opposite is true, implying that $A_1 \neq A_2$. The first spatial derivative of the transmembrane potential will contain an impulse, and the second spatial derivative will contain a doublet. On the other hand, substituting the drive term, equation (3.27), into the time-independent equation yields

$$-\lambda_c^2 \frac{d^2 \hat{V}_m}{dz^2} + \hat{V}_m = \lambda_c^2 E_o \delta(z).$$

Since this equation contains no doublets, $\hat{V}_m$ must be continuous at the origin. Letting $A_1 = A_2 = A$, we have

$$\hat{V}_m = Ae^{-|z|/\lambda_c}.$$

The coefficient A can be found by the impulse matching argument illustrated in Figure 3-13 and is

$$A = \frac{\lambda_c E_o}{2}.$$

Finally, the transmembrane potential created by a spatial impulse activating function is

$$\hat{V}_m = \frac{\lambda_c E_o}{2} e^{-|z|/\lambda_c}. \tag{3.28}$$

3.3.4 Interpretation of the time-independent solutions

Recall the stimulus paradigm illustrated in Figure 3-2b. In order to determine the transmembrane potentials induced in the axon model by the parallel plates, it will be necessary to find the associated activating function. Consider the profiles plotted in Figure 3-14. Neglecting both fringing and also the influence of the axon model on the extracellular voltage, current will pass between the plates uniformly in the horizontal direction. Extracellular voltages will be constant outside of the plates where no current is flowing, and decrease linearly with z between the plates at $z = -d/2$ and $z = d/2$, as drawn in Figure 3-14a. The corresponding electric field profile is drawn in Figure 3-14b, and the activating function in Figure 3-14c. The activating function is simply two impulses of equal area E_o and opposite magnitude. Since the circuit model for the longitudinal axon is linear and time-invariant, we can find the total response of the induced transmembrane potential for this activating function by superposing two impulse responses of opposite magnitude and separated by a distance d. Thus

$$\boxed{V_m(z) = \frac{E_o \lambda_c}{2}(-e^{-|z+\frac{d}{2}|/\lambda_c} + e^{-|z-\frac{d}{2}|/\lambda_c}).} \tag{3.29}$$

It is clear from the plot of Figure 3-15a that, if $d \gg \lambda_c$, the individual impulse responses at $z = -d/2$ and $z = d/2$ appear distinctly. The point of maximal depolarization - the physiologically significant feature - occurs at $z = d/2$. As d is decreased, the individual impulse responses tend to cancel each other out as shown in Figure 3-15b. The total amount of maximal depolarization decreases, but still occurs at $z = d/2$. The value of this depolarization is given by

$$V_m|_{z=d/2} = \frac{E_o \lambda_c}{2}(1 - e^{-d/\lambda_c}). \tag{3.30}$$

Note that the depolarization is maximal when d is infinitely large and decreases to zero as d goes to zero. In addition, the above relation allows us to predict the amount of electric field needed to produce a depolarization $V_{m,o}$:

$$E_o = \frac{2V_{m,o}}{\lambda_c}/(1 - e^{-d/\lambda_c}). \tag{3.31}$$

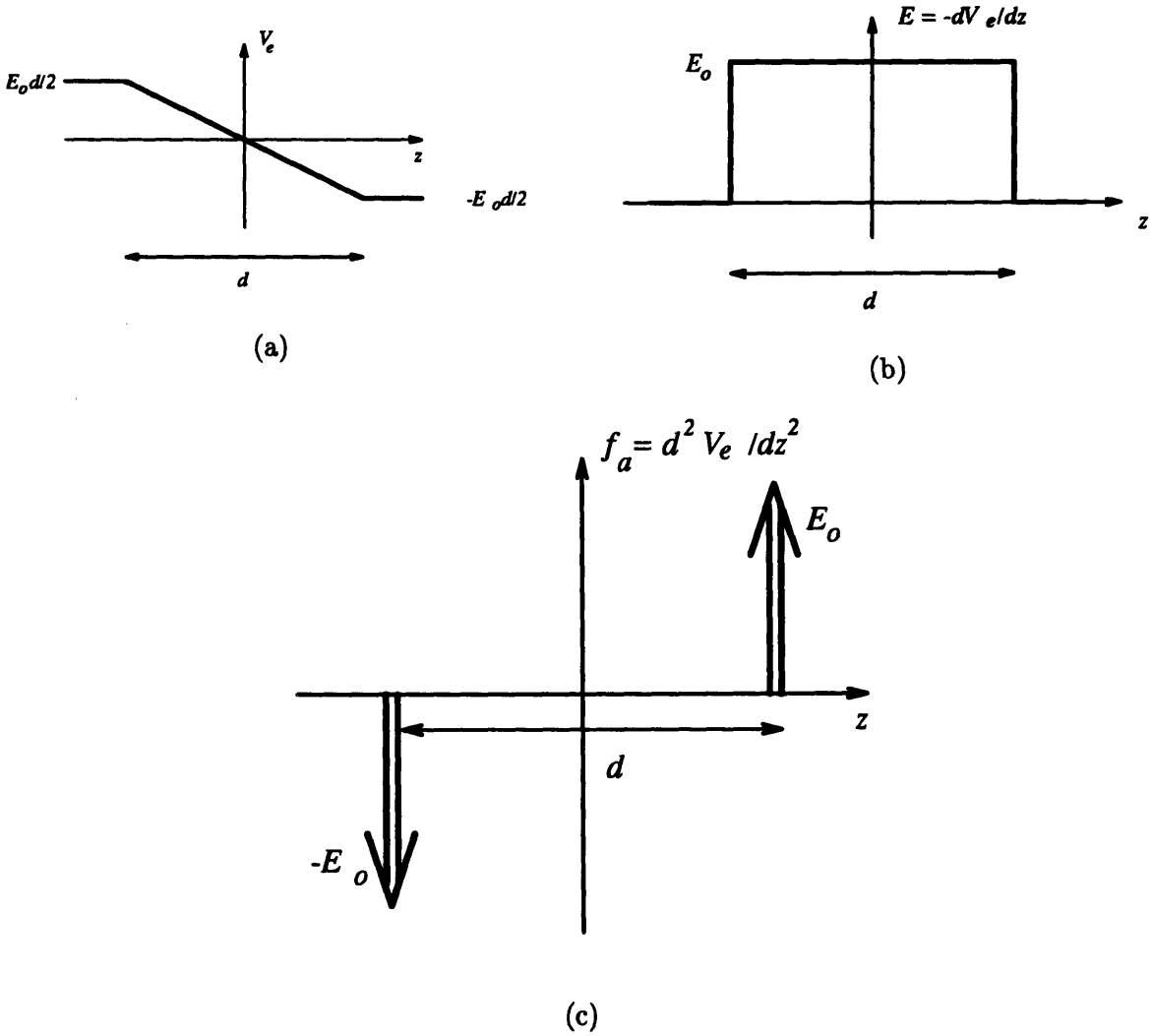

Figure 3-14: Profiles created by parallel plates with spacing d of (a) Extracellular voltage; (b) Extracellular electric field; and (c) Activating function

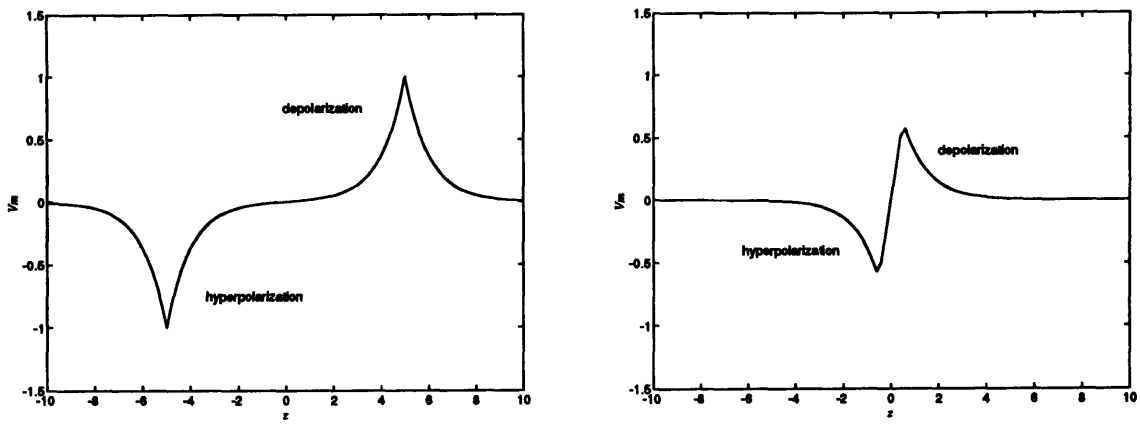

(a) (b)

Figure 3-15: Transmembrane potential profiles for plate spacing (a) $d = 10\lambda_c$; (b) $d = \lambda_c$. $E_o = 2$ and $\lambda_c = 1$ were used to produce plots.

Potential averaging property

As in the case of the spherical cell body model, induced transmembrane potentials are the result of an averaging process. To see this, let $h(z)$ be the transmembrane potential induced by an impulse of extracellular voltage $V_e = \delta(z)$. This response is found by taking the second spatial derivative of equation (3.28) and neglecting the coefficient E_o, yielding

$$h(z) = \frac{1}{2\lambda_c} e^{-|z|/\lambda_c} - \delta(z).$$

Now note that the induced transmembrane voltage for arbitrary extracellular voltages may be found from the convolution integral

$$V_m(z) = \int_{-\infty}^{\infty} V_e(\xi) h(z - \xi) d\xi.$$

Substituting the impulse response into the convolution integral yields

$$V_m(z) = \int_{-\infty}^{\infty} \frac{V_e(\xi)}{2\lambda_c} e^{-|z-\xi|/\lambda_c} d\xi - V_e(z).$$

And, finally, substituting equation (3.22) for V_m, we have

$$V_i(z) = \int_{-\infty}^{\infty} \frac{V_e(\xi)}{2\lambda_c} e^{-|z-\xi|/\lambda_c} d\xi. \tag{3.32}$$

Inspection of equation (3.32) reveals that the intracellular voltage at some location z along the axon consists of a weighted sum of the extracellular potentials. Furthermore, the weighting function is greatest at the "observation point" z, decreases monotonically and symmetrically as you move away from z, and has area 1. The potential averaging process implied by equation (3.32) is illustrated in Figure 3-16. The intracellular and extracellular potentials differ only near breakpoints ($|z| \approx 5$) where the extracellular potential is not the average of its neighboring values.

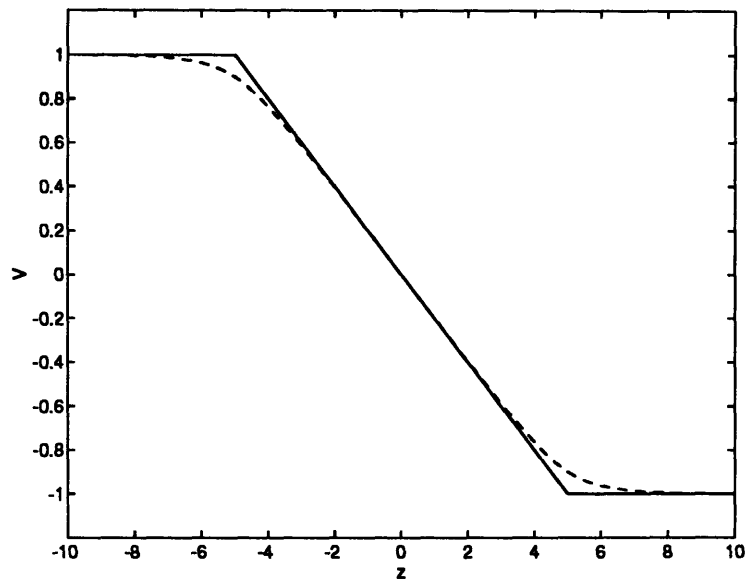

Figure 3-16: Extracellular (solid line) and intracellular (dashed line) voltages for parallel plate electrode with $\lambda_c = 1$, $d = 10\lambda_c$, and $E_o d = 2$. Intracellular potentials are found by adding the extracellular potentials to V_m.

3.4 Comparison of thresholds

In the previous two sections, linear models were used to obtain closed-form solutions for the induced transmembrane potential. By assumption (see section 3.1), these models are valid only when the transmembrane potential is below some fixed threshold. Let this threshold be denoted by $V_{m,th}$, and assume that it is the maximum depolarization produced when an electric field E_{th} is established between the electrode plates. Suppose also that the maximal depolarization produced by an electric field E_o is denoted $V_{m,max}$. Express these relationships as

$$E_{th} \longrightarrow V_{m,th},$$

$$E_o \longrightarrow V_{m,max}.$$

Without loss of generality, we can write

$$V_{m,max} = kV_{th},$$

where k is an arbitrary real number. Thus, to produce the threshold depolarization, we wish to find the stimulus which yields $V_{th} = V_{m,max}/k$. Since our models are linear, we have

$$\frac{E_o}{k} \longrightarrow \frac{V_{m,max}}{k} = V_{th}.$$

Substituting for k in this last result, we have

$$E_{th} = \frac{V_{th}}{V_{m,max}} E_o. \tag{3.33}$$

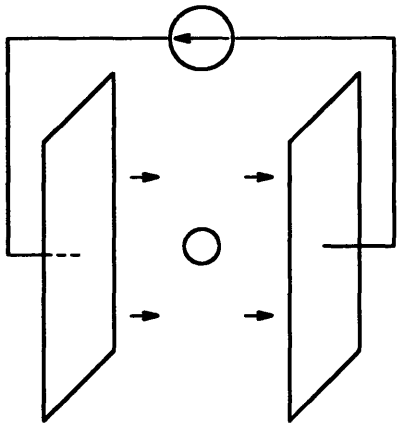

$$V_m = \frac{3\sigma_i\sigma_e R}{\sigma_i G_m R + 2\sigma_e G_m R + 2\sigma_i\sigma_e} E_o \cos\theta$$

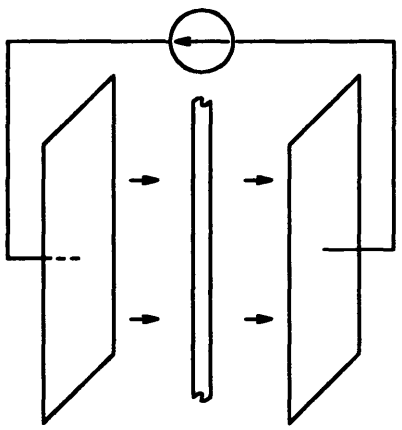

$$V_m = \frac{2\sigma_i\sigma_e R}{\sigma_i G_m R + \sigma_e G_m R + \sigma_i\sigma_e} E_o \cos\phi$$

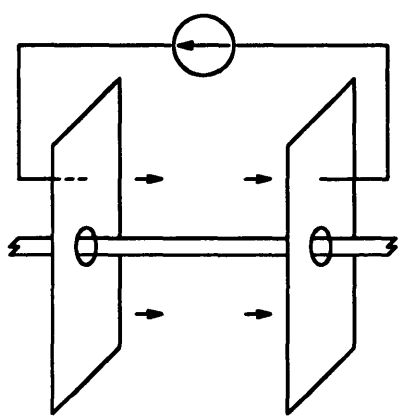

$$V_m(z) = \frac{E_o\lambda_c}{2}(-e^{-|z+\frac{d}{2}|/\lambda_c} + e^{-|z-\frac{d}{2}|/\lambda_c})$$

Figure 3-17: Summary of analytical derivations; transmembrane potentials for cell body in a uniform electric field (top), axon in a uniform, transverse field (middle) and axon in a longitudinal field (bottom).

From equation (3.33), we see that *the threshold electric field is inversely proportional to the maximum depolarization induced in the linear models by a (fixed) stimulating field E_o*. This fact will now be used to compare the thresholds for generating action potentials using the three stimulus paradigms of Figure 3-2.

A summary of the steady-state induced transmembrane potentials for the stimulus paradigms is provided by Figure 3-17. As discussed at the beginning of this chapter, the derivation and interpretation of the transmembrane potentials induced in an axon model by a uniform, transverse field are quite similar to those for the spherical cell body model. This analysis was therefore left out of the chapter, and may be found in Appendix A.2.

Using an axon radius of $R_a = 0.5\mu$m[26][4], a cell body radius of $R_{cb} = 10\mu$m[26] and the electrical parameters listed in Table 3.2, it can be shown that

$$V_{mcb} \approx 1.5 R_{cb} E_o \cos\theta,$$

$$V_{mta} \approx 2 R_a E_o \cos\phi,$$

where the subscript *cb* refers to the cell body and the subscript *ta* refers to the axon in a transverse field. Now consider the maximum levels of depolarization induced in the three models by the parallel plate electrode. For the cell body model, this occurs at $\theta = 0$, for the axon in the transverse field at $\phi = 0$, and for the axon in the longitudinal field at $z = d/2$. The maximum depolarizations are given by

$$V_{mcb,max} = 1.5 R_{cb} E_o,$$

$$V_{mta,max} = 2 R_a E_o,$$

$$V_{mla,max} = \frac{E_o \lambda_c}{2},$$

where the last formula applies for the case where d is much larger than the space constant.

Cell body vs. axon in transverse field

Taking the ratio of maximal depolarizations of the cell body and the axon in a transverse field yields

$$\frac{V_{mcb,max}}{V_{mta,max}} = 0.75 R_{cb}/R_a = 15.$$

Thus, the relative amount of transmembrane potential induced in the two models by the uniform electric field is proportional to the ratio of cell body radius to axonal radius. Using the radii given above, this ratio of depolarizations turns out to be 15. This result is qualitatively consistent with the discussion of section 3.2.3, where it was concluded that the total amount of polarization created in a cell body model was proportional to its radius. In light of equation (3.33), the threshold for stimulating axons with a transverse field will be 15 times higher than that for stimulating cell bodies.

[4]Radius of a rabbit retinal ganglion cell axon. See footnote 3.

Axon in longitudinal field vs. axon in transverse field

In general, an extracellular electric field will have components longitudinal to an axon as well as transverse to it. We can compare the relative effects of the two electric field components by taking the ratio

$$\frac{V_{mla,max}}{V_{mta,max}} = \lambda_c/4R_a \approx 56.$$

To determine this ratio numerically it will be necessary to determine the length constant λ_c of the axon model. This may be found from the definition given by equation (3.20) and by noting that $g_m \approx G_m(2\pi R_a)$ and $r_i = 1/\sigma_i \pi R_a^2$.

$$\lambda_c = \sqrt{\frac{\sigma_i R_a}{2G_m}}.$$

Using the numbers in Table 3.2, λ_c is calculated to be about 112μm. Plugging in the values for the axonal radius and length constant yields a depolarization ratio of about 56. The threshold for stimulating axons with a transverse field will therefore be 56 times higher than that for stimulating the axon with a longitudinal field.

An important distinction must be made when considering this comparison, however. Only a spatially constant electric field E_o is required to induce depolarizations in the axon when the field is applied transversely to it. By contrast, spatial gradients in E_o are necessary to induce transmembrane potentials when the field is longitudinal to the axon. To put it precisely, the ratio computed above is a comparison of the depolarization created by a uniform, transverse electric field and that created by a *step* in electric field of equal magnitude in a direction longitudinal to the axon.

Is this a reasonable comparison to make? I believe so for two reasons. First, consider the vast difference between the radius $R \approx 0.5\mu$m of an axon and the length constant $\lambda_c \approx 112\mu$m. A transversely applied field may be considered uniform if it does not change significantly within several radii of the axon, whereas a longitudinally applied field may be considered uniform if it does not change significantly over the course of several length constants. Since $\lambda_c \gg R$, spatial gradients in electric field will more likely be of consequence in the longitudinal direction than in the transverse direction. Second, the comparison may simply be viewed as that between two stimulus paradigms. The ratio computed above is simply an expression of the relative effects of the same electrode configuration in two different orientations.

Axon in longitudinal field vs. cell body

The depolarizations created in the cell body model and the axon model in a longitudinal field may be compared by taking the ratio of the previous two ratios,

$$\frac{V_{mla,max}}{V_{mcb,max}} \approx 56/15 \approx 4.$$

Thus the parallel plate electrode is almost four times more effective in depolarizing the axon model than the cell body model. Furthermore, the threshold for stimulating cell bodies will be about four times that for stimulating axons with a longitudinal field.

3.5 Limitations of approach

A large number of assumptions were made to arrive at the analytical results of this chapter. To determine the quantitative effect that these assumptions will have on the derived results would be beyond the scope of this thesis. Instead, the purpose of the following section is to acknowledge the more critical of our assumptions and discuss their drawbacks.

3.5.1 Nonlinearity of the cell membrane

The consequences of ignoring active and nonlinear responses of nerve membranes were discussed in section 3.1. To recapitulate, passive and linear models fail to reproduce the familiar resting potential and action potentials. Linearizing the electrical properties of cell membranes about the rest potential permits the use of straightforward analytical techniques to determine the effects of extracellular electric fields. Analysis of this type reveals *how* and *where* membrane depolarizations and hyperpolarizations will be induced in cell body and axon models by an extracellular stimulus. In order to determine the relative excitability of cells in the three stimulus paradigms, it was assumed that the linear models were valid until a fixed threshold depolarization was reached. There are several indications that the threshold for extracellular stimulation may depend on the time pattern of the stimulus (see below). This may not be an issue if the stimuli used in the three paradigms have the same time pattern. On the other hand, linear models are only valid up until some fraction of the threshold.

3.5.2 Time-dependent behavior

In this chapter, only steady-state responses were examined. Experimental nerve preparations involve time-dependent stimuli (even a constant stimulus must be turned on at some point) and time-dependent cellular responses. How might the approach of this chapter be generalized to account for time-dependent behavior? If the linear approximation were valid up to some fixed threshold, a simple approach could be taken: calculate the time-dependent responses of the different models for a time-dependent electric field, and determine excitability based on how much time and field strength are needed to produce the threshold depolarization in each of the models. Does there exist a critical threshold depolarization at which action potentials are always produced? To answer this question, consider the phenomenon of accommodation and the strength-duration relation.

Accommodation

A step in applied current may cause a nerve cell to activate, while a slow ramp attaining the same final value of current does not[63]. Clearly, this accommodating behavior demonstrates that the time pattern of a stimulus is critical in determining whether or not a cell will be excited. Note that, for both "slow" and "fast" stimuli, the same amount of steady-state depolarization would be produced in a linear model of a cell. This suggests that the threshold for generating action potentials is dependent on the time pattern of the stimulus. On the other hand, it is well known that as threshold is approached, linear models of cells break down. If this were the case, the same steady-state applied current might not produce the same depolarization for the two types of stimuli.

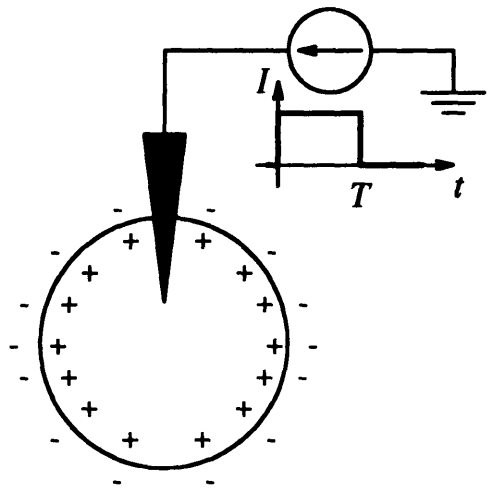

Figure 3-18: Intracellular stimulation with square pulses of current.

Strength-duration relation

A common finding in electrophysiological experiments is that, when using a square pulse of current, the threshold strength required to elicit action potentials is a function of the pulse duration. Many strength-duration curves fit the empirical equation

$$I_{th} = I_r(1 + C/T)$$

, where I_{th} is the threshold current, I_r is the *rheobase* current, T is the pulse duration, and C is called *chronaxie*[46]. Note that for pulse durations which are small compared to the chronaxie $I_{th} \approx I_r C/T$. Thus there is a threshold charge $Q_{th} = I_{th}T = I_r C$ which is independent of T for small T. Suppose this charge is applied to the inside of a cell with lumped capacitance $C_M = 4\pi R^2 C_m$, as in Figure 3-18. A potential

$$V_{th} = Q_{th}/C_M$$

will be established across the membrane. Thus, for intracellular stimuli of short duration, the cell membrane demonstrates a fixed membrane potential at which action potentials will be generated. This fact is rigorously demonstrated by Weiss for the space-clamped Hodgkin-Huxley model of the squid axon[63]. Furthermore, the strength-duration is approximated over the entire range of durations with a parallel RC model of the cell membrane which charges up to a fixed threshold[63].

Unfortunately, interpreting the strength-duration relation is less straightforward for extracellular stimuli. In contrast to charge applied intracellularly to a cell body or space-clamped axon, extracellularly applied charge will not build up uniformly against cell membranes. As a consequence, lumped-parameter circuit models must be replaced with distributed models such as those used in the previous sections. The time constants of the linear models analyzed in this chapter are determined in appendices A.1,A.2.3 and B. These are summarized in Table 3.4. The time constants of the spherical cell model and axon in a transverse field are so small that such models reach steady-state within a microsecond. If the membranes generated action potentials at a fixed threshold V_{th} as hypothesized above,

Model	Time constant
Cell body	225ns
Axon/transverse field	12.5ns
Axon/longitudinal field	0.4ms

Table 3.4: Time constants for different models.

it would be difficult to explain changes in threshold for pulse durations much greater than a few microseconds with these models. This is not consistent with the fact that chronaxies determined in extracellular stimulation experiments are typically tens of microseconds or more[45]. The time constant for the model of the axon in a longitudinal field is substantially larger, and might in fact be consistent with the notion of a fixed threshold. McNeal numerically determined the strength-duration curve for a Frankenhauser-Huxley model frog myelinated nerve which was stimulated by a monopolar spherical electrode located 1mm away from one of the nodes. McNeal's calculations, however, fail to demonstrate a constant voltage threshold, even at pulse durations as low as $10\mu s$. It is unclear whether this behavior is a property of the electrode configuration, the Frankenhauser-Huxley equations, or a combination of both.

In light of what is known about accommodation and the strength-duration relation, the threshold depolarization for generating action potentials appears to depend on the time pattern of the stimulus used.

3.5.3 Role of the cell in determining the extracellular voltage

In cases where circuit models were analyzed (see Figures 3-9 and 3-12) it was assumed that the extracellular voltage produced by the stimulating electrode was not deformed by the presence of the cell. It is clear, however, from the electroquasistatic models that this approximation is weakest in the region of greatest interest to the circuit models: immediately outside the cell. For example, the extracellular voltage in Figure 3-5 deviates maximally from a straight line at $|z| = R$.

3.5.4 Inhomogeneity of biological tissue

To determine the extracellular electric field produced by the parallel plate electrode, it was assumed that cells reside in a homogeneous extracellular medium. In general this is not the case. In the retina, for example, the extracellular space between its neural and glial cells is confined to gaps about 20nm wide (see chapter 2).

3.5.5 Anode-break excitation

A common phenomenon in electrophysiology occurs when a hyperpolarizing extracellular stimulus (an anode) is suddenly turned off[63]. Cells have been known to activate in some such cases, indicating that depolarizing a cell's membrane is not the only way to generate action potentials.

3.5.6 Non-uniformity of the cell membrane

It has been asserted that light evoked action potentials are initiated at the initial segment of amphibian retinal ganglion cell axons [7]. Studies yielding similar results for extracellular electrical stimulation of nerve cells have been cited by Ranck[46]. The existence of such "trigger zones" indicates that cell membranes may not have uniform electrical properties.

Chapter 4

Electrode Design

In this thesis we are interested in preferentially stimulating retinal ganglion cell bodies. Ideally, current delivered by our stimulating electrode will produce action potentials in cell bodies while evoking only passive responses from nearby axons. Thus in the ideal case the threshold for stimulating axons will be much higher than that for stimulating cell bodies.

Our design strategy is based on the assumption that the depolarization produced in the linear models is inversely related to the threshold for generating action potentials. It was found in chapter 3 that depolarizations could be induced in a spherical cell body model by a spatially uniform electric field. Due to the symmetry of the model, the orientation of the electric field is arbitrary. On the other hand, the depolarizations induced in the axon model depend strongly on the electric field orientation. A uniform electric field crossing the model in a transverse direction is sufficient to induce a depolarization, whereas a field parallel to the model must have a nonzero first derivative in that direction.

These results suggest that a stimulating electric field with carefully chosen spatial properties might provide some selectivity for cell bodies over axons. The spatial pattern of the electric field will be determined to a large extent by the geometry of the stimulating electrode. We therefore view the problem of selective stimulation as one of choosing the right electrode geometry.

This chapter is divided into three sections. The first section describes an electrode geometry which we believe will preferentially stimulate cell bodies. The second section provides the details of how the electrode was constructed. Finally, the third section discusses a model for predicting the electric field produced by the electrode.

4.1 Geometry

Consider the ideal parallel plate electrode analyzed in the previous chapter. Suppose a single axon model, oriented parallel to the plates, and a single cell body model reside between the plates of this electrode. If the cell body and axon models are far enough apart that they may be considered "in isolation", then the results of section 3.4 are applicable to this case. It was found in that section that the depolarization in each of the models is proportional to its size. Since the constants of proportionality are similar and ganglion cells are somewhat larger than axons, the amount of depolarization created in the cell body model is greater than that in the axon model. Furthermore, since the plates in this case are arbitrarily large, the applied electric field will have no component longitudinal to the axon model. Thus no additional depolarization will be created by longitudinal effects.

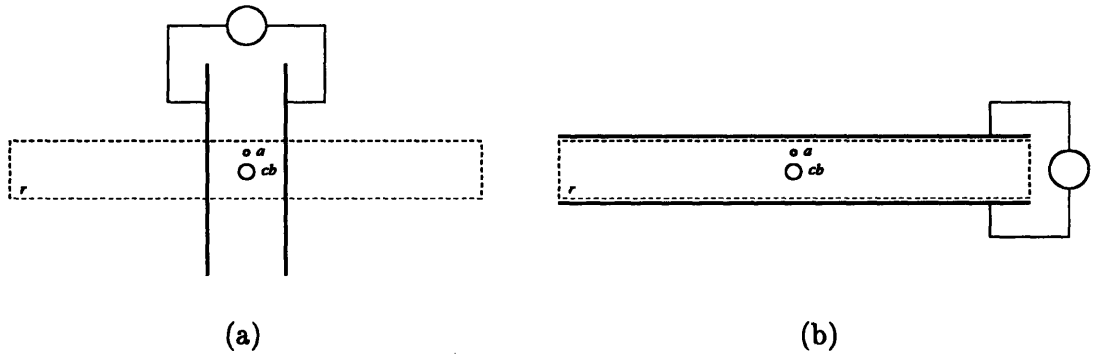

Figure 4-1: Schematic of parallel plate electrode in two different orientations relative to the retina. (a) Plates oriented perpendicular to the retinal surface; (b) Plates oriented parallel to the retinal surface. Abbreviations: *r* - retina; *a* - axon; *cb* - cell body.

Figures 4-1a and 4-1b illustrate how we apply this reasoning to stimulation of retinal cells. In the Figure, large parallel plate electrodes are arranged in two different orientations relative to the retina. The axon, which projects perpendicular to the page in both cases, is parallel to the plates. Our (admittedly simplified) model posits the retina as a linear, isotropic, and homogeneous conductor. In addition, the cell body and axon models are assumed to be far enough apart to be considered in isolation. Under these assumptions and based on the comparison of section 3.4 above, we might expect to find lower thresholds for cell bodies than for axons with the parallel plate electrode.

Unfortunately, this electrode is impractical for use with a retinal implant. The orientation shown in Figure 4-1a is undesirable because it penetrates the retina, which would damage the tissue. The orientation in Figure 4-1b is undesirable because it places a plate on either side of the retina. By contrast, the implant's stimulating electrodes will all reside at the inner surface. Furthermore, due to their large size, both electrode configurations will influence the cells over vast regions of the retina. The implant, on the other hand, is to be used to stimulate cells in localized regions. Thus, alternatives to the electrode configurations of Figure 4-1 must be found.

One such alternative is to approximate the electrode of Figure 4-1a by using only its cross-section in the plane of the retina. This cross-section consists of two parallel, infinitely long wires. Limiting the length of the wires results in the electrode shown in Figure 4-2. If the wires' length is substantially larger their spacing, there will be regions of uniform electric field between the wires. By the reasoning presented above, this electrode might also be used to preferentially stimulate ganglion cells.

Some warnings must be made regarding the approximation of Figure 4-2. First, unlike the parallel plate electrode, the strength of electric field created by this electrode will decrease with distance from the retinal surface. Electric fields passing through nearby axons will be stronger than those passing through the more distant cell bodies. The applicability of the comparison of section 3.4 to the electrode of Figure 4-2 therefore depends on how rapidly the electric field decays with distance. Second, as suggested in the Figure, there will be fringing of the electric field around ends of wires. If all retinal axons were centered exactly between wires, fringe fields would cross the axons in a purely transverse direction.

However, in addition to the single axon drawn in the Figure, there are many other ganglion cell axons at the inner retinal surface. Fringe fields will produce longitudinal effects in axons which are closer to one or the other of the wires, perhaps increasing the total amount of depolarization created by the electrode. Thus, axons directly under the wires might be just as likely or even more likely to be stimulated than the cell bodies beneath them.

The disadvantages inherent in the parallel wire geometry are hard to quantify without a detailed knowledge of the electric field it produces. A model for predicting the field will be proposed in section 4.3. Electrodes were constructed in the absence of this knowledge, with the thought in mind that their ultimate effectiveness (or lack thereof) would be determined in experiments.

4.2 Construction

Electrodes with the geometry of Figure 4-2 were constructed by the author at MIT Lincoln Laboratory during the summer of 1993 and the month of January, 1994. Note that only the general shape of the electrode is indicated by the reasoning above. The additional variables of *materials* and *size* must be determined in order to completely specify the electrode. A number of factors including biocompatibility of materials, availability of materials, and various practical considerations influenced the final determination of these less conceptually important variables. Such factors will be discussed where appropriate in the outline of electrode construction presented below.

The stimulating electrodes used by the retinal implant will be created using photolithography techniques commonly employed in microelectronics fabrication. Using such techniques, arrays of electrodes having complex geometries can be routinely produced. It was decided, however, that the time and resources required for successful microfabrication made such electrodes impractical for this thesis. A more economical though less flexible method for producing single electrodes was employed. This method is illustrated step by step in the six panels of Figure 4-3. Each of these steps will now be described in detail:

1. **Cut a thin strip of conductor-insulator-conductor sandwich.** The starting material for the electrode was a square piece of fused silica which had been coated on either side with a 5μm thick layer of gold (MIC Technology, Richardson, TX). Coated substrates such as this are commonly patterned and used for high performance Hybrid Microwave Integrated Circuits. For our purposes, this conductor-insulator-conductor "sandwich" provided a convenient way to obtain the electrode geometry illustrated in Figure 4-2. The shaded square and rectangle in the upper part of Figure 4-3.1 represent a head-on view of the material, before and after a thin slice was cut along the dashed line with a wafer saw. The lower portion of Figure 4-3.1 is a cross-sectional view showing the insulator (white) sandwiched between the two conductors (shaded).

   The thickness of the fused silica in the conductor-insulator-conductor sandwich determined the electrode wire spacing (d in Figure 4-4b). This material was available in two thicknesses, one corresponding to a wire of spacing 127μm and the other yielding a spacing of 254μm. The length of the wires (l in Figure 4-4b) was equal to the width of the slice in Figure 4-3.1. Presumably, the greater the wires' length relative to their spacing, the better the uniform field approximation between the middle portions of the wires. Conductors could not be made arbitrarily long, however, because relatively small electrode tips were required for experiments (see Chapter 5). Slices of

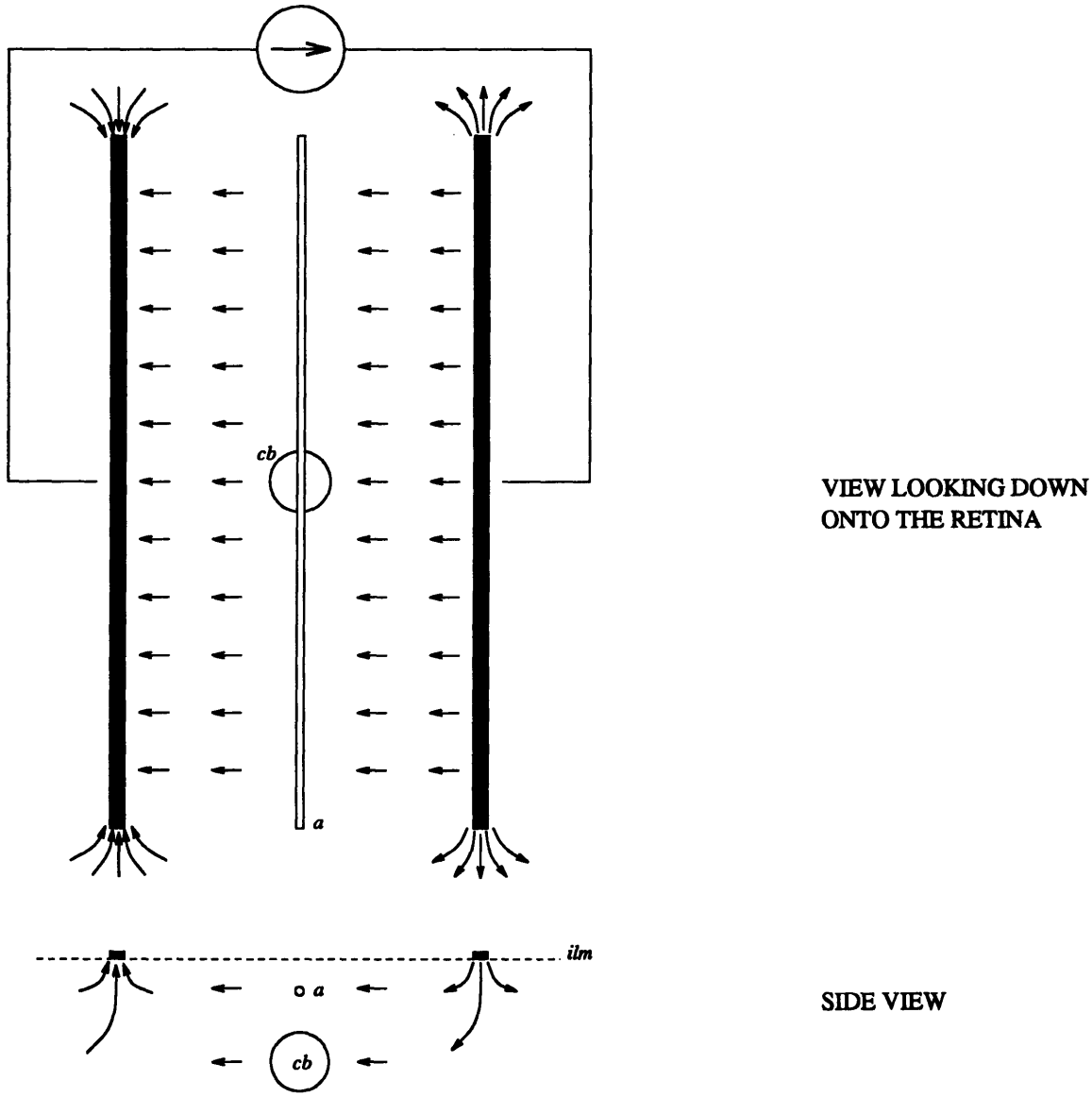

Figure 4-2: Schematic drawing of parallel wire electrode. Hypothesized electric field lines, including fringing, are drawn in. Abbreviations: *a* - axon; *cb* - cell body; *ilm* - inner limiting membrane.

this material were cut so that the conductor length was at least 2.5 times the conductors spacing (see Table 4.1 and Figure 4-4b for a complete specification of electrode dimensions). The width of the wires themselves was 5μm in all cases.

Early electrode designs used a copper-clad insulator to obtain the geometry of Figure 4-2. This material was abundantly available at Lincoln and could easily be cut into thin strips using a metal shear. However, copper may react with tissue and produce cell destruction when used in long-term experiments [12]. Even though our experiments were short-term (12 hours at most) in nature, we decided to use gold because it is considered "biologically inert" and therefore less likely to produce tissue damage.

A significant disadvantage of gold is that it is relatively soft. It was often found during electrode construction that the gold had been smeared or deformed in some way, either in the process of being cut by the wafer saw or during tip grinding. If the deformation was severe enough to obscure the basic parallel conductor geometry, the electrode was discarded.

In addition to gold, several other metals are considered biologically safe, including platinum, silver, stainless steel, and tantalum [12, 16]. Of these, only gold was readily available in the conductor-insulator-conductor form described above.

2. **Bond copper wires to the strip.** Insulated copper wires were stripped of their insulation at one end and soldered to either side of the strip obtained in step 1. Electrical contacts were tested by placing an ohm-meter between each wire (insulation removed at the other end as well) and the corresponding conductor, as depicted in Figure 4-3.2. If the resistance was small (10Ω or less) and the solder joint was mechanically robust, good electrical contact was assumed. Also, the resistance between the two wires was checked. If this resistance was large (off the scale of the ohm-meter), it was assumed that the two poles of the electrode weren't shorted together.

3. **Fill a glass tube with liquid epoxy.** A glass capillary tube (Drummond Scientific Co., Broomall, PA[1]) was then filled with Clear 2-Ton Epoxy (True Value Hardware, Cambridge, MA). The liquid (uncured) epoxy was drawn into the thin capillary tube by suction, as shown in Figure 4-3.3. A hypodermic needle of suitable diameter was attached to a syringe and inserted into the tube. Duct tape (not shown) was then wrapped around the base of the hypodermic and adjacent end of the glass tube to form an air-tight seal. Pulling back on the plunger of the syringe created a pressure vacuum inside of the capillary tube, drawing the epoxy up into it.

   Glass capillary tubing was used in the construction of the electrodes for a several reasons. First, encapsulating the conductor-insulator-conductor strip in the tube provided a straightforward way to electrically insulate its side faces from one another. Filling the space between the tube and the strip with epoxy (a good insulator) assured that there were no conductance paths between the side faces. This was done to prevent such conductance paths from shunting current away from the electrode tip. Alternatively, the strip could have been coated by dipping it in epoxy or some other insulator. This was tried with some success, but in general the insulated strip

[1]Three sizes, each specified by an inner diameter (*id*) and an outer diameter (*od*) listed in Table 4.1. The corresponding capillary tube volumes were 25, 50, and 100μL.

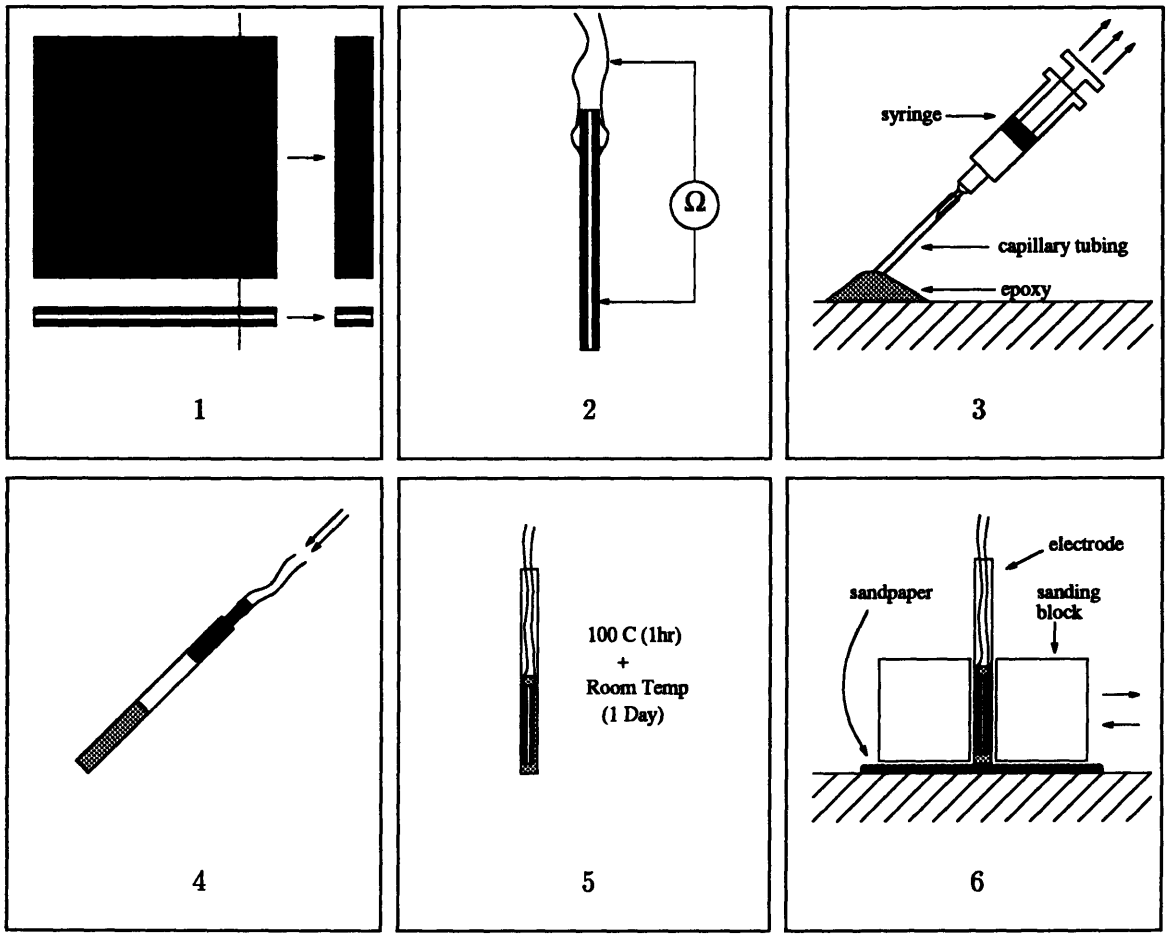

Figure 4-3: Electrode construction step by step. Not drawn to scale.

was difficult to work with due to its irregular shape. The second reason for using the glass tubing, then, was that its circular-cylindrical shape made it easy to work with. The sanding block in Figure 4-3.6, for example, was made by simply drilling a hole of suitable diameter in a block of teflon. Finally, the combined properties of small size, rigidity, and electrical insulation made the glass tubing advantageous. A small tube was needed for careful positioning of the electrode tip (see Chapter 5). In addition, a rigid tube was needed in order to have good control over the tip as it was lowered onto a preparation. Finally, an insulating tube was used to prevent stray coupling between electrode wires and their housing, which could have deformed the effective electrode geometry.

A disadvantage of using glass was that it was fragile and broke often. Metal tubes such as hypodermic needles are small, rigid, and more robust than glass. On the other hand, metal tubes conduct electricity, and were considered undesirable based on the reasoning above.

4. **Insert the strip.** The strip prepared previously was then inserted in the tube as shown in Figure 4-3.4. Though the strip was somewhat shorter than the tube, it

Design	d (μm)	l (μm)	id (μm)	od (μm)
1	127	572	660	991
2	254	635	736	1080
3	254	889	991	1370

Table 4.1: Electrode tip dimensions for three designs. d - conductor spacing; l - conductor length; id - inner diameter of the glass capillary tube; od - outer diameter of the capillary tube.

could be inserted far into the tube by pushing on the attached wires. A small epoxy-filled gap was left between the end of the strip and the end of the tube, as shown in Figure 4-3.5. This was done because bubbles often formed in the epoxy at the end of the tube as it cured. A small distance away from the end of the tube, the epoxy cured more uniformly, filling the space between the strip and the glass.

5. **Cure the epoxy.** The glass capillary tube, epoxy, and strip were then heated in an oven at 100°C for an hour. This helped to speed the curing time of the epoxy. After the tube was taken out of the oven, it was stored at room temperature for an additional 24 hours to insure that the epoxy had cured completely.

6. **Grind and polish the tip.** Once the epoxy was dry, it could be ground down with sandpaper. Using a sanding block as depicted in Figure 4-3.6, the end of the electrode was sanded at a right angle until the edge of the conductor-insulator-conductor sandwich could be clearly seen under a microscope. At this point, the tip of the electrode was polished by sanding with increasingly finer grades of sandpaper.

   A hard-curing epoxy was required for this step. The Clear 2-Ton epoxy was chosen because, of the epoxies tested, it cured the hardest. Even so, this epoxy may not have been hard enough. When electrode tips were viewed under the microscope (as in Figure 4-4a), it sometimes appeared as if the epoxy had smeared over the conductor surface. In addition, as one might observe directly from Figure 4-4, the bits of visible sandpaper grit (see step 6) embedded in the cured epoxy indicate that it was still substantially deformable. Furthermore, after several hours of immersion in saline solution, the epoxy appeared to have deformed somewhat. This was evidenced by visible peaks or valleys in the formerly flat surface of the electrode tip. Despite complications with the epoxy, the electrode's ability to pass current was uncompromised in all cases.

Pictures were taken of some of the electrode tips upon completion. A example is shown in Figure 4-4a. Below the picture in Figure 4-4b is a schematic drawing of the tip. Electrode tips of three different dimensions were made. These are listed in Table 4.1

Electrodes were tested prior to animal experiments using the apparatus of Figure 4-5. A voltage waveform V_i was established across the terminals of the circuit by the signal generator, and the resulting current flow through the electrode (if any) was measured as a voltage V_r across a known resistance. This provided a second check (in addition to that performed in step 2) that the poles of the electrode were not shorted together: if

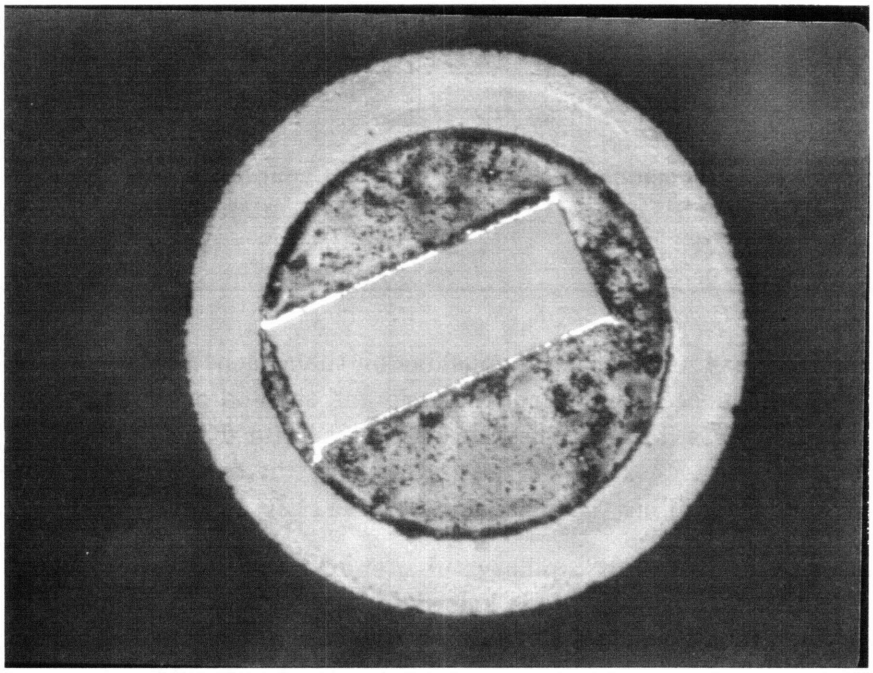

(a)

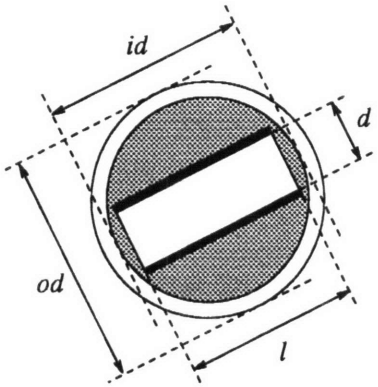

(b)

Figure 4-4: Electrode tip. (a) Photograph of a design 2 electrode; (b) Schematic of the tip with dimension variables labeled. The white annulus represents the edge of the capillary tube, which has inner diameter *id* and outer diameter *od*. The rectangle in the center represents a slice of conductor-insulator-conductor sandwich yielding wire length *l*. The white rectangle in the center is the fused silica, which had thickness *d*, and the thin black rectangles represent the gold wires, which in all cases were 5μm thick. The shaded region between the strip and the capillary tube represents the epoxy. Electrode tips of three different dimensions were made. These are listed in Table 4.1

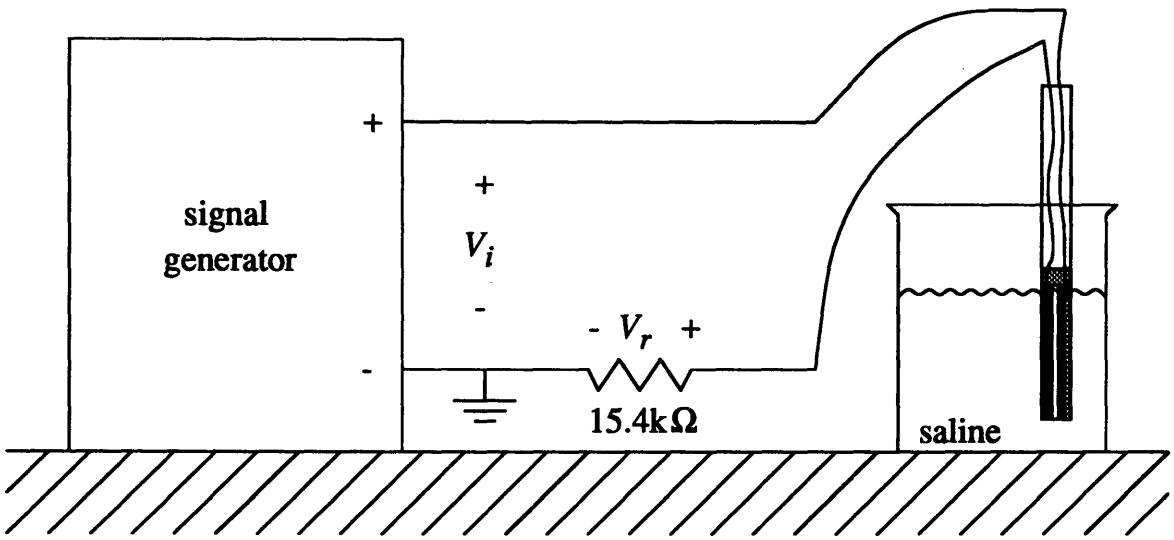

Figure 4-5: Apparatus for testing electrodes in saline.

the electrode was suspended in air, no direct current should flow between the poles of the electrode when it is connected to the signal generator. The apparatus of Figure 4-5 might also be used to determine the electrical characteristics of the electrode in physiological saline solution.

4.3 Predicting the electric field

Preliminary attempts have been made to model the electric fields produced in the retina by the electrodes constructed for this thesis. Such fields are produced by the flow of ions in the biological fluid. The ionic flow is made possible by electrochemical reactions at the electrode:solution interfaces. Our approach has neglected these interactions in the interest of simplicity. More detailed descriptions of electrode-surface reactions and related phenomena are found in [16, 17, 50, 56, 58].

To find the electric field produced by the electrode, Laplace's equation must be solved within some volume which contains the tip[2]. For the moment, let this volume be arbitrary, and consider a surface which bounds it. If either the potential on the surface (Dirichlet boundary condition) or the derivative of the potential normal to the surface (Neumann boundary condition) is specified for every point on the surface, then a unique solution for Laplace's equation exists within the volume.

Now assume that the electrode tip forms one side of the bounding surface. Because they are equipotentials, the conducting regions of the electrode tip are conveniently modeled using Dirichlet boundary conditions. Note that the electrode is symmetrical about a line parallel to and lying between the two wires. Due to this symmetry, the wires will be at

[2]As in Chapter 3, we assume that there are no fixed charges near the electrode, and that Laplace's equation will be solved within a material that is linear, isotropic, and homogeneous.

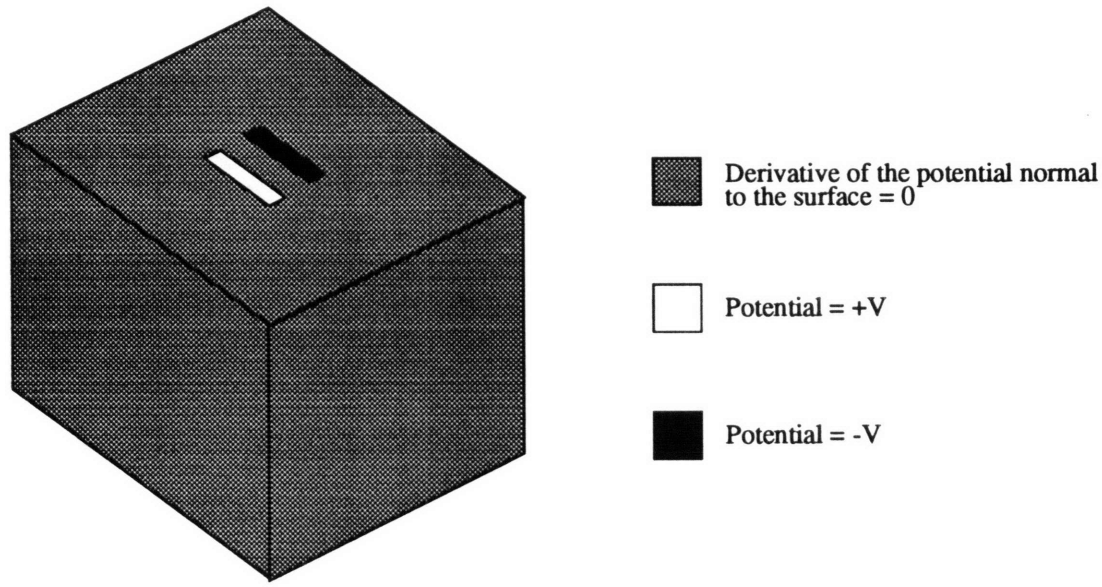

Figure 4-6: Model for predicting the electric fields generated using the stimulating electrode described in this chapter.

equal and opposite voltages when stimuli are applied. The epoxy and glass are modeled as perfect insulators through which no current will flow. This requires that the current density normal to the surface in such regions is zero. Since the normal current density is proportional to the normal derivative of the potential, Neumann boundary conditions are used to represent the non-conducting portions of the electrode tip. Assume further that the remaining portions of the bounding surface are far away from the bipolar electrode. Like the regions of the bounding surface representing insulators, no current will flow through these regions. Neumann boundary conditions are therefore established at these regions as well.

Laplace's equation subject to the boundary conditions described above does not lend itself readily to analytical techniques. However, we may be able to solve this problem efficiently using a numerical algorithm. To facilitate this process, the bounding surface is chosen to be a box. Our model for predicting the electric field produced by the electrode is shown in Figure 4-6. An algorithm for solving this problem has not yet been implemented.

Chapter 5

On experimental verification

Preliminary attempts were made to experimentally test the electrodes of chapter 4. A total of seven experiments were conducted. Two of these were performed by Dr. Ralph Jensen (Southern College of Optometry, Memphis, TN) using a small slice of the rabbit retina. This preparation has been used extensively for other retinal implant project experiments [64], and is described in detail elsewhere [27]. The remaining five experiments were performed by Dr. Lyle Borg-Graham (visiting scientist at MIT during the month of February, 1994; currently at the Institut Alfred Fessard, CNRS, Gif-sur-Yvette, France) and the author using an isolated turtle retina preparation, also described elsewhere [4].

This chapter is divided into three sections. In the first section, three hypotheses which might be tested in an experiment are presented. These will help to motivate the experimental procedures outlined in the second section. Results obtained using the methods described were on the whole inconclusive. This was due in part to the relatively small number of experiments conducted. More importantly, though, results were inconclusive due to several unresolved experimental issues. These will be described in the third section of the chapter. Such issues must be addressed in future experiments if the hypotheses are to be tested in a conclusive manner. For the most part, results from the experiments will not be presented.

5.1 Three hypotheses

It was argued in chapter 4 that the parallel wire electrode could be used to selectively stimulate cell bodies. This argument was based on a comparison made in section 3.4 for the parallel plate electrode. Two additional comparisons for the parallel plates were made in that section. These might also be applicable to the parallel wire electrode.

The comparisons assume that the spacing of the plates is much larger than the space constant of the axon. To a first approximation, this assumption might be modified for the electrodes of chapter 4 by requiring that the spacing of the *wires* is much larger than the space constant. Does this modified assumption hold? Using "typical" values for the electrical properties of nerve membranes, we calculated in chapter 3 that the length constant was about 112μm. From Table 4.1, we see that the wire spacing is just over one length constant for the design 1 electrode and about two length constants for designs 2 and 3. Thus, the assumption does not hold strictly for the electrodes designed in chapter 4.

To bring the electrodes in line with the assumptions of chapter 3, larger wire spacings could have been incorporated into the design. This would have required that the wire length also be larger (see section 4.1), and the resulting electrode tip would have increased

λ_c (μm)	Plate spacing (in λ_c's)	$V_{mla,max}/V_{mta,max}$	$V_{mla,max}/V_{mcb,max}$
112	2 (Designs 2,3)	48	3.2
112	1 (Design 1)	35	2.4
922	1/4 (Designs 2,3)	102	6.8
922	1/8 (Design 1)	54	3.6

Table 5.1: Depolarization ratios for plate spacings corresponding to the electrode designs in chapter 4 and for two different values of the length constant. $V_{mla,max}$ is the maximum depolarization induced in an axon model by a longitudinal field, $V_{mta,max}$ is the maximum depolarization induced by a transverse field, and $V_{mcb,max}$ is the maximum depolarization induced in a cell body model.

in size. As we will see below, small electrodes were desired when positioning the stimulating electrodes. The electrode dimensions listed in Table 4.1 represent a design tradeoff between the constraints of large wire spacing and small electrode tip size.

Table 5.1 summarizes the depolarization ratios which result from several nonideal plate spacings. The first and second rows of the Table present the ratios for plate spacings corresponding to the wire spacings of the chapter 4 electrodes. The length constant used to calculate these ratios was 112μm as before. After the electrodes were constructed, it was discovered that the membrane conductance per unit area for ganglion cell axons may be closer to $1/(68,000\Omega\cdot\text{cm}^2)$ [9], much lower than the value listed in Table 3.2. In this case, the length constant would be 922μm. The resulting depolarization ratios for the chapter 4 electrodes are listed in the third and fourth rows of Table 5.1. Note that, even though the plate spacings are reduced to 1/4 (designs 2 and 3) and 1/8 (design 1) of the length constant, the depolarization ratios are larger than those listed in the first two rows. While increasing the length constant causes a decrease in the effective plate spacing, which would lower $V_{mla,max}$ for a fixed λ_c, we also see from equation (3.29) that $V_{mla,max}$ increases in proportion to λ_c for a fixed d.

Table 5.1 suggests that for all length constants and electrode wire spacings considered, the same qualitative differences in thresholds will be found. The analysis portion of this thesis therefore leads to three hypotheses which can be tested in experiments using the electrodes of chapter 4:

Hypothesis 1 *The threshold for stimulating cell bodies is lower than that for stimulating axons when the electrode wires are parallel to the axons.*

Hypothesis 2 *The threshold for stimulating axons is higher when the electrode wires are parallel to the axons than when when the wires are perpendicular to them.*

Hypothesis 3 *The threshold for stimulating cell bodies is higher than that for stimulating axons when the electrode wires are perpendicular to the axons.*

Note that, unlike in chapter 3 or in Table 5.1, we are not predicting the relative thresholds in quantitative terms. Due to both the large number of assumptions which were made to facilitate analysis (see sections 3.1 and 3.5) and also to the fact that the parallel wires are only an approximation to the parallel plates, we expect that experiments would at best yield qualitative verification of the hypotheses.

5.2 Outline of the experimental procedure

All experiments followed the same basic procedure. This procedure is outlined below:

1. **Dissection.**

   Experiments were done *in vitro*. Retinas were removed from either rabbits, as described in [27], or turtles, as described in [4], and mounted on a holder over which physiological fluids were perfused. Such fluids help to prolong the life of the retina after removal from the eye.

2. **Position the recording and stimulating electrodes.**

   Testing the hypotheses of the previous section requires the use of two types of electrodes. A stimulating electrode, such as those described in chapter 4, is used to deliver current to a ganglion cell, while a recording electrode is used to determine if the cell produced an action potential as a result. In all experiments, the recording electrode was placed outside of but very close to a ganglion cell body or axon. Furthermore, the recording and stimulating electrodes were always placed as far apart from one another as possible to circumvent the problem of stimulus artifact, which will be discussed in section 5.3.

   Experimental efforts concentrated mainly on Hypothesis 2 above. To test this hypothesis, the recording electrode was positioned near a cell body, and stimuli were delivered to the axon at a distant location. Action potentials generated by the stimulating electrode and picked up by the recording electrode in this arrangement were conducted *antidromically*, or towards the cell body. The stimulating electrode was oriented so that the wires were either parallel to the axon, as in Figure 5-1a, or perpendicular to the axon, as in Figure 5-1b.

   In order to test Hypotheses 1 or 3, it would be necessary to record action potentials from the axon at a location near the optic disk. In this case the stimulating electrode would be placed closer to the cell body. Action potentials generated by the stimulating electrode and picked up by the recording electrode in this arrangement would be conducted *orthodromically*, or away from the cell body. The stimulating electrode would either be placed over the cell body, as in Figure 5-1c, or over a segment of the axon, as in Figure 5-1d. Note that the stimulating electrode in Figure 5-1d is oriented so that the wires are parallel to the axon. This orientation would be used to test Hypothesis 1. To test Hypothesis 3, the electrode wires would be oriented perpendicular to the axon (not shown).

3. **Determine threshold.**

   The amplitude of the stimulus was then adjusted until the minimum amount of current required to produce action potentials was found.

4. **Move the stimulating electrode.**

   The stimulating electrode was then shifted from one of the positions and orientations described above to another, and threshold determination repeated.

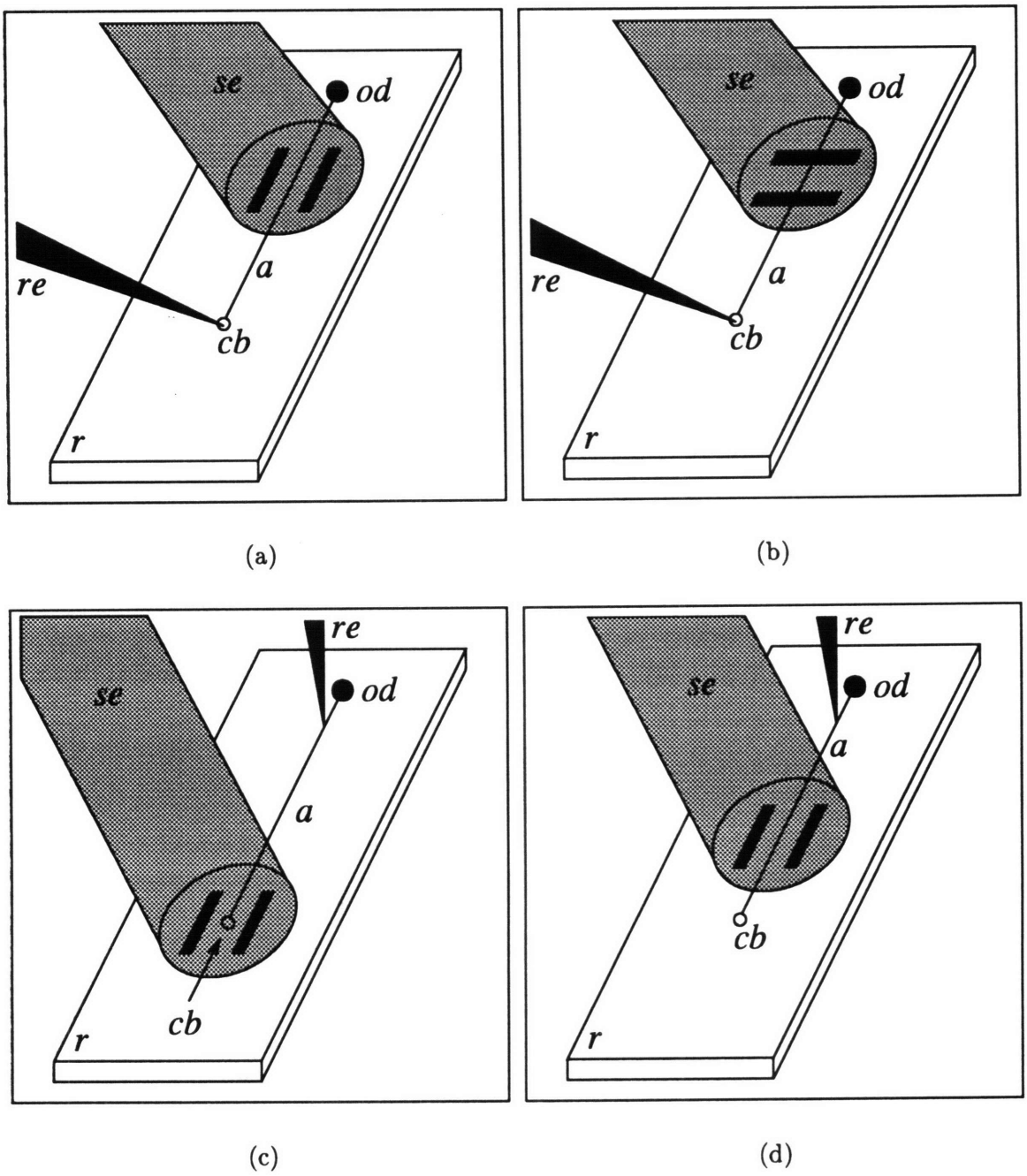

Figure 5-1: Schematic diagrams illustrating several arrangements of the recording and stimulating electrodes. Abbreviations: *cb* - cell body; *a* - axon; *od* - optic disk; *re* - recording electrode; *se* - stimulating electrode; *r* - retina.

5.3 Unresolved experimental issues

Several difficulties were encountered during experimentation which hindered our ability to obtain conclusive results. Many of these point to problems with our current experimental methods which have yet to be resolved. A discussion of these unresolved experimental issues is undertaken in this section.

5.3.1 Stimulus artifact

When current is applied to the stimulating electrode in preparations such as those of Figure 5-1, electrical activity is invariably picked up by the recording electrode. This activity is called the *stimulus artifact.* The stimulus artifact may outlast the stimulating current itself and can be substantially larger than extracellularly recorded action potentials. The former effect is thought to be due to saturation of recording amplifiers [46]. Because action potentials propagate along an axon with a finite velocity, it will take a finite amount of time for them to travel from their site of origin, near the stimulating electrode, to the recording electrode. If the two electrodes are placed far enough apart, the artifact will have died out by the time action potentials are recorded. This was the case for the experiments on rabbit retina, where the distance separating the electrodes was about 1cm. If the stimulating and recording electrodes are fairly close to one another, on the other hand, action potentials will arrive at the recording electrode while the stimulus artifact is still dominant. This was the case for the turtle retina experiments, where electrode separation was less than 0.5mm. Unfortunately, the stimulating and recording electrodes could not be placed further apart due to the small size of the turtle retina preparation. In this second case, we could not tell whether or not we were generating action potentials because, if they were occurring, they were obscured by the stimulus artifact.

5.3.2 Position of the stimulating electrode relative to the cell

The locations of ganglion cells were not known *a priori.* Had we been able to visually identify cells under a microscope, the recording and stimulating electrodes could have been positioned as discussed in section 5.2 in a straightforward manner. With the exception of the rabbit retinal ganglion cell axons, however, the cells of the rabbit and turtle retinas are completely transparent. The rabbit axons are ensheathed in white myelin near the optic disk, but are also grouped in clusters which makes them hard to identify individually. On the other hand, various staining techniques have been used for visualizing cell bodies. For example, see [28]. It was found that the staining process altered the sensitivity of cells to electrical stimuli [26]. For this reason, we did not stain ganglion cells in our experiments.

Because the locations of individual cells were unknown, a certain amount of guesswork was required when positioning the recording and stimulating electrodes. The recording electrode, for example, was positioned by repeatedly lowering it onto different portions of the retina until it was close enough to a cell body or axon to record action potentials from it reliably. This method, though at times tedious, was fairly consistent. More problematic was the positioning of the stimulating electrode.

Position in the plane of the retina

The placement of the stimulating electrode in the plane of the retina depended in part on the position of the recording electrode. For example, if recordings were being made from a

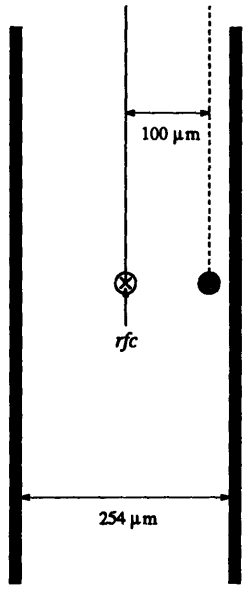

Figure 5-2: Two possible positions of the cell body (white and shaded circles). A stimulating electrode with wire spacing 254μm centered over the receptive field center (*rfc*).

cell body, as in Figures 5-1c and 5-1d, the path of the axon was approximated as the straight line from the recording electrode to the optic disk. On the other hand, if recordings were being made from an axon, as in Figures 5-1a and 5-1b, the cell body location was inferred from the location of the cell's receptive field center, and the axon was assumed to follow the straight line between the cell body and recording electrode. The stimulating electrode was placed over the desired region of retina based on these approximations.

An example will help to illustrate the potential difficulties involved in the placement methods described above. Consider an experiment in which we wish to stimulate a ganglion cell near the cell body, as in Figure 5-1c. The exact location of the cell body is unknown, but the center of the cell's receptive field can be determined by shining a small spot of light on different parts of the retina while monitoring cellular responses with the recording electrode. For rabbit retina, we estimate that ganglion cell bodies are within about 100μm (in the plane of the retina) of the cell's receptive field center [26]. Suppose that, in the absence of more detailed knowledge of the cell body location, a stimulating electrode with wire spacing 254μm (design 2 or design 3) is centered over the receptive field center. Figure 5-2 illustrates both the ideal situation, in which the cell body (white circle) is at the same location as the receptive field center, and a less desirable situation, in which the cell body (shaded circle) is displaced 100μm from the receptive field center.

The stimulating fields experienced by the cell in the two cases may be quite different, leading to ambiguities in the interpretation of thresholds. If the cell is centered between the wires, for instance, we might expect the uniform field approximation to be a good one. On the other hand, if the cell is closer to one of the electrode wires, we might expect fringing fields to be substantial (see Figure 4-2 for hypothesized stimulating fields). Since the position of the stimulating electrode relative to the cell will determine the shape of the effective stimulating field, we might expect thresholds to vary with electrode position.

However, since for a given experiment the electrode position relative to the cell is unknown, we would be unable to determine which thresholds corresponded to which positions.

Ambiguities of this sort might be eliminated if the stimulating electrode wires were spaced far enough apart. However, increasing the wire spacing will increase the overall size of the electrode tip. To some extent, our ability to place the electrode over the receptive field center accurately depends on the size of the electrode tip. The larger the tip, the less accurate electrode placement will be.

Another way to tackle this problem might be to record the thresholds at a series of points on the retinal surface, and then try to deduce the location of a cell body or axon by hypothesizing how the thresholds will change with position. This strategy involves moving the stimulating electrode from its initial position, which entails additional complications. These are considered in section 5.3.3.

Placement above the retina

The discussion thus far has focused on the position of the electrode relative to the cell in the plane of the retina. The height of the electrode above the cell is also an important consideration in the interpretation of threshold measurements. In general, we expect the threshold to rise as the electrode height is increased, since an increase in the electrode-to-cell distance is accompanied by a decrease in the effective stimulating field. In order to impose some measure of consistency on the electrode-to-cell height, attempts were made to place the stimulating electrode directly against the inner limiting membrane. Using such a scheme, the variability in the vertical electrode to cell height is constrained to the variation of cell body or axon depths within their respective layers (see Figure 2-3).

Two different methods were used to place the electrode against the inner limiting membrane. In both cases, the task amounted to lowering the electrode as close to the retina as possible without compressing so much that cell damage resulted. The first method, used with the turtle preparation, involved lowering the electrode under visual control. As the electrode was lowered, we watched for visible signs that the edges of the electrode tip were compressing the retina. It was important for the electrode tip to have small diameter for this method, so that the entire tip could be seen at a reasonably high magnification. In general, this method was complicated by the fact that the retina itself is transparent, and also by the fact that the optics were often blurred by the electrode tip or by the fluids flowing over the retina. It remains unclear whether or not the electrode tip was indeed against the inner limiting membrane when this method was used. The second method, used with the rabbit retina, relied on threshold information to infer electrode height. Thresholds were measured as the electrode was moved progressively closer to the retina. Up until a certain point, thresholds decreased as the electrode was lowered. When the threshold stopped decreasing, the electrode was assumed to be apposed to or slightly compressing the inner limiting membrane.

Control experiment

A control experiment was performed to determine the precision of the second method. Using that method, the electrode was repeatedly lowered onto and withdrawn from the same spot on the retinal surface using a micromanipulator. The micromanipulator could be used to maneuver the electrode in any of three orthogonal directions, the manipulator *axes*. Motion along each axis was controlled with a separate knob, and the distance moved in each

Trial	Threshold (μA)	z-micrometer (mm)
1	140	6.740
2	160	6.694
3	165	6.712
4	165	6.743

Table 5.2: Results from a control experiment conducted to determine how precisely the electrode could be placed against the inner limiting membrane using the second method described in the text. Lifting the electrode off of the retina corresponded to lowering the micrometer reading. Trials are listed in chronological order.

direction could be measured from a micrometer. A single direction, which we referred to as z and which was approximately perpendicular to the table, was used in this experiment. Each time the final height was determined, with the electrode presumably against the inner limiting membrane, the threshold and z-micrometer reading were recorded. Table 5.2 summarizes these results.

Several observations may be made from the Table. Most importantly, the final z-micrometer readings for the 4 trials varied over a range of about 50μm. Assuming that the inner limiting membrane had not moved relative to the table on which the micromanipulator rested, this value would ideally have been constant. Is 50μm a tolerable amount of uncertainty? In other work, such a difference in electrode height led on the average to a 2.5-fold increase in threshold [64]. We see from Table 5.2 that the total change in threshold over the 4 trials amounted to a less dramatic increase. However, note that in this experiment the threshold did not necessarily increase with the electrode height. From Trial 2 to Trial 3, the electrode was lowered 18μm closer to the retina while the threshold increased by 5μA. Rather than increasing with electrode height, the thresholds appear to be increasing with time. We will return to this subject in section 5.3.4.

On the whole, the control experiment was inconclusive. Thus the precision of the second method described above for placing the stimulating electrode against the inner limiting membrane still remains in doubt.

5.3.3 Movement of the stimulating electrode

It was often necessary to move the stimulating electrode from its initial position and orientation to another one. This might have been done to determine the location of a cell as described above, or simply in order to shift the stimulating electrode between the arrangements of Figure 5-1. In order to avoid dragging the retina, the electrode was lifted off of the tissue before making such changes, and then then lowered again.

In order to properly interpret changes in threshold with electrode position or orientation, we must have a detailed knowledge of how the electrode moved relative to the cell. To illustrate this point, consider an experiment to test Hypothesis 2. Cross sectional views of the stimulating electrode in the configurations of Figures 5-1a and 5-1b are shown in Figures 5-3a and 5-3b, respectively. Suppose that, as drawn in Figure 5-3, the height of the electrode has been inadvertently raised after rotation of the wires. If the threshold rose from Figure 5-3a to Figure 5-3b, we would not be able to conclude whether the increase was

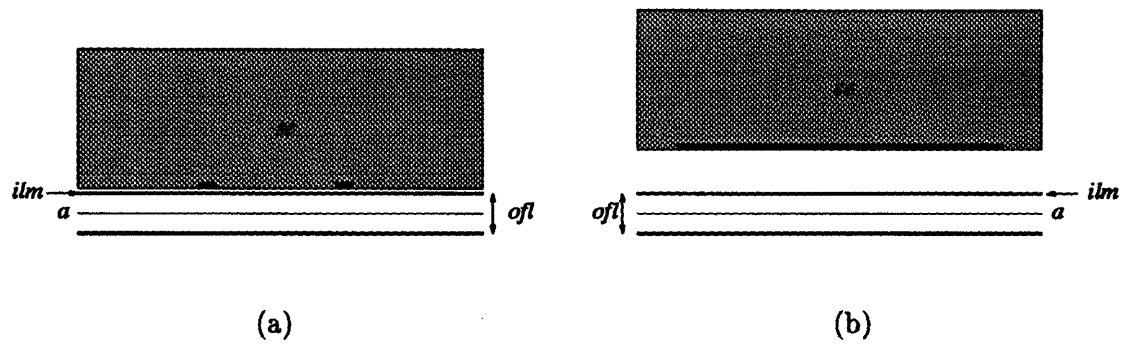

Figure 5-3: Examples of electrode placement over the retina. (a) Electrode oriented so that its wires are perpendicular to an axon, as in Figure 5-1a; (b) electrode oriented so that its wires are parallel to the axon, as in Figure 5-1b. Abbreviations: *a* - axon; *se* - stimulating electrode; *ilm* - inner limiting membrane; *ofl* - optic nerve fiber layer.

due to the change in electrode orientation or to the increase in electrode height. Results would be inconclusive in this case.

A further objection to moving the stimulating electrode is that, as mentioned above, it must be lifted off of and then lowered back down onto the retina. If it were lifting or compressing the retina in the process, this might result in cell damage. Again ambiguities would arise in the interpretation of threshold measurements. Thresholds might increase due either a change in electrode position or due to cell damage.

Finally, a warning must be made about moving the electrode "in the plane of the retina". In order to facilitate fluid flow over the rabbit retina, the retina was mounted at a 30° angle from the horizontal. If the micromanipulator axes were not properly aligned, movements of the stimulating electrode might be misinterpreted. For example, Figure 5-4 depicts the case in which one of the micromanipulator axes - call it the y-axis - is aligned so that motion in the corresponding direction is parallel to the table. Since the retina is at an angle, moving the micromanipulator arm 50μm in the y direction corresponds to a somewhat larger displacement in the plane of the retina, as shown in the Figure.

5.3.4 Variations with time

When the retina is removed from the turtle or rabbit, its cells begin to die. In a typical experiment using a rabbit retina, stable light-evoked responses may be recorded many hours after removal of the retina. It was sometimes noted in experiments, however, that with all of the stimulus parameters held constant, thresholds increased significantly over the course of several minutes. The fact that thresholds varied over such a short time interval indicates that the properties of some element in the experimental apparatus are changing with time. The most likely candidates for such behavior are the electrode tip and the cell itself. The passage of current through the electrode will tend to corrode its surface to some extent. Furthermore, the health of the cell might be comprised by stimulation, either due to toxic byproducts produced at the electrode tip or from fatigue due to continuous stimulation. Corrosion and toxicity problems may be reduced through the use of biphasic, charge-balanced pulses [12]. In general, though, more control experiments need to be done

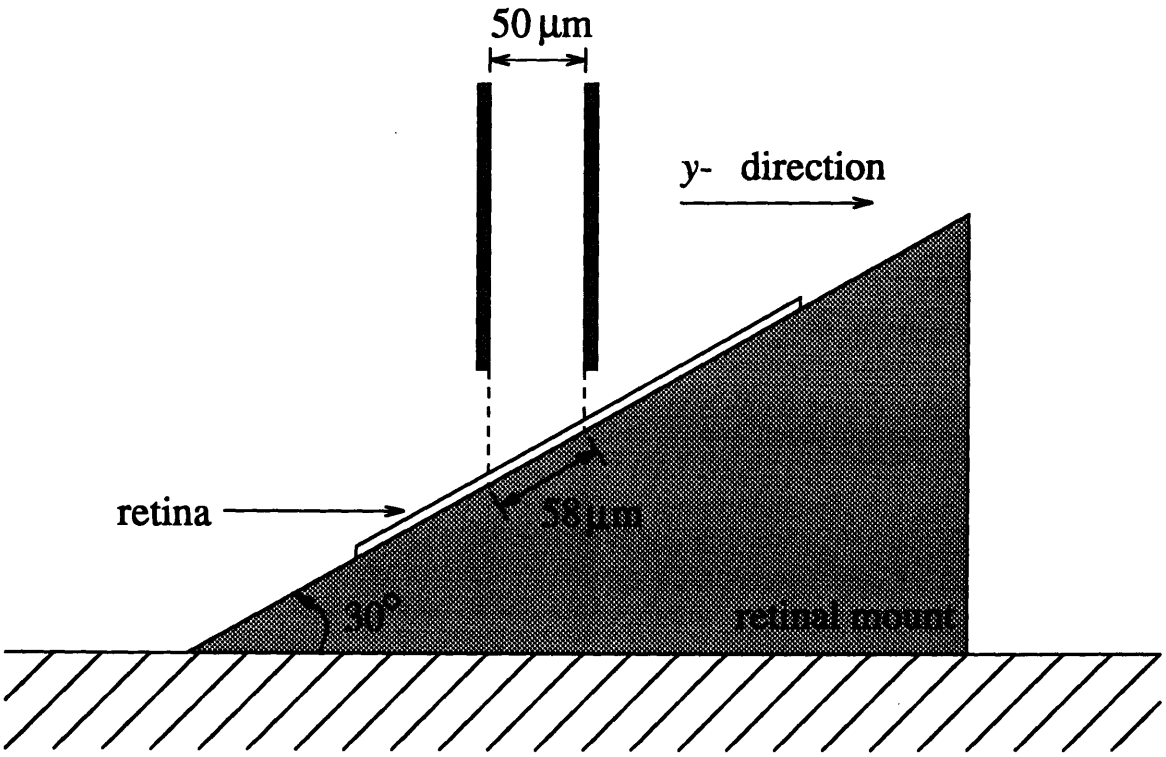

Figure 5-4: Movement of the stimulating electrode in a direction which is not parallel to the retina.

to investigate variations with time in our experimental apparatus.

Chapter 6

Conclusion

6.1 Summary

Through a discussion of the retina and of the retinal implant, Chapter 2 provided the relevant background material for the thesis. In this chapter, the anatomy and physiology of the retina were discussed, the motivation for and a functional description of the retinal implant were given, and the literature on electrical stimulation of retinal cells was reviewed. The chapter concluded with a formulation of the thesis problem. This problem was addressed in the following chapters using a combination of theoretical and experimental approaches. In Chapter 3 the theory of extracellular electrical stimulation was examined. Threshold comparisons were made based on the analysis of linear models of nerve cells in steady-state elèctric fields of fairly simple shape. The design and construction of a practical stimulating electrode, which we believe can be used for selective stimulation of ganglion cell bodies, is presented in Chapter 4. At the end of the chapter, a model for numerically predicting the electric fields produced by the electrode was presented. Finally, Chapter 5 describes the experiments that were performed to test three hypotheses stemming from the results of Chapter 3. For a number of reasons presented at the end of the chapter, these experiments yielded inconclusive results. The results themselves were not presented.

6.2 Suggestions for further study

Opportunities arose frequently during the course of this work to pursue some new line of inquiry, to refine the electrode design or construction, or to improve on our experimental methods. Many of these opportunities were not taken for one reason or another, and are therefore presented below as suggestions for future study.

6.2.1 Modeling and analysis

A number of fairly strong assumptions were made to facilitate the analysis of Chapter 3. A natural extension of this work would be to determine if any if these assumptions might be relaxed without making the problem analytically intractable. Some initial steps are taken to do this in appendices A and B, where the time-dependent responses of the linear cell models are examined. It was discovered in appendix A that the quasistatic models of the cell body and axon (in a transverse field) had time constants which were roughly a factor of 1000 smaller than the membrane RC time constant. Additional thought should be given

to the astonishing rapidity at which these models reach steady-state.

Other assumptions might be tackled numerically. Consider for instance the circuit model for the axon in a longitudinal field. To analyze the effects of a parallel-plate electrode on this model, we assumed that the axon itself did not play a role in determining the extracellular voltages. We would not expect this assumption to hold in a strict sense. To what extent would the axon model influence the extracellular electric field?

The problem amounts to solving Laplace's equation at the exterior surface of the model. In appendix A, a three-dimensional electroquasistic model for an unmyelinated axon was analyzed in a uniform, transverse electric field. Due to the symmetries of the model and of the stimulating field, analytical solutions for Laplace's equation could be found in a straightforward manner. Solutions which account for longitudinally nonuniform boundary conditions would be substantially more complex. Thus a numerical algorithm might be employed to find such solutions.

A second numerical problem was introduced at the end of Chapter 4. To predict the electric fields generated by the experimental stimulating electrode, a set of boundary conditions on Laplace's equation were established. A numerical algorithm has yet to be implemented to find the unique solution entailed by these boundary conditions.

6.2.2 Electrode construction

Three significant improvements can be made in the construction of single electrodes described in Chapter 4. First, the Clear 2-Ton epoxy (used to encapsulate the electrode and to cement it into the glass tube) leaves much to be desired. A harder-curing epoxy would be less susceptible to smearing during tip-grinding. When the 2-Ton epoxy smeared onto the electrode conductor surfaces, it might have changed their electrical properties, potentially altering the effective electrode geometry. Ideally the epoxy should not soften after prolonged exposure to salt water, either. Soft epoxy might be smeared over conductor surfaces in the course of electrode manipulation during an experiment. Again, this could lead to an alteration of the effective electrode geometry. Second, an alternative to glass needs to be found for the electrode housing. The glass capillary tubes were quite fragile and broke far too often. If a small metal tube (such as a hypodermic needle) is used, it will be necessary to insulate the conductor-insulator-conductor sandwich to circumvent stray shorts to the housing. Third, attempts could be made plate the electrode tip. Plating electrode tips using colloidal suspensions of gold or platinum black will lower the tip resistance, and possibly reduce the likelihood of tip corrosion and/or subsequent toxicity problems.

6.2.3 Experimental methods

If the experimental procedures described in Chapter 5 are to be continued, systematic attempts should be made to address each of the unresolved issues raised at the end of the chapter. More controls - and more experiments in general - need to be performed.

The problems with stimulus artifact encountered in the turtle preparation might be solved if the recording and stimulating electrodes could be placed further apart. Unfortunately, the size of the preparation is quite small to begin with (two to three millimeters in diameter), making this solution impractical. Given the constraint of a relatively small electrode separation, attempts might be made to minimize the amplitude and duration of the stimulus artifact. It was suggested in section 5.3, for example, that stimulus artifacts outlast stimulus pulses due to saturation of the recording amplifiers. If this is indeed the

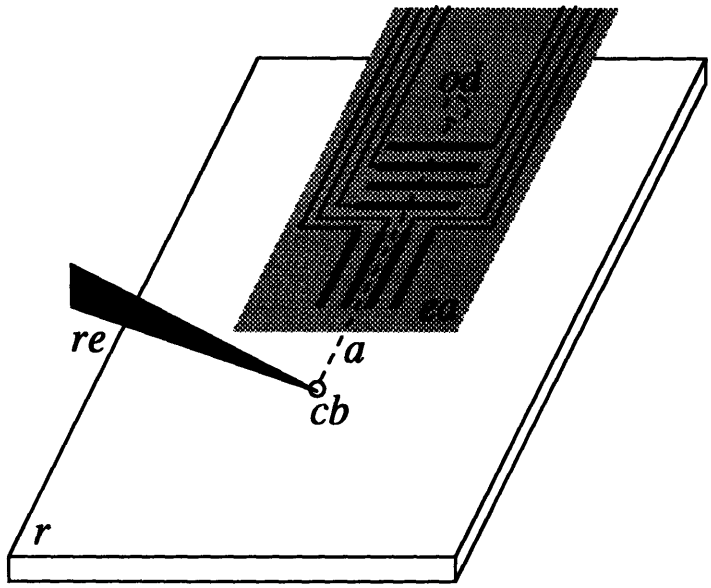

Figure 6-1: Stimulation of the retina with an electrode array (shaded). The thicker black lines on the array represent exposed conductor surfaces, while the thin lines represent wires which are insulated from the tissue. Abbreviations: *r* - retina; *a* - axon; *cb* - cell body; *od* - optic disk; *ea* - electrode array; *re* - recording electrode.

case, the duration of the artifacts might be minimized by disconnecting the leads of the recording electrode from the amplifiers during the application of stimulus pulses.

Other unresolved issues might be addressed successfully using an array of stimulating electrodes, such as that depicted in Figure 6-1. Rather than moving a stimulating electrode physically, the electrode could be moved "virtually" by connecting the stimulator across different pairs of conductors within the array. If the array is placed against the inner limiting membrane, variations in the electrode height above cells would be constrained to the biological variability of cell depth within the retina. This would remedy ambiguities of the sort illustrated in Figure 5-3. With the electrode free to move, the positions of cell bodies and axons might be deduced by plotting out thresholds obtained with the stimulating electrode in several different locations.

Appendix A

Additional mathematical derivations

A.1 Time dependent responses of cell body in a uniform field

Equations (3.3)-(3.8) describe a dynamic system. What type of response will it exhibit if the driving field $E_o(t)$ is not constant in time? In this section the time-dependent response of the plate/cell body system will be examined. This analysis will be directed at finding the time constants of the system and also on finding a circuit representation for the system dynamics.

In order to understand the time-dependent response of this system in terms of a circuit model, it is helpful to solve equations (3.3)-(3.8) in for the surface charge densities σ^i_{su} and σ^e_{su}. To do this it will be necessary to eliminate a, b, c, and d. First, solve for b and c in terms of a and d using equations (3.3) and (3.4).

$$\begin{aligned} b &= a - \frac{(R+\Delta)^3}{(R+\Delta)^3 - R^3}\left[a - \frac{d}{(R+\Delta)^3} + E_o(t)\right], \\ c &= \frac{(R+\Delta)^3 R^3}{(R+\Delta)^3 - R^3}\left[a - \frac{d}{(R+\Delta)^3} + E_o(t)\right]. \end{aligned}$$

Substitute these formulas for b and c into equations (3.5) and (3.6) and collect terms.

$$\begin{aligned} a\left[\epsilon_f + \epsilon_m \frac{2(R+\Delta)^3 + R^3}{(R+\Delta)^3 - R^3}\right] + \frac{d}{(R+\Delta)^3}\left[-\epsilon_m \frac{3(R+\Delta)^3}{(R+\Delta)^3 - R^3}\right] \\ = \frac{\sigma^i_{su}}{\cos\theta} + E_o(t)\left[-\epsilon_m \frac{3(R+\Delta)^3}{(R+\Delta)^3 - R^3}\right], \\ a\left[-\epsilon_m \frac{3R^3}{(R+\Delta)^3 - R^3}\right] + \frac{d}{(R+\Delta)^3}\left[2\epsilon_f + \epsilon_m \frac{(R+\Delta)^3 + 2R^3}{(R+\Delta)^3 - R^3}\right] \\ = \frac{\sigma^e_{su}}{\cos\theta} + E_o(t)\left[-\epsilon_f + \epsilon_m \frac{(R+\Delta)^3 + 2R^3}{(R+\Delta)^3 - R^3}\right]. \end{aligned}$$

The above equations can be greatly simplified by factoring a Δ out of the denominators,

$$(R+\Delta)^3 - R^3 = \Delta(3R^2 + 3R\Delta + \Delta^2),$$

noting the definition of membrane capacitance per unit area,

$$C_m = \epsilon_m/\Delta,$$

and using the approximation $\Delta \approx 0$ since $\Delta \ll R$. The results of the simplification are as follows.

$$a(\epsilon_f + C_m R) + d\left(\frac{-C_m}{R^2}\right) = \frac{\sigma^i_{su}}{\cos\theta} + E_o(t)(-C_m R), \tag{A.1}$$

$$a(-C_m R) + d\left(\frac{2\epsilon_f}{R^3} + \frac{C_m}{R^2}\right) = \frac{\sigma^e_{su}}{\cos\theta} + E_o(t)(-\epsilon_f + C_m R). \tag{A.2}$$

[Note in the above equations that if $\epsilon_f \ll C_m R$, $\sigma^i_{su} \approx -\sigma^e_{su}$ and we no longer have a second order system.]

b and c can be eliminated from equations (3.7) and (3.8) in a nearly identical manner, but this time using the definition of membrane conductance per unit area,

$$G_m = \sigma_m/\Delta.$$

The results are as follows

$$a(\sigma_i + G_m R) + d\left(-\frac{G_m}{R^2}\right) = -\frac{\dot{\sigma}^i_{su}}{\cos\theta} + E_o(t)(-G_m R), \tag{A.3}$$

$$a(-G_m R) + d\left(\frac{2\sigma_e}{R^3} + \frac{G_m}{R^2}\right) = -\frac{\dot{\sigma}^e_{su}}{\cos\theta} + E_o(t)(-\sigma_e + G_m R). \tag{A.4}$$

Now solve equations (A.3) and (A.4) for a and d. In matrix notation,

$$\begin{bmatrix} a \\ d \end{bmatrix} = -\left(\frac{R^3}{\cos\theta}\right) \frac{\begin{bmatrix} \frac{2\sigma_e}{R^3} + \frac{G_m}{R^2} & \frac{G_m}{R^2} \\ G_m R & \sigma_i + G_m R \end{bmatrix} \begin{bmatrix} \dot{\sigma}^i_{su} \\ \dot{\sigma}^e_{su} \end{bmatrix}}{2\sigma_i\sigma_e + 2\sigma_e G_m R + \sigma_i G_m R} + \frac{\begin{bmatrix} -\frac{3\sigma_e G_m}{R^2} \\ -\sigma_i\sigma_e \end{bmatrix} R^3 E_o(t)}{2\sigma_i\sigma_e + 2\sigma_e G_m R + \sigma_i G_m R}. \tag{A.5}$$

Substituting the above result into equations (A.1) and (A.2) yields the following ordinary differential equation in surface charge density.

$$-\frac{\begin{bmatrix} \epsilon_f + C_m R & -C_m R \\ -C_m R & 2\epsilon_f + C_m R \end{bmatrix} \begin{bmatrix} 2\sigma_e + G_m R & G_m R \\ G_m R & \sigma_i + G_m R \end{bmatrix} \begin{bmatrix} \dot{\sigma}^i_{su} \\ \dot{\sigma}^e_{su} \end{bmatrix}}{2\sigma_i\sigma_e + 2\sigma_e G_m R + \sigma_i G_m R} = \begin{bmatrix} \sigma^i_{su} \\ \sigma^e_{su} \end{bmatrix} + \begin{bmatrix} f_1 \\ f_2 \end{bmatrix} E_o(t)\cos\theta, \tag{A.6}$$

where

$$f_1 = \frac{3\epsilon_f\sigma_e G_m R + \sigma_e G_m C_m R^2 - \sigma_i C_m G_m R^2 - 3\sigma_i\sigma_e C_m R}{2\sigma_i\sigma_e + 2\sigma_e G_m R + \sigma_i G_m R}, \tag{A.7}$$

$$f_2 = \frac{-2\epsilon_f\sigma_e G_m R - \sigma_e G_m C_m R^2 + \sigma_i C_m G_m R^2 + 3\sigma_i\sigma_e C_m R - \epsilon_f\sigma_i G_m R}{2\sigma_i\sigma_e + 2\sigma_e G_m R + \sigma_i G_m R}. \tag{A.8}$$

Two important pieces of information come out of equation (A.6). The first is a circuit representation of the nerve membrane dynamics. [not sorted out yet, but see Figure A-1].

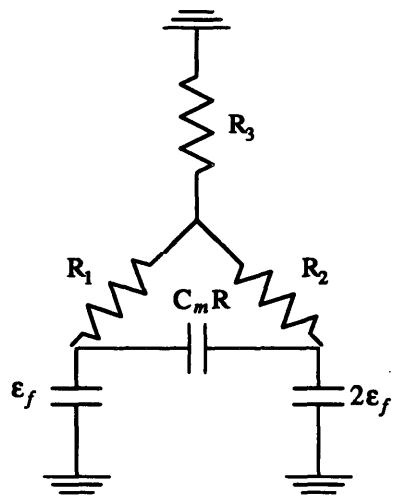

$$R_1 = \frac{2\sigma_e}{2\sigma_i\sigma_e + 2\sigma_e G_m R + \sigma_i G_m R}$$

$$R_2 = \frac{\sigma_i}{2\sigma_i\sigma_e + 2\sigma_e G_m R + \sigma_i G_m R}$$

$$R_3 = \frac{G_m R}{2\sigma_i\sigma_e + 2\sigma_e G_m R + \sigma_i G_m R}$$

Figure A-1: Circuit model for spherical cell.

The second important piece of information that can be obtained from equation (A.6) are the time constants of the system. The equation is of the general form

$$-A\,\dot{\mathbf{x}} = \mathbf{x} + \text{drive terms},$$

where A is a 2 by 2 matrix. The time constants of the system are simply the eigenvalues of the A matrix. Using the approximation that $\epsilon_f \ll C_m R$ to simplify things, it can be shown that

$$\tau = 0,\ \frac{C_m R(\sigma_i + 2\sigma_e)}{2\sigma_i\sigma_e + G_m R(\sigma_i + 2\sigma_e)}. \tag{A.9}$$

The zero-valued time constant is nonzero if the above approximation is not made. The zero-valued time constant represents a very fast equilibration of the two surface charge densities, σ^i_{su} and σ^e_{su}. The second time constant can be rewritten,

$$\frac{1}{\tau_2} = \frac{1}{R_m C_m} + \frac{2\sigma_i\sigma_e}{C_m R(\sigma_i + 2\sigma_e)}, \tag{A.10}$$

where

$$R_m = \frac{1}{G_m}$$

is the membrane sheet resistance. The first expression appearing on the right of equation (A.10) resembles a circuit RC time constant for the membrane. The second expression is determined by the membrane capacitance C_m but also by the radius of the cell R and the intracellular and extracellular conductivities σ_i and σ_e. To get an idea of the size of these quantities, we use the typical cell data listed in Table A.1. Also, the radius of a typical ganglion cell body is $R = 10^{-5}$m. Using these data,

$$\frac{1}{R_m C_m} = 10^3 \text{ s},$$

$$\frac{2\sigma_i\sigma_e}{C_m R(\sigma_i + 2\sigma_e)} = 4.44 \times 10^6 \text{ s},$$

$R_m = 1000\Omega \cdot \text{cm}^2$	$C_m = 1 \times 10^{-6}\text{F/cm}^2$
$\sigma_e = 0.02$ S/cm	$\sigma_i = 0.005$ S/cm

Table A.1: Typical cell data. From Cartee and Plonsey (1992)

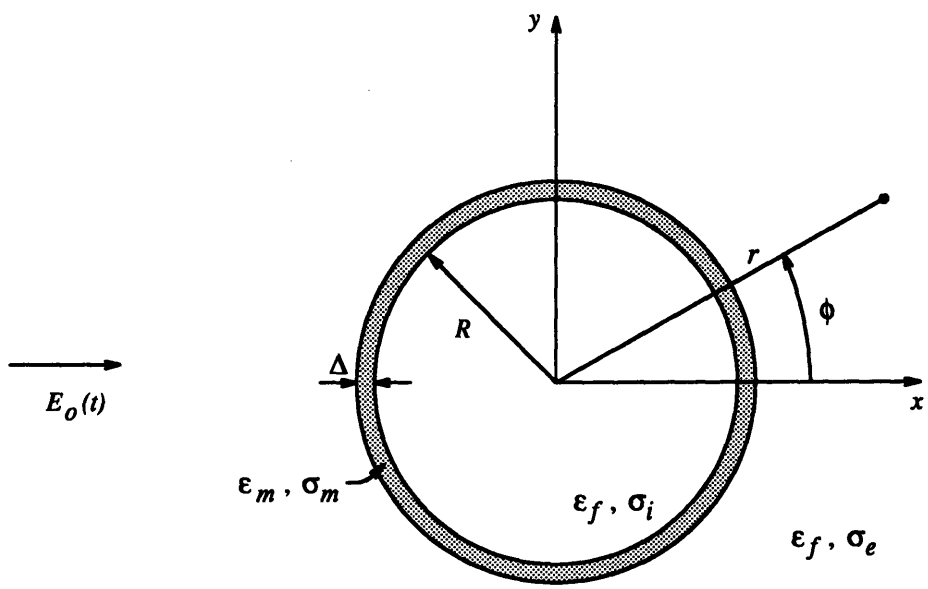

Figure A-2: Axon model.

$$\tau_2 = 2.25 \times 10^{-7} \text{ s.}$$

In such a case, the second term dominates the τ_2, making it much smaller than the $R_m C_m$ product.

A.2 Axon in a uniform, transverse field

The same approach that was used to analyze the cell body in sections 3.2 and A.1 will now be applied to the axon.

A.2.1 Solution form and boundary conditions

An axon is modeled as an infinitely long cylindrical shell, as shown in Figure A-2.

The solution for the electric potential is of the form

$$\Phi = \begin{cases} a(t) r \cos\phi & \text{for } r < R, \\ b(t) r \cos\phi + \frac{c(t)}{r} \cos\phi & \text{for } R < r < R + \Delta, \\ -E_o(t) r \cos\phi + \frac{d(t)}{r} \cos\phi & \text{for } r > R + \Delta. \end{cases} \tag{A.11}$$

Before the boundary conditions for the problem are established, a couple of comments will be made about the solution form. First, for large r, the potential is approximately

$-E_o(t)r\cos\phi$ or simply $-E_o(t)x$. This agrees with the previously established condition that the field is uniform and horizontally directed far from the cell. Second, note that there is no z-variation in the potential. This is due to the uniformly applied field and infinite length of the axon model. More importantly, it points to the relative simplicity of the solution, which for other applied fields and axon geometries would likely be a modal expansion in polar coordinates. Now we will establish the boundary conditions which apply to the solution given above.

The functions $a(t), b(t), c(t)$ and $d(t)$ can be related to each other and to the surface charge densities on the membrane:solution boundaries using continuity conditions established in subsection 3.2.1. Using the definition of electric potential, equation (3.2), the first of the three continuity conditions becomes

$$\frac{\partial\Phi^a}{\partial\phi} = \frac{\partial\Phi^b}{\partial\phi}.$$

The remaining two continuity conditions simplify to

$$-\epsilon_a\frac{\partial\Phi^a}{\partial r} + \epsilon_b\frac{\partial\Phi^b}{\partial r} = \sigma_{su},$$

$$-\sigma_a\frac{\partial\Phi^a}{\partial r} + \sigma_b\frac{\partial\Phi^b}{\partial r} = -\dot{\sigma}_{su},$$

as before. Note that in this Section r represents the polar coordinate radius as defined in Figure (A-2), whereas in the previous section r represented the spherical coordinate radius as defined in Figure (3-3).

Application of the continuity conditions at $r = R$ and $r = R + \Delta$ yield the following equations.

$$bR + \frac{c}{R} = aR, \tag{A.12}$$

$$-E_o(t)(R+\Delta) + \frac{d}{R+\Delta} = b(R+\Delta) + \frac{c}{R+\Delta}, \tag{A.13}$$

$$-\epsilon_m\left(b - \frac{c}{R^2}\right)\cos\phi + \epsilon_f a\cos\phi = \sigma^i_{su}, \tag{A.14}$$

$$-\epsilon_f\left[-E_o(t) - \frac{d}{(R+\Delta)^2}\right]\cos\phi + \epsilon_m\left[b - \frac{c}{(R+\Delta)^2}\right]\cos\phi = \sigma^e_{su}, \tag{A.15}$$

$$-\sigma_m\left(b - \frac{c}{R^2}\right)\cos\phi + \sigma_i a\cos\phi = -\dot{\sigma}^i_{su}, \tag{A.16}$$

$$-\sigma_e\left[-E_o(t) - \frac{d}{(R+\Delta)^2}\right]\cos\phi + \sigma_m\left[b - \frac{c}{(R+\Delta)^2}\right]\cos\phi = -\dot{\sigma}^e_{su}. \tag{A.17}$$

In the above equations, $a = a(t)$, $b = b(t)$, $c = c(t)$, $d = d(t)$, and σ^i_{su} and σ^e_{su} are the surface charge densities on the intracellular and extracellular membrane:solution boundaries, respectively. These equations completely describe a linear time-invariant system in six variables (a, b, c, d, σ^i_{su}, and σ^e_{su}) which can be solved completely for a given $E_o(t)$.

A.2.2 Time-independent solution

If the applied field is held constant at E_o, and the system described above is in steady state, the time derivatives in equations (A.16) and (A.17) will be zero. In such a case, equations (A.12),(A.13), (A.16), and (A.17) can be solved for a, b, c, and d.

From equations (A.12) and (A.13), it can be shown that

$$b = a - \frac{(R+\Delta)^2}{(R+\Delta)^2 - R^2}\left[a - \frac{d}{(R+\Delta)^2} + E_o\right], \tag{A.18}$$

$$c = \frac{(R+\Delta)^2 R^2}{(R+\Delta)^2 - R^2}\left[a - \frac{d}{(R+\Delta)^2} + E_o\right]. \tag{A.19}$$

Substituting into equations (A.16) and (A.17), noting that the time derivatives are zero, and collecting terms yields

$$a\left[\sigma_i + \sigma_m \frac{(R+\Delta)^2+R^2}{(R+\Delta)^2-R^2}\right] + \frac{d}{(R+\Delta)^2}\left[-\sigma_m \frac{2(R+\Delta)^2}{(R+\Delta)^2-R^2}\right] = E_o\left[-\sigma_m \frac{2(R+\Delta)^2}{(R+\Delta)^2-R^2}\right],$$

$$a\left[-\sigma_m \frac{2R^2}{(R+\Delta)^2-R^2}\right] + \frac{d}{(R+\Delta)^2}\left[\sigma_e + \sigma_m \frac{(R+\Delta)^2+R^2}{(R+\Delta)^2-R^2}\right] = E_o\left[-\sigma_e + \sigma_m \frac{(R+\Delta)^2+R^2}{(R+\Delta)^2-R^2}\right].$$

Several of the expressions in the two preceding equations can be written in terms of the membrane conductance per unit area defined in equation (3.11) by noting that

$$\frac{\sigma_m}{(R+\Delta)^2 - R^2} = \frac{G_m}{2R+\Delta}.$$

After making this substitution, we have

$$a\left[\sigma_i + G_m \frac{(R+\Delta)^2+R^2}{2R+\Delta}\right] + \frac{d}{(R+\Delta)^2}\left[-G_m \frac{2(R+\Delta)^2}{2R+\Delta}\right] = E_o\left[-G_m \frac{2(R+\Delta)^2}{2R+\Delta}\right],$$

$$a\left[-G_m \frac{2R^2}{2R+\Delta}\right] + \frac{d}{(R+\Delta)^2}\left[\sigma_e + G_m \frac{(R+\Delta)^2+R^2}{2R+\Delta}\right] = E_o\left[-\sigma_e + G_m \frac{(R+\Delta)^2+R^2}{2R+\Delta}\right].$$

The equations that have been derived thus far can now be greatly simplified by recognizing that membrane thickness Δ is much less than the axon radius R. Specifically, cell membranes thickness is on the order of 75Å, whereas the radius of a typical axon is roughly 0.5μm[26]. Thus the axon radius is almost 100 times greater than the cell membrane thickness. Based on this comparison, we make the approximation $\Delta \approx 0$ to obtain

$$a(\sigma_i + G_m R) + d\left(-\frac{G_m}{R}\right) = E_o(-G_m R),$$

$$a(-G_m R) + d\left(\frac{\sigma_e}{R^2} + \frac{G_m}{R}\right) = E_o(-\sigma_e + G_m R).$$

Now a and d can be found fairly easily, and are given by

$$a = -\frac{2\sigma_e G_m R}{\sigma_i G_m R + \sigma_e G_m R + \sigma_i \sigma_e} E_o, \tag{A.20}$$

$$d = \frac{\sigma_i G_m R^3 - \sigma_e G_m R^3 - \sigma_i \sigma_e R^2}{\sigma_i G_m R + \sigma_e G_m R + \sigma_i \sigma_e} E_o. \tag{A.21}$$

Equations (A.11), (A.20) and (A.21) provide a complete solution for the electric potential inside and outside of the axon model. To determine the potential inside of the cell

membrane, it would be necessary to find b and c. This could be done by substituting the solutions for a and d back into equations (A.18) and (A.19). As in the case of the cell body model, however, the potential inside the membrane is not of critical importance, so we will neglect b and c altogether.

Applying the definition of transmembrane potential given in equation (3.14) to the solution above gives

$$\boxed{V_m = \frac{2\sigma_i\sigma_e R}{\sigma_i G_m R + \sigma_e G_m R + \sigma_i\sigma_e} E_o \cos\phi.} \tag{A.22}$$

Note the similarity between the induced transmembrane potential for the cylindrical and spherical models. All of the major points made in Subsection 3.2.3 apply to the cylindrical axon model.

A.2.3 Time-dependent solutions

In this section the system dynamics of equations (A.12)-(A.17) are examined. The derivations parallel those used for the spherical cell.

The four coefficients a, b, c and d may be eliminated from equations (A.12)-(A.17), leaving an ordinary differential equation in the surface charge densities, σ^i_{su} and σ^e_{su}. Solve for b and c in terms of a and d using equations (A.12) and (A.13).

$$\begin{aligned} b &= a - \frac{(R+\Delta)^2}{(R+\Delta)^2 - R^2}\left[a - \frac{d}{(R+\Delta)^2} + E_o(t)\right], \\ c &= \frac{(R+\Delta)^2 R^2}{(R+\Delta)^2 - R^2}\left[a - \frac{d}{(R+\Delta)^2} + E_o(t)\right]. \end{aligned}$$

Substitute formulas for b and c into equations (A.14) and (A.15) and collect terms.

$$\begin{aligned} a\left[\epsilon_f + \epsilon_m \frac{(R+\Delta)^2 + R^2}{(R+\Delta)^2 - R^2}\right] + \frac{d}{(R+\Delta)^2}\left[-\epsilon_m \frac{2(R+\Delta)^2}{(R+\Delta)^2 - R^2}\right] \\ = \frac{\sigma^i_{su}}{\cos\phi} + E_o(t)\left[-\epsilon_m \frac{2(R+\Delta)^2}{(R+\Delta)^2 - R^2}\right], \\ a\left[-\epsilon_m \frac{2R^2}{(R+\Delta)^2 - R^2}\right] + \frac{d}{(R+\Delta)^2}\left[\epsilon_f + \epsilon_m \frac{(R+\Delta)^2 + R^2}{(R+\Delta)^2 - R^2}\right] \\ = \frac{\sigma^e_{su}}{\cos\phi} + E_o(t)\left[-\epsilon_f + \epsilon_m \frac{(R+\Delta)^2 + R^2}{(R+\Delta)^2 - R^2}\right]. \end{aligned}$$

Factor a Δ out of the denominators,

$$(R+\Delta)^2 - R^2 = \Delta(2R+\Delta),$$

make use of the definition of membrane capacitance per unit area, $C_m = \epsilon_m/\Delta$, and approximate $\Delta \approx 0$ since $\Delta \ll R$.

$$a(\epsilon_f + C_m R) + d\left(-\frac{C_m}{R}\right) = \frac{\sigma^i_{su}}{\cos\phi} + E_o(t)(-C_m R), \tag{A.23}$$

$$a(-C_m R) + d\left(\frac{\epsilon_f}{R^2} + \frac{C_m}{R}\right) = \frac{\sigma^e_{su}}{\cos\phi} + E_o(t)(-\epsilon_f + C_m R). \tag{A.24}$$

[Note in the above equations that if $\epsilon_f \ll C_m R$, $\sigma^i_{su} \approx -\sigma^e_{su}$ and we no longer have a second order system.]

b and c may be eliminated from equations (A.16) and (A.17) in a nearly identical manner, but this time using the definition of membrane conductance per unit area, $G_m = \sigma_m/\Delta$. Derivations yield

$$a(\sigma_i + G_m R) + d\left(-\frac{G_m}{R}\right) = \frac{-\dot{\sigma}^i_{su}}{\cos\phi} + E_o(t)(-G_m R), \tag{A.25}$$

$$a(-G_m R) + d\left(\frac{\sigma_e}{R^2} + \frac{G_m}{R}\right) = \frac{-\dot{\sigma}^e_{su}}{\cos\phi} + E_o(t)(-\sigma_e + G_m R). \tag{A.26}$$

Now solve equations (A.25) and (A.26) for a and d. In matrix notation,

$$\begin{bmatrix} a \\ d \end{bmatrix} = \left(\frac{-R^2}{\cos\phi}\right) \frac{\begin{bmatrix} \frac{\sigma_e}{R^2} + \frac{G_m}{R} & \frac{G_m}{R} \\ G_m R & \sigma_i + G_m R \end{bmatrix} \begin{bmatrix} \dot{\sigma}^i_{su} \\ \dot{\sigma}^e_{su} \end{bmatrix}}{\sigma_i\sigma_e + \sigma_i G_m R + \sigma_e G_m R} + \frac{\begin{bmatrix} \frac{-2\sigma_e G_m}{R} \\ -\sigma_i\sigma_e \end{bmatrix} R^2 E_o(t)}{\sigma_i\sigma_e + \sigma_i G_m R + \sigma_e G_m R}. \tag{A.27}$$

Substituting the above results into equations (A.23) and (A.24) yields the following ordinary differential equation in surface charge density.

$$-\frac{\begin{bmatrix} \epsilon_f + C_m R & -C_m R \\ -C_m R & \epsilon_f + C_m R \end{bmatrix} \begin{bmatrix} \sigma_e + G_m R & G_m R \\ G_m R & \sigma_i + G_m R \end{bmatrix} \begin{bmatrix} \dot{\sigma}^i_{su} \\ \dot{\sigma}^e_{su} \end{bmatrix}}{\sigma_i\sigma_e + \sigma_i G_m R + \sigma_e G_m R} = \begin{bmatrix} \sigma^i_{su} \\ \sigma^e_{su} \end{bmatrix} + \begin{bmatrix} f_1 \\ f_2 \end{bmatrix} E_o(t)\cos\phi, \tag{A.28}$$

where

$$f_1 = \frac{2\epsilon_f\sigma_e G_m R + \sigma_e C_m G_m R^2 - \sigma_i C_m G_m R^2 - 2\sigma_i\sigma_e C_m R}{\sigma_i\sigma_e + \sigma_i G_m R + \sigma_e G_m R}, \tag{A.29}$$

$$f_2 = \frac{-\epsilon_f\sigma_e G_m R - \sigma_e C_m G_m R^2 + \sigma_i C_m G_m R^2 + 2\sigma_i\sigma_e C_m R - \epsilon_f\sigma_i G_m R}{\sigma_i\sigma_e + \sigma_i G_m R + \sigma_e G_m R}. \tag{A.30}$$

As in the case of the sphere, two important pieces of information can be found in equation (A.28); a circuit representation of the system and the system time constants. The circuit representation is shown in Figure A-3. Its topology is identical to that of the sphere, but the resistor values are slightly different. Also, the cylinder radius R is somewhat smaller than that of the sphere.

To find the time constants of the system, note again that equation (A.28) is of the form

$$-A\,\dot{\mathbf{x}} = \mathbf{x} + \text{drive terms}.$$

The time constants of the system are the eigenvalues of the A matrix. Using the fact that $\epsilon_f \ll C_m R$, the time constants are found to be

$$\tau = 0,\ \frac{C_m R(\sigma_i + \sigma_e)}{\sigma_i\sigma_e + G_m R(\sigma_i + \sigma_e)}. \tag{A.31}$$

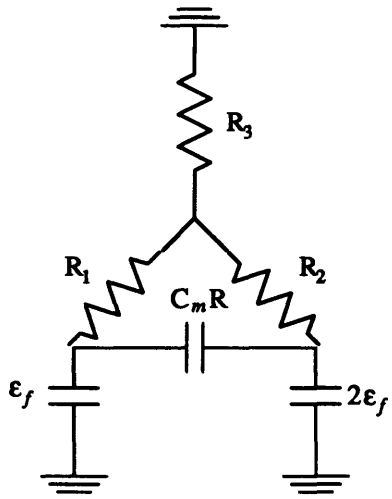

$$R_1 = \frac{\sigma_e}{\sigma_i \sigma_e + \sigma_e G_m R + \sigma_i G_m R}$$

$$R_2 = \frac{\sigma_i}{\sigma_i \sigma_e + \sigma_e G_m R + \sigma_i G_m R}$$

$$R_3 = \frac{G_m R}{\sigma_i \sigma_e + \sigma_e G_m R + \sigma_i G_m R}$$

Figure A-3: Circuit model for cylindrical cell.

The zero-valued time constant arises because the approximation $\epsilon_f \approx 0$ was made. The second time constant can be rewritten

$$\frac{1}{\tau_2} = \frac{1}{R_m C_m} + \frac{\sigma_i \sigma_e}{C_m R(\sigma_i + \sigma_e)}. \tag{A.32}$$

The first expression appearing on the right of equation (A.32) resembles a circuit RC time constant for the membrane. The second expression, as in the case of the sphere, is determined by the membrane capacitance C_m, the radius of the cell R and the intracellular and extracellular conductivities σ_i and σ_e. Again the time constant will be dominated by the second expression. Since the axon radius $R \approx 5 \times 10^{-7}$m is somewhat smaller than that of the sphere, the time constant for the axon will be somewhat smaller than that of the sphere. Using the data of Table A.1,

$$\frac{1}{R_m C_m} = 10^3 \text{ s},$$

$$\frac{\sigma_i \sigma_e}{C_m R(\sigma_i + \sigma_e)} = 8 \times 10^9 \text{ s},$$

$$\tau_2 = 1.25 \times 10^{-8} \text{ s}.$$

Appendix B

SPICE simulation of axon in longitudinal field

To examine the time-dependent behavior of the model for an axon in a longitudinal field, a SPICE simulation was run on the circuit of Figure B-1. An abbreviated version of the input file is given at the end of this appendix.

B.1 Circuit description

A small unit of axonal length Δ is represented by the circuit block in the dashed enclosure. Using the notation of section 3.3, we see from the Figure that

$$c_m = \frac{1\text{mF}}{\Delta},$$

$$g_m = \frac{1/1\Omega}{\Delta},$$

$$r_i = \frac{0.01\Omega}{\Delta}.$$

From equation (3.20),

$$\lambda_c = \sqrt{\frac{\Delta^2}{(1/1\Omega)(0.01\Omega)}} = 10\Delta,$$

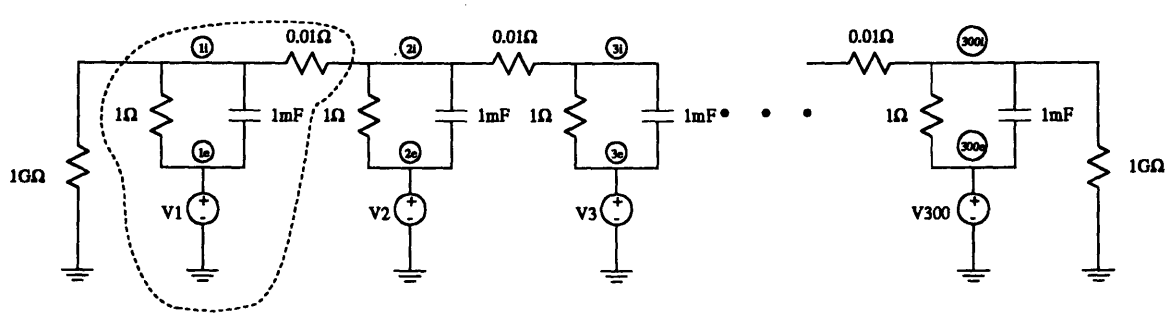

Figure B-1: SPICE simulation circuit for axon in a longitudinal field.

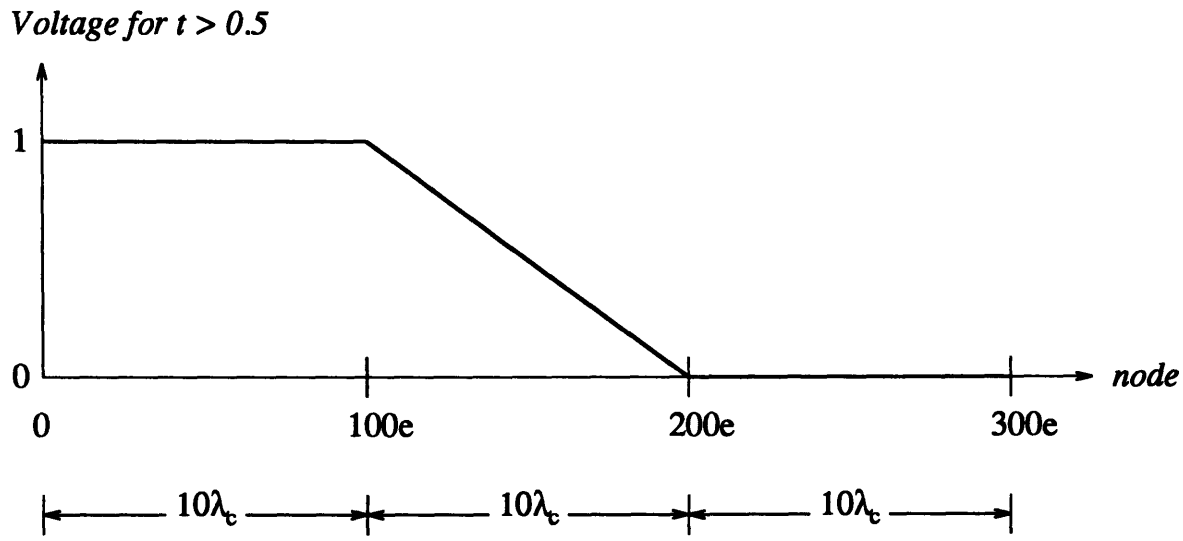

Figure B-2: Distribution of source voltages along the axon model circuit.

Thus, the circuit of Figure B-1 represents an axon which is $300\Delta = 30\lambda_c$ long. From equation (3.21),

$$\tau_m = \frac{0.001\text{F}}{1/1\Omega} = 1\text{ms}.$$

This is the same as the membrane RC time constant found in section A.1.

The circled numbers in Figure B-1 represent the nodes of the circuit model between each of the length-Δ segments. Nodes 1i-300i represent intracellular voltages of the circuit model, and nodes 1e-300e represent the extracellular voltages at corresponding locations. Applied extracellular voltages are modeled with perfect voltage sources V1-V300. To find the step response of the circuit, the voltages were initially set to zero. For $t > 0.5$ms the voltage sources were assigned as in Figure B-2. Note that segments of length $10\lambda_c$ surround the two breakpoints at nodes 100e and 200e. These breakpoints represent impulses in the activating function (see section 3.3), and were intentionally placed "far away" from each other and from the left and right boundaries of the circuit.

B.2 Results

Plotted in Figure B-3 is the intracellular voltage at several nodes in the rightmost portion of the circuit. Since the extracellular voltage at these locations is zero, the intracellular voltage is equal to the induced transmembrane potential. The solid line, which represents the transmembrane potential at one of the breakpoints, rises fastest. The dotted vertical and horizontal lines indicate that this quantity reaches 63% of its final value at

$$\tau = 0.4\text{ms}$$

after the extracellular voltages are switched on. Note that *this interval is less than the membrane RC time constant.* Further away from the breakpoint, the intracellular voltages rise more slowly and attain lower final values.

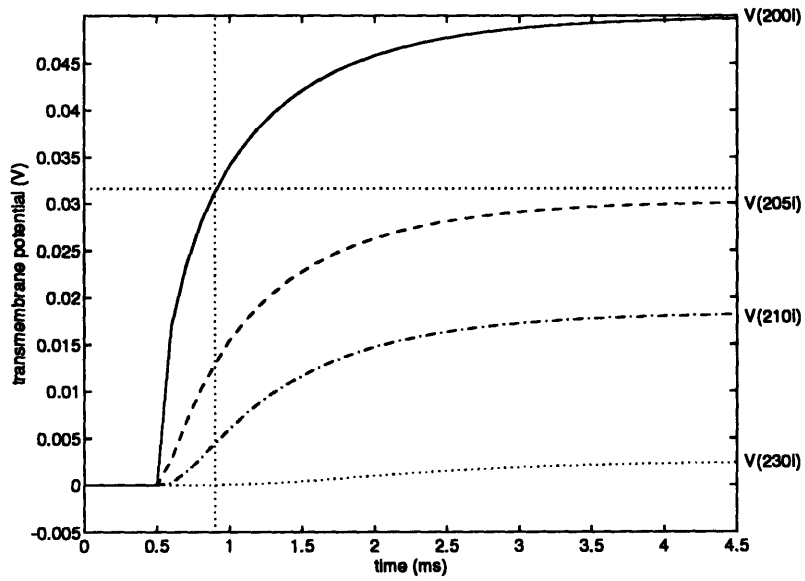

Figure B-3: "Intracellular" voltage vs. time.

B.3 Abbreviated SPICE input file

```
* ladder network

.subckt ladder 1 2 3
r1 1 2 0.01
r2 2 3 1
c1 2 3 0.001
.ends

*** rc ladder network

*** left side
r1 1000 0 1G * terminate with large resistance to ground
x1 1000 1 vl ladder
x2 1 2 vl ladder
x3 2 3 vl ladder
.
.
.
x98 97 98 vl ladder
x99 98 99 vl ladder
x100 99 100 vl ladder

vleft vl 0 dc 0 pulse(0 1 0.5m 2u 2u 10m 20m)

*** middle
```

```
x101 100 101 500 ladder
x102 101 102 501 ladder
x103 102 103 502 ladder
.
.
.
x197 196 197 596 ladder
x198 197 198 597 ladder
x199 198 199 598 ladder
x200 199 200 599 ladder

e101 500 0 (vl,0) 0.990000
e102 501 0 (vl,0) 0.980000
e103 502 0 (vl,0) 0.970000
.
.
.
e198 597 0 (vl,0) 0.020000
e199 598 0 (vl,0) 0.010000
e200 599 0 (vl,0) 0.000000


*** right side
x201 200 201 0 ladder
x202 201 202 0 ladder
x203 202 203 0 ladder
.
.
.
x298 297 298 0 ladder
x299 298 299 0 ladder
x300 299 1001 0 ladder
r2 1001 0 1G * terminate with large resistor
***
.op
.tran 0.1m 10m
.print tran v(200) v(205) v(210) v(230)
.options nomod ingold=2 numdgt=8 post
.end
```

References

[1] F.R. Amthor, C.W. Oyster, and E.S. Takahashi. Quantitative morphology of rabbit retinal ganglion cells. *Proc. R. Soc. Lond. B*, 217, 1983.

[2] A. Benjamin, M. Humayun, D. Hickingbotham, E. de Juan, Jr., and C. van den Honert. Characterization of retinal responses to electrical stimulation of retinal surface of rana catesbeiana. *Investigative Opthalmology and Visual Science*, 35(4):1832, March 15 1994. ARVO abstract.

[3] E. Berson. Retinitis pigmentosa. *Investigative Opthalmology and Visual Science*, 34(5):1659–1676, April 1993.

[4] L. Borg-Graham. On directional selectivity in vertebrate retina: An experimental and computational study. Technical Report 1350, MIT Artificial Intelligence Laboratory, 1992.

[5] R. Brancato, R. Pratesi, G. Leoni, G. Trabucchi, and U. Vanni. Histopathology of diode and argon laser lesions in rabbit retina: a comparative study. *Investigative Opthalmology and Visual Science*, 30(7):1504–1510, July 1989.

[6] G.S. Brindley. The site of electrical excitation of the human eye. *Journal of Physiology*, 127:189–200, 1955.

[7] Peter Carras, Paul Coleman, and Robert Miller. Site of action potential initiation in amphibian retinal ganglion cells. *Journal of Neurophysiology*, 67(2):292–304, February 1992.

[8] L. Cartee and R. Plonsey. The transient subthreshold response of spherical and cylindrical cell models to extracellular stimulation. *IEEE Transactions on Biomedical Engineering*, 39(1):76–85, January 1992.

[9] P. Coleman and R. Miller. Measurement of passive membrane parameters with whole-cell recording from neurons in the intact amphibian retina. *Journal of Neurophysiology*, 61(1):218–230, January 1989.

[10] D. Crapper and W. Noell. Retinal excitation and inhibition from direct electrical stimulation. *Journal of Neurophysiology*, 26:924–947, 1963.

[11] W. Dawson and N. Radtke. The electrical stimulation of the retina by indwelling electrodes. *Investigative Opthalmology and Visual Science*, 16(3):249–252, March 1977.

[12] J. M. R. Delgado. Electrodes for extracellular stimulation and recording. In W.L. Nastuk, editor, *Physical Techniques in Biological Research*, volume V: Electrophysiological Methods, Part A. Academic Press, 1964.

[13] R. Doty and F. Grimm. Cortical responses to local electrical stimulation of retina. *Experimental Neurology*, 5:319–334, 1962.

[14] J. Dowling. *The Retina: An Approachable Part of the Brain.* The Belknap Press of Harvard University Press, 1987.

[15] J. Dowling and B. Boycott. Retinal ganglion cells: A correlation of anatomical and physiological approaches. In B. Straatsma, M. Hall, R. Allen, and F. Crescitelli, editors, *The Retina: Morphology, Function, and Clinical Characteristics.* University of California Press, 1969.

[16] C.D. Ferris. *Introduction to Bioelectrodes.* Plenum Press, 1974.

[17] K. Frank and M. Becker. Microelectrodes for recording and stimulation. In W.L. Nastuk, editor, *Physical Techniques in Biological Research*, volume V: Electrophysiological Methods, Part A. Academic Press, 1964.

[18] B. Gernandt and R. Granit. Single fibre analysis of inhibition and the polarity of the retinal elements. *Journal of Neurophysiology*, 10:295–302, 1947.

[19] R. Granit. The distribution of excitation and inhibition in single-fibre responses from a polarized retina. *Journal of Physiology*, 105:45–53, 1946.

[20] R. Granit. Neural organization of the retinal elements, as revealed by polarization. *Journal of Neurophysiology*, 11:239–251, 1948.

[21] A.L. Hodgkin and A.F. Huxley. A quantitative description of membrane current and its application to conduction and excitation in nerve. *Journal of Physiology*, 117:500–544, 1952.

[22] A.L. Hodgkin and W.A.H. Rushton. The electrical constants of a crustacean nerve fiber. *Proc. Roy. Soc. Lond. B.*, 133:444–479, 1946.

[23] C. Howarth. Strength duration curves for electrical stimulation of the human eye. *The Quarterly Journal of Experimental Psychology*, 6:47–61, 1954.

[24] M. Humayun, R. Propst, E. de Juan, Jr., K. McCormick, and D. Hickingbotham. Bipolar surface electrical stimulation of the vertebrate retina. *Archives of Opthalmology*, 112:110–116, January 1994.

[25] M.S. Humayun, R.H. Propst, D. Hickingbotham, E. de Juan, Jr., and G. Dagnelie. Visual sensations produced by electrical stimulation of the retinal surface in patients with end-stage retinitis-pigmentosa. *Investigative Opthalmology and Visual Science*, 34(4):834, March 15 1993. ARVO abstract.

[26] R. Jensen. Personal communication.

[27] R. Jensen. Mechanism and site of action of a dopamine D1 antagonist in the rabbit retina. *Visual Neuroscience*, 3:573–585, 1989.

[28] R. Jensen. Intracellular recording of light responsees from visually identified ganglion cells in the rabbit retina. *Journal of Neuroscience Methods*, 40:101–112, 1991.

[29] R. Knighton. An electrically evoked slow potential of the frog's retina. I. properties of response. *Journal of Neurophysiology*, 38:185–197, 1975.

[30] R. Knighton. An electrically evoked slow potential of the frog's retina. II. identification with PII component of electroretinogram. *Journal of Neurophysiology*, 38:198–209, 1975.

[31] S. Kuffler. Discharge patterns and functional organization of mammalian retina. *Journal of Neurophysiology*, 16:37–68, 1953.

[32] S. Kuffler, J. Nicholls, and A. Martin. *From Neuron to Brain: A Cellular Approach to the Function of the Nervous System.* Sinauer Associates Inc., 1984.

[33] D.R. McNeal. Analysis of a model for excitation of myelinated nerve. *IEEE Transactions on Biomedical Engineering*, 23(4):329–337, July 1976.

[34] M. Meister, J. Pine, and D. Baylor. Multi-neuronal signals from the retina: acquisition and analysis. *Journal of Neuroscience Methods*, 51:95–106, 1994.

[35] S. Molotchnikoff. Transient responses of rabbit retinal ganglion cells to photic and electrical stimuli. *The Canadian Journal of Neurological Sciences*, pages 73–79, February 1976.

[36] S. Molotchnikoff. Lateral geniculate cell responses to electrical stimulation of the retina. *Brain Research*, 152:81–95, 1978.

[37] K. Motokawa. Retinal processes and their role in color vision. *Journal of Neurophysiology*, 12(5):291–303, September 1949.

[38] M. Narayanan, J. Rizzo, D. Edell, and J. Wyatt. Development of a silicon retinal implant: cortical evoked potentials following stimulation of the rabbit retina with light and electricity. *Investigative Opthalmology and Visual Science*, 35(4):1380, March 15 1994. ARVO abstract.

[39] T. Ogden and K. Brown. Intraretinal responses of the cynamolgus monkey to electrical stimulation of the optic nerve and retina. *Journal of Neurophysiology*, 27:682–705, 1964.

[40] R. Pagon. Retinitis pigmentosa. *Survey of Opthalmology*, 33(3):137–177, November-December 1988.

[41] R. Plonsey and K. Altman. Electrical stimulation of excitable cells - a model approach. *Proceedings of the IEEE*, 76(9):1122–1128, September 1988.

[42] S. Polyak. *The Retina.* The University of Chicago Press, 1941.

[43] A. Potts and J. Inoue. The electrically evoked resonse (EER) of the visual system. ii. effect of adaptation and retinitis pigmentosa. *Investigative Opthalmology and Visual Science*, 8(6):605–612, December 1969.

[44] A. Potts, J. Inoue, and D. Buffum. The electrically evoked resonse of the visual system (EER). *Investigative Opthalmology and Visual Science*, 7(3):269–278, June 1968.

[45] James B. Ranck, Jr. Which elements are excited in electrical stimulation of mammalian central nervous system: a review. *Brain Research*, 98:417–440, 1975.

[46] James B. Ranck, Jr. Extracellular stimulation. In M. Patterson and R. Kesner, editors, *Electrical Stimulation Research Techniques.* Academic Press, 1981.

[47] Frank Rattay. Analysis of models for external stimulation of axons. *IEEE Transactions on Biomedical Engineering*, BME-33(10):974–977, October 1986.

[48] Frank Rattay. Analysis of models for extracellular fiber stimulation. *IEEE Transactions on Biomedical Engineering*, 36(7):676–682, July 1989.

[49] J. Rizzo. Personal communication.

[50] L.S. Robblee and T.L. Rose. The electrochemistry of electrical stimulation. *Annual International Conference of the IEEE Engineering in Medicine and Biology Society*, 12(4):1479–80, 1990.

[51] J.T. Rubinstein. Analytical theory for extracellular electrical stimulation of nerve with focal electrodes. II. passive myelinated axon. *Biophysical Journal*, 60:538–555, September 1991.

[52] J.T. Rubinstein and F.A. Spelman. Analytical theory for extracellular electrical stimulation of nerve with focal electrodes. I. passive unmyelinated axon. *Biophysical Journal*, 54:975–981, December 1988.

[53] W.A.H. Rushton. The effect upon the threshold for nervous excitation of the length of nerve exposed, and the angle between current and nerve. *Journal of Physiology*, 63:357–377, 1927.

[54] P. Schiller. The on and off channels of the visual system. *Trends in Neurosciences*, 15(3):86–92, 1992.

[55] P. Schiller and N. Logothetis. The color-opponent and broad-band channels of the primate visual system. *Trends in Neurosciences*, 13(10):392–398, 1990.

[56] H.P. Schwan. Determination of biological impedances. In W.L. Nastuk, editor, *Physical Techniques in Biological Research*, volume VI: Electrophysiological Methods, Part B. Academic Press, 1963.

[57] W. Smiddy and E. Hernandez. Histopathologic results of retinal diode laser photocoagulation in rabbit eyes. *Archives of Opthalmology*, 110:693–698, May 1992.

[58] K. Spiegler and M. Wyllie. Electric potential differences. In G. Oster and A. Pollister, editors, *Physical Techniques in Biological Research*, volume II: Physical Chemical Techniques. Academic Press, 1956.

[59] J. Stone. *Parallel Processing in the Visual System.* Plenum Press, 1983.

[60] J. Stone, W. Barlow, M. Humayun, E. de Juan, Jr., and A. Milam. Morphometric analysis of macular photoreceptors and ganglion cells in retinas with retinitis pigmentosa. *Archives of Opthalmology*, 110:1634–1639, November 1992.

[61] E.N. Warman, W.M. Grill, and D. Durand. Modeling the effects of electric fields on nerve fibers: Determination of excitation thresholds. *IEEE Transactions on Biomedical Engineering*, 39(12):1244–1254, December 1992.

[62] H. Wässle and B. Boycott. Functional architecture of the mammalian retina. *Physiological Reviews*, 71(2):447–480, April 1991.

[63] T.F. Weiss. *A Textbook of Cellular Physiology and Biophysics.* MIT 6.021J Course Notes, 1992.

[64] J. Wyatt, J. Rizzo, A. Grumet, D. Edell, and R. Jensen. Development of a silicon retinal implant: epiretinal stimulation of retinal ganglion cells in the rabbit. *Investigative Opthalmology and Visual Science*, 35(4):1380, March 15 1994. ARVO abstract.

[65] R. Young. Pathophysiology of age-related macular degeneration. *Survey of Opthalmology*, 31(5):291–306, March-April 1987.